Report on the CCPR-S2 Supplementary Comparison of Area Measurements of Apertures for Radiometry

Final Report
January 4, 2007

Prepared by

Maritoni Litorja and Joel Fowler
National Institute of Standards and Technology

Table of Contents

List of Tables

List of Figures

1. Introduction

The Consultative Committee on Photometry and Radiometry in 1999 decided to undertake an international comparison of the capabilities of member laboratories to measure the geometric area of apertures used for radiometry. The accuracy of aperture areas is deemed vital to many radiometric and photometric measurements and thereby affects the accuracy of radiometric and photometric standards. This supplementary comparison is carried out within the framework of the Mutual Recognition Arrangement for national measurement standards and follows the *Guidelines for CIPM key comparisons*.

The National Institute of Standards and Technology, NIST, the national metrological institute (NMI) of the United States of America was chosen as the Pilot Laboratory for this supplementary comparison S2. The Pilot Laboratory was responsible for the fabrication, initial and periodic measurements during the comparison, and circulation of the transfer apertures used in the supplementary comparison.

2. Organization of the comparison

The Supplementary Comparison S2 was designed to determine laboratory differences in area measurements of apertures commonly used in radiometry and photometry. A total of eight apertures were circulated for the comparison, heretofore referred to as transfer apertures. Seven apertures were manufactured at NIST while another one was supplied by the Physikalische Technische Bundesanstalt (PTB), the NMI of Germany. All transfer apertures were measured at NIST prior to circulation. The comparison was conducted in a star pattern (A-B-A-C-A-D-A…) where A is the Pilot Laboratory. For this comparison, the NIST non-contact aperture area measurement facility was the pilot laboratory. The areas of the apertures for circulation were measured prior to shipping to the participant laboratory, and again measured after it was received from the participant laboratory. A set of control apertures was also measured at certain times during the comparison.

The comparison commenced in January 1999 and the last measurement at NIST was taken in November 2003. The time taken by each round (A-Lab-A) is not uniform throughout the comparison for a variety of reasons, such as unavailability of measuring instrument at the participant laboratory or at NIST, or both. Due to instrumental limitations, not all participant laboratories measured all transfer apertures.

3. Description of apertures and measurement methods

3.1. Description of apertures

Eight different apertures were used in the comparison, varying in size (small vs. large), fabrication method (diamond turned vs. conventionally turned), material (copper, aluminum bronze), and edge type (knife edged vs. cylindrical (with land)).

There were three aperture sets with eight different apertures in each set, one for circulation (transfer), one kept at NIST as control and one spare. Each set consisted of four diamond-turned apertures and three conventionally machine turned, ground, and polished apertures and one diamond turned aperture fabricated in Germany. The apertures from Germany have a 10 μm-thick land and the edge has a radius of about 1 μm.

The NIST apertures (APT 01 to 19) were all nominally 50 mm outer diameter by 6 mm thick. Two inside diameters (IDs) nominally 5.0 mm and 25.0 mm, two edge types and two types of material were manufactured, using each fabrication method. The edge is either sharp (knife-edged), where the edge is only a few micrometers thick, if not thinner, or cylinder type, where the edge has a thickness of 50-100 micrometers, also called a land. The knife-edged apertures could only be measured using a non-contact technique while apertures with a land can be measured using either non-contact or contact method. The PTB aperture can also only be measured by non-contact method.

Figure 3.1. Photographs of some of the transfer apertures, in their shipping containers

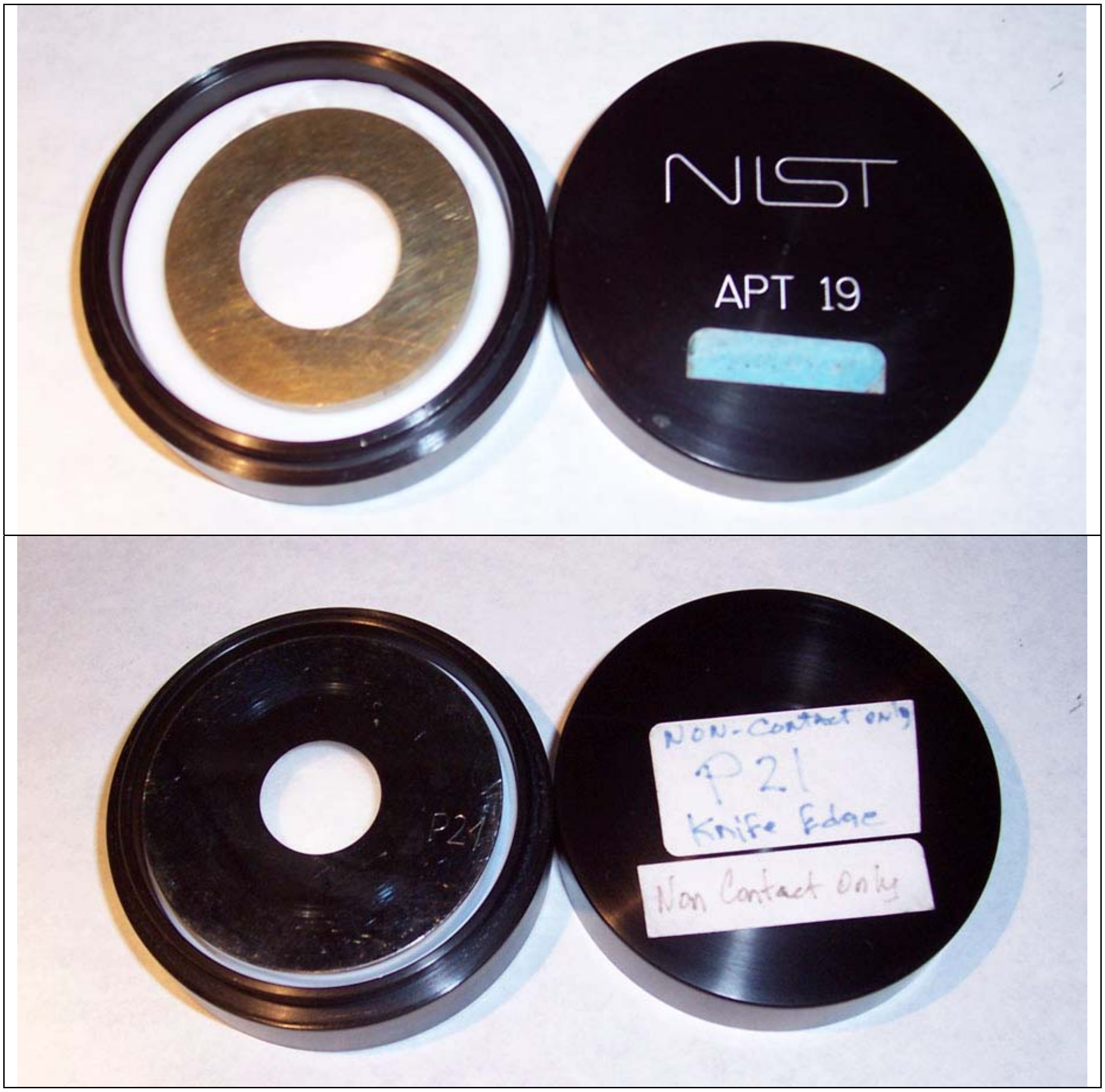

Electron micrographs of the edges of the transfer apertures were taken by the PTB and shown in Appendix B.

Table 3.1. is a summary of the apertures used for the comparison. There are three nominal sizes, three types of material, two edge types, and two fabrication methods. There are nine participating laboratories and two general methods of measurement, either non-contact or contact, where the measuring device comes in contact with the edge. Apt 01 to APT 06 are made from UBAC[1] copper-plated oxygen- free high-conductivity (OFHC) copper inserts.

[1] UBAC is a registered trademark for UDYLITE Bright Acid Copper by the Enthone-OMI, Inc. subsidiary of ASARCO. Their address is 21441 HOOVER Road, Warren, Michigan 48089 USA. The phone number is 313-497-9100.

Table 3.1. List of apertures used for the S2 intercomparison

ID number	Diameter [mm]	Material	Edge type	Fabrication
1-3	25	Cu	sharp	Diamond turned
4-6	5	Cu	sharp	Diamond turned
7-9	25	Al bronze	cylinder	Diamond turned
10-12	5	Al bronze	cylinder	Diamond turned
13-15	25	Al bronze	sharp	conventional
16-18	5	Al bronze	sharp	conventional
19-21	25	Al bronze	cylinder	conventional
P21-P23	20	Al	sharp	Diamond-turned

3.2. Description of measurement methods

The measurement methods used by most of the participant laboratories fell into two general categories: (1) non contact method where the edges are located optically, and (2) contact method, where a mechanical probe touches the aperture edge to find its position. For either method, edge locations are used to determine the radius or diameter of the circular aperture. MIKES and BIPM are two laboratories using the non-contact method to determine the effective area of the aperture by directly measuring radiation throughput, rather than the geometric area.

Table 3.2 lists the participant laboratories, the apertures measured and the measurement method, which is either the non-contact (1) or contact (2) method. Not every participant laboratory could measure all the transfer apertures due to certain instrumental limitations. Some laboratories (PTB, NPL, NIST, OMH) were able to measure the apertures using both non-contact and contact methods. The laboratories that made contact measurements are affixed with a lower case c after the laboratory name to distinguish them from the non-contact methods. NIST using non-contact method is the pilot laboratory and NIST using contact method is treated as a participant separate from the pilot laboratory.

Table 3.2 List of participating laboratories in the S2 comparison

Lab	1=non-contact	Apertures Measured							
	2=contact	1	4	7	10/11	13	16	19	P21
PTB	1	●	●	●	●	●	●		●
PTBc	2			●	●			●	
NPL	1	●	●	●	●	●	●	●	●
NPLc	2			●	●				
BNM[2]	1	●	●	●	●	●	●	●	●
VNIIOFI	1	●	●	●	●	●	●	●	●
HUT[3]	1		●		●		●		
BIPM	1		●		●		●		●
OMH	1	●	●		●	●	●	●	●
OMHc	2			●				●	
NISTc	2			●	●			●	
NRCc	2			●	●			●	
NIST	1	●	●	●	●	●	●	●	●

[2] BNM was renamed in January 2005 as the LNE-INM and heretofore will be referred to as such

[3] Helsinki University of Technology (HUT) and the Centre for Metrology and Accreditation (MIKES) have established a joint laboratory in Jan. 2005. The laboratory name will in future comparisons be abbreviated as MIKES.

4. Measurement results from participating laboratories

The participant laboratories' description of their measurement method and their tables of uncertainty are presented in Appendix A. Each participant laboratory measured each aperture five times, unless otherwise noted, according to the laboratory's measurement protocol. The reported areas (*A*) are the means of the replicate measurements, expressed in mm^2 and corrected for thermal expansion if necessary, to 20°C. Uncertainties in area (*u*(*A*)) are also expressed in mm^2 as a combined standard uncertainty. The NIST measurement results are further discussed in the next section.

The first laboratory, PTB, reported edge damage to Apt 10 after their contact measurement. Even though the NIST measurement of Apt 10 upon return did not show significant difference to that prior to shipping to PTB, Apt 10 was replaced by Apt 11 in the subsequent measurements. Hence, only PTB measured Apt 10, while the rest of the participants measured Apt 11.

Tables 4.1.1 through 4.8.1 present the reported results of each laboratory's measurement of the apertures. The NIST results are presented in the next section.

4.1. PTB (Germany)

Table 4.1 Mean area measurements by the PTB non-contact method (n=5)

Aperture	Area, *A* [mm^2]	*u*(*A*) [mm^2]
Apt 1	550.7791	0.0126
Apt 4	34.0262	0.0031
Apt 7	505.1476	0.0509
Apt 10	23.2684	0.0109
Apt 13*	526.2817	0.1235
Apt 16*	21.3865	0.0193
Apt 21	314.1847	0.0273

*After Draft A was distributed, PTB notified the Pilot lab that there were errors they made in the reported values for Apt 13 and Apt 16, and submitted corrected results. The values shown here are original reported values. The results of the comparison including the corrected values of these apertures are shown in Appendix D.

Table 4.1.2 Mean area measurements by the PTB contact method (n=10)

Aperture	Area, *A* [mm^2]	*u(A)* [mm^2]
Apt 7	505.1755	0.0080
Apt 10	23.2591	0.0085
Apt 19	518.2533	0.0303

4.2. NPL (United Kingdom)

Table 4.2.1 Mean area measurements by the NPL non-contact method (n=5)

Aperture	Area, A [mm^2]	$u(A)$ [mm^2]
Apt 01	550.5900	0.0140
Apt 04	34.0189	0.0017
Apt 07	505.1140	0.0130
Apt 11	23.3131	0.0016
Apt 13	525.5218	0.0130
Apt 16	21.3082	0.0024
Apt 21	314.1180	0.0070

Table 4.2.2 Mean area measurements by the NPL contact method (n=4)

Aperture	Area, A [mm^2]	$u(A)$ [mm^2]
Apt 07	505.1827	0.0048
Apt 11	23.3115	0.0010

4.3. LNE-INM (France)

Table 4.3 Mean area measurements by the LNE-INM non-contact method (n=5)

Aperture	Area, A [mm^2]	$u(A)$ [mm^2]
Apt 01	550.8918	0.0710
Apt 04	34.0340	0.0054
Apt 07	505.2272	0.0410
Apt 11	23.3061	0.0055
Apt 13	525.6808	0.0490
Apt 16	21.2887	0.0043
Apt 19	518.3052	0.0420
Apt P21	314.1258	0.0200

4.4. VNIIOFI (Russia)

Table 4.4 Mean area measurements by the VNIIOFI non-contact method (n=5)

Aperture	Area, A [mm^2]	$u(A)$ [mm^2]
Apt 01	550.6220	0.0050
Apt 04	33.9905	0.0022
Apt 07	504.8890	0.0060
Apt 11	23.2870	0.0040
Apt 13	525.4000	0.0110
Apt 16	21.2624	0.0009
Apt 19	517.8230	0.0080
Apt 21	313.9440	0.0050

4.5. MIKES (Finland)

Table 4.5 Mean area measurements by MIKES non-contact method (n=5)

Aperture	Area, A [mm^2]	$u(A)$ [mm^2]
Apt 04	34.0240	0.0145
Apt 11	23.3020	0.0105
Apt 16	21.2690	0.0095

4.6. BIPM

Table 4.6 Mean area measurements by the BIPM non-contact method (n=5)

Aperture	Area, A [mm^2]	$u(A)$ [mm^2]
Apt 04	34.0260	0.0016
Apt 11	23.3094	0.0016
Apt 16	21.2786	0.0011
Apt 21	314.1170	0.0328

4.7. OMH (Hungary)

Table 4.7.1 Mean area measurements by the OMH non-contact method (n=5)

Aperture	Area, A [mm^2]	$u(A)$ [mm^2]
Apt 01	550.6747	0.0663
Apt 04	34.0046	0.0179
Apt 07	505.0377	0.0877
Apt 11	23.2657	0.0160
Apt 13	525.5362	0.0620
Apt 16	21.2535	0.0109
Apt 19	518.0051	0.1096
Apt 21	314.0771	0.0391

Table 4.7.2 Mean area measurements by the OMH contact method (n=5)

Aperture	Area, *A* [mm^2]	*u(A)* [mm^2]
Apt 07	505.1665	0.0378
Apt 19	518.2138	0.0363

4.8. NIST (USA)

The contact method measurements were performed by another NIST laboratory, completely independent of the non-contact measurements lab.

Table 4.8 Mean area measurements by the NIST contact method (n=5)

Aperture	Area, *A* [mm^2]	*u(A)* [mm^2]
Apt 07	505.1902	0.0026
Apt 11	23.3141	0.0005
Apt 19	518.2163	0.0024

4.9. NRC (Canada)

Table 4.9 Mean area measurements by the NRC contact method (n=4 or 5)

Aperture	Area, *A* [mm^2]	*u(A)* [mm^2]
Apt 07	505.1750	0.0080
Apt 11	23.3003	0.0021
Apt 19	518.2088	0.0081

5. NIST measurements and uncertainty

5.1. Pilot lab Facility

NIST as the pilot laboratory, used an instrument employing non-contact method. The instrument is an interferometrically-controlled XY stage with green-filtered white light for illumination in transmission mode, a microscope objective and CCD for edge detection. Edge point positions around the circular apertures are collected and used in a circle fitting routine to determine radius and area of the aperture.

The estimated relative standard uncertainty of aperture area measurement for apertures having perfect edges is 4.6×10^{-5} for apertures of 5 mm diameter, and 2.8×10^{-5} for apertures of 25 mm diameter. The uncertainties of area measurements vary depending on type and conditions of edges. See Appendix A for further details of the instrument and detailed uncertainty budget.

5.2. Measurement scheme

NIST as the pilot laboratory measured the transfer apertures in replicate, before and after each deployment to the participant laboratory. The mean of each pilot data set *h* (a set of replicate NIST measurements between deployments) for each aperture *j*, $\overline{A}_{\mathrm{NIST},j,h}$, was taken. Each laboratory *i* measurement was basically compared to the pair of NIST measurement sets bracketing deployments to lab *i* for most of the apertures. The overall NIST mean was used rather than the pair, for Apt 11 and Apt 16, both of which exhibited comparably large variances relative to the rest of the transfer apertures.

The overall mean of NIST measurements for each aperture, $\overline{A}_{\mathrm{NIST},j}$, is determined as a mean of all the pilot data sets and used as the NIST official measurement as a participant laboratory. The deviation of each pilot data set mean $\overline{A}_{\mathrm{NIST},j,h}$ from $\overline{A}_{\mathrm{NIST},j}$ reflects artifact effects

5.3. Stability of the transfer apertures

The charts 5.3.1 through 5.3.8 present the relative deviation (in percent) of each pilot data set mean $\overline{A}_{\mathrm{NIST},j,h}$ from the overall mean $\overline{A}_{\mathrm{NIST},j}$ plotted against the date of the measurement. Control apertures of the same type were measured with the transfer apertures and these results are shown together in each figure. The variation of results for the transfer apertures, if significantly larger than that of control apertures, reflect the changes (artifact effects) of the transfer apertures during the comparison. The measurement by participant laboratories occurred in between the NIST measurements of the transfer apertures.

Linear regression analysis of the transfer and control aperture data were performed to determine transfer aperture drift (artifact effect) vs. NIST measurement drift (lab effect). No significant measurement drift was observed, but some of the transfer apertures showed artifact effects. In many cases, the variations of transfer apertures were larger than control apertures (Apt 01/03, 04/06, 16/17, 19/20), which indicate that there have been some changes of these transfer apertures during the comparison. In some other cases, variations of transfer apertures and control apertures were comparable (Apt. 7/8, 11/12, 13/14, 21/23), in which case changes of the transfer apertures are not notable. Based on these observations, the data analysis strategies as described in section 5.2 were taken.

Another view of the stability of the transfer apertures in the comparison is shown in the charts 5.3.9 through 5.3.16. Instead of percent relative deviation, the ordinate axis is the absolute deviation from the overall mean area, expressed in mm^2.

Figure 5.3.1 Relative Deviation (%) of Apt 01/02

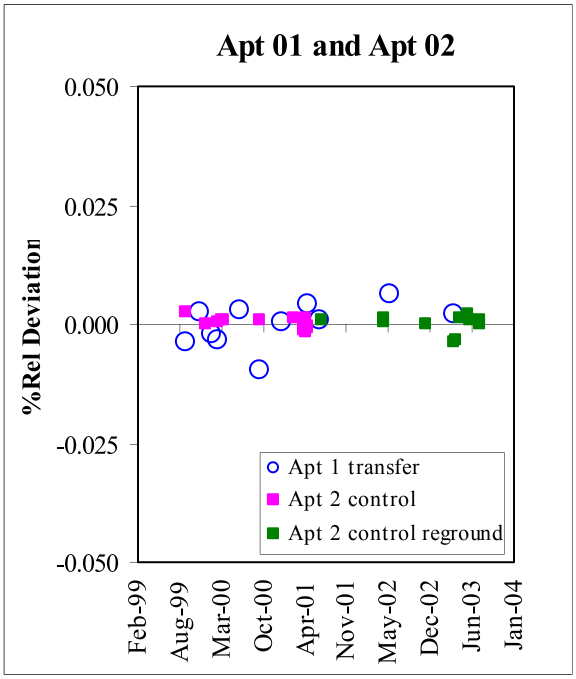

Figure 5.3.2 Relative Deviation (%) of Apt 04/06

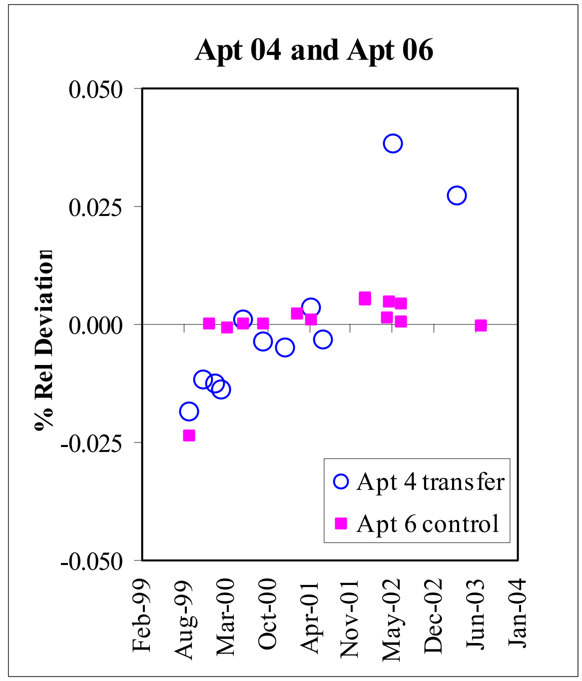

Figure 5.3.3 Relative Deviation (%) of Apt 07/08

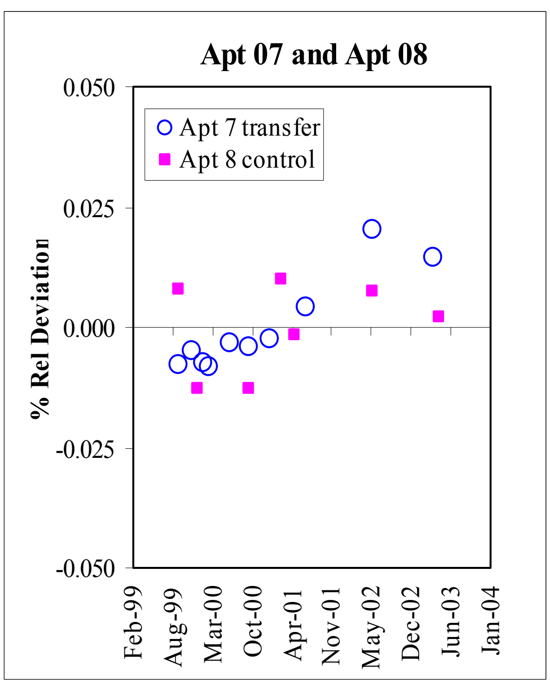

Figure 5.3.4 Relative Deviation (%) of Apt 11/12

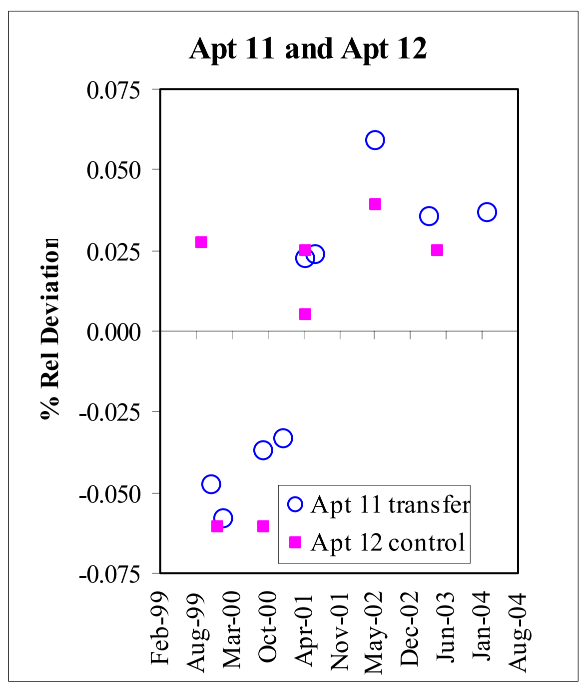

Figure 5.3.5 Relative Deviation (%) of Apt 13/14

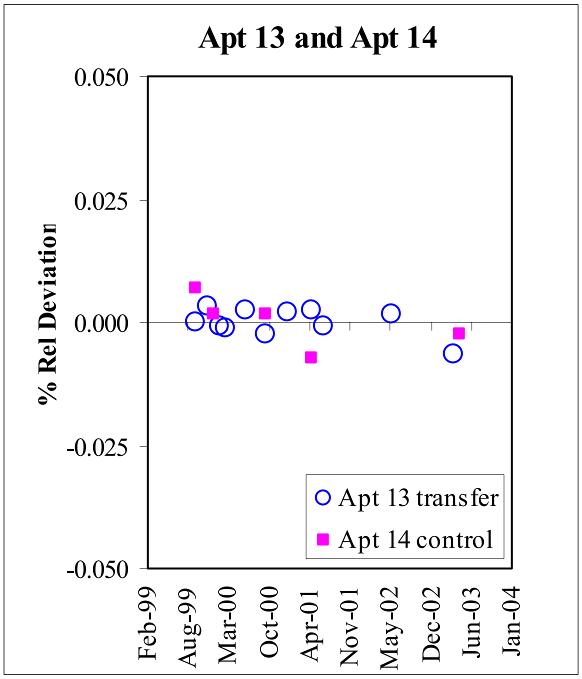

Figure 5.3.6 Relative Deviation (%) of Apt 16/17

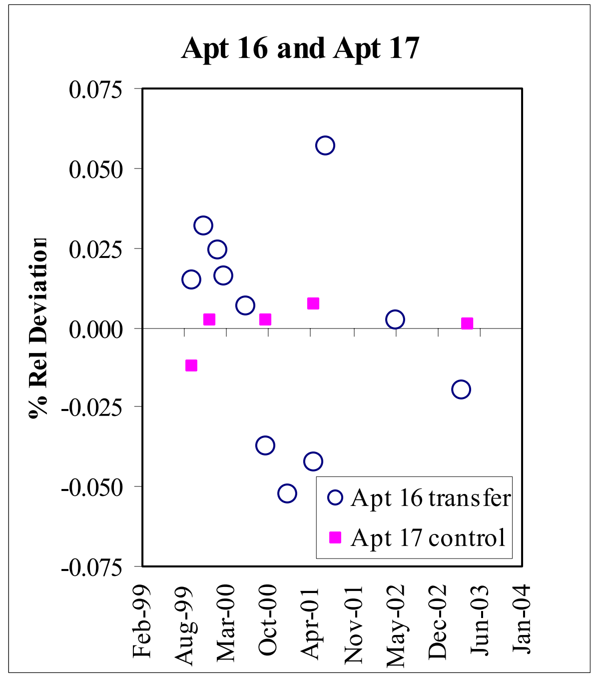

Figure 5.3.7 Relative Deviation (%) of Apt 19/20

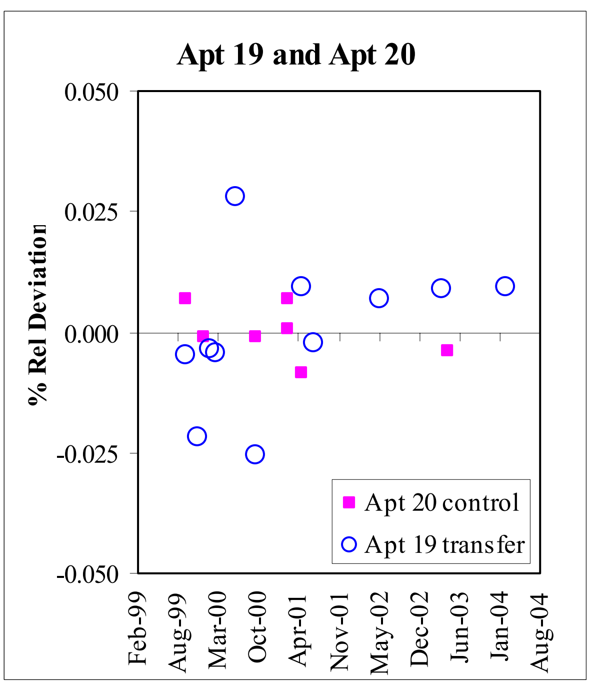

Figure 5.3.8 Relative Deviation (%) of Apt P21/P23

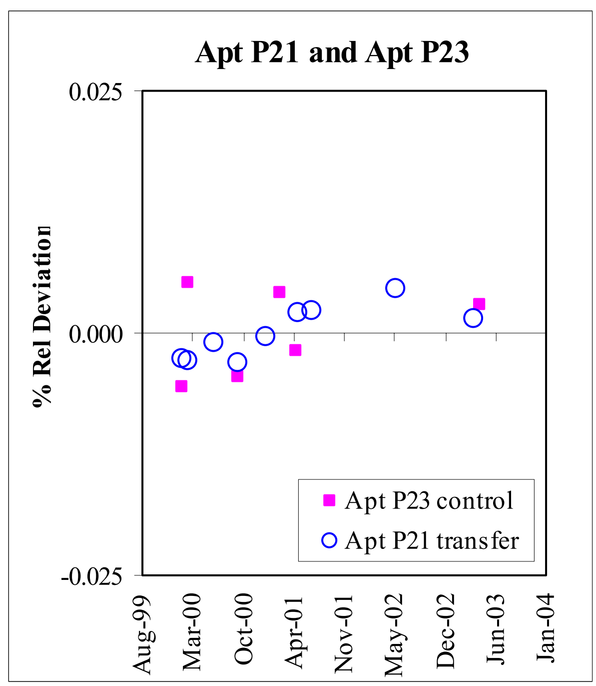

Figure 5.3.9 Dev. from mean of Apt 01/02 (mm^2)

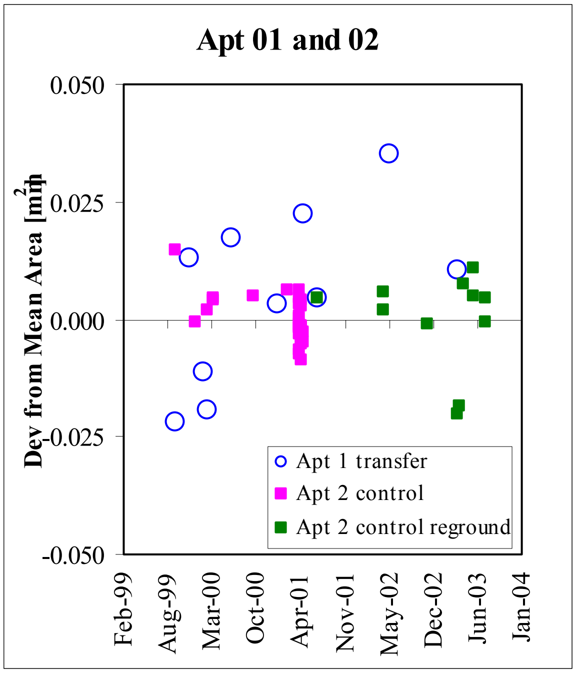

Figure 5.3.10 Dev. from mean of Apt 04/06 (mm^2)

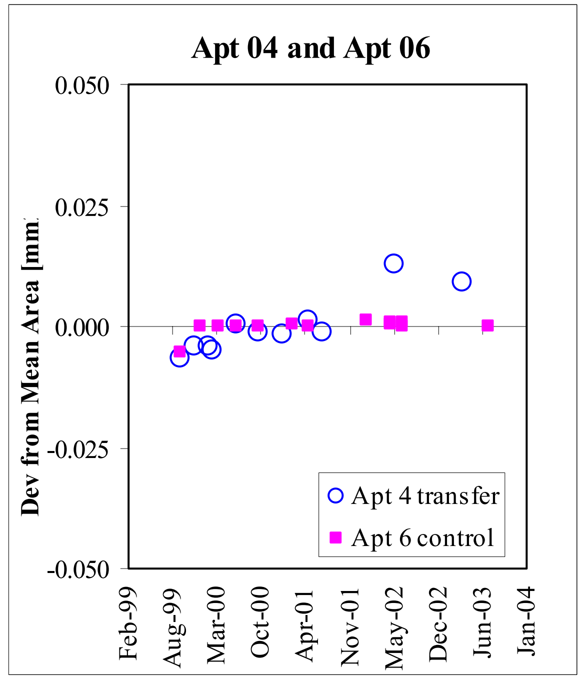

Figure 5.3.11 Dev. from mean of Apt 07/08 (mm^2)

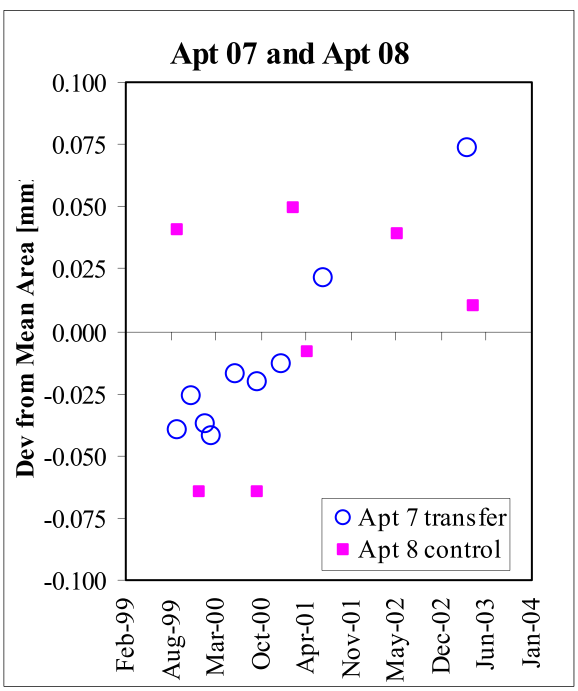

Figure 5.3.12 Dev. from mean of Apt 11/12 (mm^2)

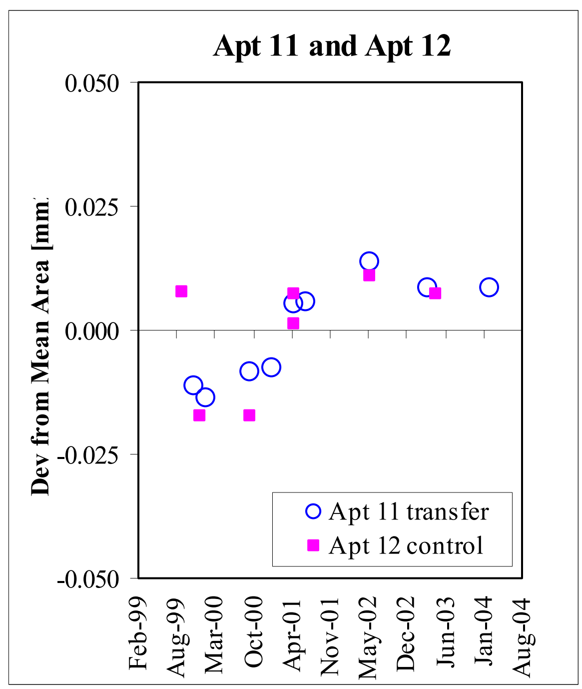

Figure 5.3.13 Dev. from mean of Apt 13/14 (mm^2)

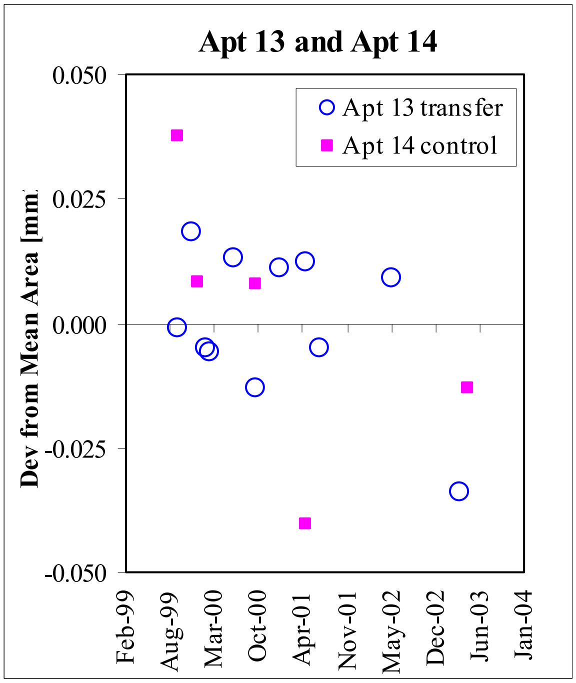

Figure 5.3.14 Dev. from mean of Apt 16/17 (mm^2)

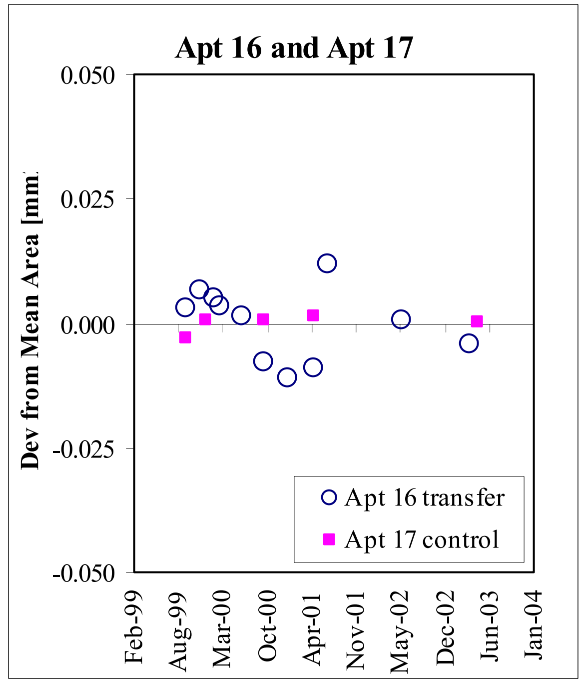

Figure 5.3.15 Dev. from mean of Apt 19/20 (mm^2)

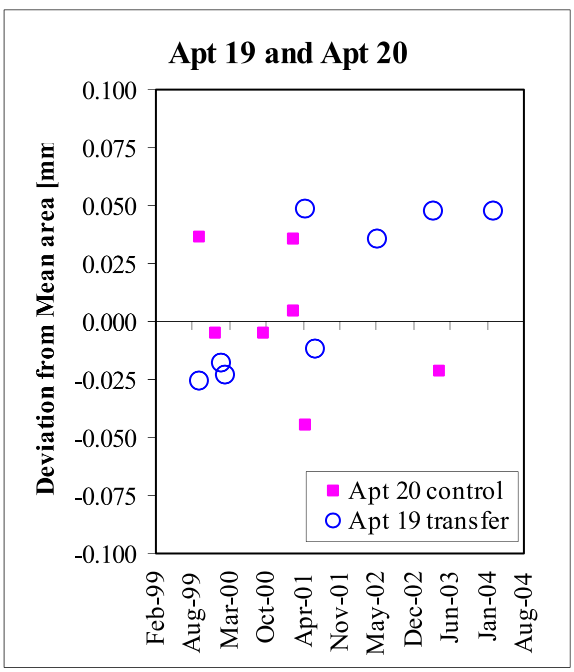

Figure 5.3.16 Dev. from mean of Apt P21/P23 (mm^2)

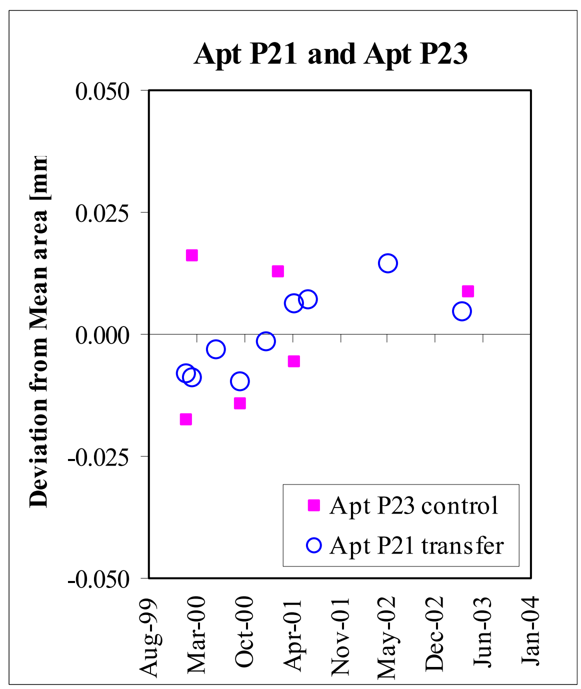

5.4. NIST measurements as participant laboratory

The measurement values for NIST (non-contact method) as a participant for each aperture *j*, is the overall mean $\overline{A}_{\mathrm{NIST},j}$ of pilot lab measurements taken over the course of the comparison. For example, the aperture area for Apt 01 is the overall mean of 11 sets of measurements of Apt 01.

The Type A uncertainty used for the NIST area measurement is the pooled standard deviation of the pilot lab measurement sets. This is the deviation within a given set of measurements and reflects short-term reproducibility. Since there are several sets of pilot lab data, the pooled standard deviation is used.

The pooled standard deviation s_p is computed according to the equation

$$s_p = u(\overline{A}_{\mathrm{NIST},j,h}) = \left[\frac{1}{k-l} \sum_h \left(A_{\mathrm{NIST},j} - \overline{A}_{\mathrm{NIST},j,h} \right)^2 \right]^{1/2} \tag{5.3}$$

where *k* is the total number of measurements for aperture *j*, and *l* is the number of pilot data sets of measurements.

Table 5.4 presents the overall mean area for aperture *j* in the second column, the Type A uncertainties as determined from (5.3), the Type B uncertainties, and the combined uncertainties, expressed in mm^2 and as relative uncertainty, for each of the transfer apertures measured with non-contact method.

Table 5.4. Mean NIST measurements of transfer apertures and uncertainties

Aperture	$\bar{A}_{\mathrm{NIST}\,j}$	Type A [mm^2]	Type B [mm^2]	$u(\bar{A}_{\mathrm{NIST},j})$ [mm^2]	$u(\bar{A}_{\mathrm{NIST},j})/\bar{A}_{\mathrm{NIST},j}$
Apt 01	550.7717	0.0046	0.0128	0.0136	0.0025%
Apt 04	34.0291	0.0012	0.0009	0.0015	0.0045%
Apt 07	505.0708	0.0176	0.0117	0.0212	0.0042%
Apt 10	23.2793	0.0004	0.0006	0.0007	0.0033%
Apt 11	23.2934	0.0030	0.0005	0.0031	0.0132%
Apt 13	525.6332	0.0090	0.0141	0.0167	0.0032%
Apt 16	21.2789	0.0004	0.0005	0.0006	0.0030%
Apt 19	518.2530	0.0203	0.0139	0.0246	0.0048%
Apt P21	314.1102	0.0152	0.0073	0.0168	0.0054%

6. Computation of a reference value

Analysis of comparison data sets usually entails the calculation of a reference value, determining its uncertainty and evaluating the degree of equivalence between participant laboratories. For this supplementary comparison, this reference value is calculated for data presentation purposes only and is not intended to be a statement about the expected value of the aperture's area. The reference value consists of the average of the aperture area and average of laboratory and transfer artifact effects.

For this comparison, we use ratios of laboratory *i* area measurements to those of NIST at each cycle (e.g., cycle 1: NIST–Lab1–NIST, cycle 2: NIST–Lab2–NIST,…) in an attempt to take into account artifact effects in each cycle (except aperture #11 and #16). We calculate the mean of the ratios, which is then the Reference Value (RV). Lab differences from the RV are computed. The details of the computation are given below. We used a simple arithmetic mean of the ratios of all participating NMIs, with agreement from all the participants, rather than weighted mean with cut-off, which is the default method agreed by CCPR. We chose this simplified method because the variations in results for many of the apertures appeared much larger than the uncertainties reported by each NMI, and the decision was made that uncertainty values reported by NMIs were not credible enough to be used for weighted mean. In addition, this is a supplementary comparison, where calculation of degree of equivalence is not required.

Steps in computation of a Reference Value for Aperture *j*

1. Take the ratio of the mean of lab *i* area measurements to the mean of the NIST (pilot) lab area measurements for aperture *j* at each participating laboratory in the intercomparison:

$$r_{i,j} = \frac{\overline{A}_{i,j}}{\overline{A}_{\mathrm{NIST},j,i}} \qquad (6.1)$$

$\overline{A}_{i,j}$ is the mean of lab *i* area measurements for aperture *j*

$\overline{A}_{\mathrm{NIST},j,i}$ is the mean of two pilot data sets $\overline{A}_{\mathrm{NIST},j,h}$ (see 5.2) taken just before and just after lab *i*'s measurements for aperture *j*. The reason for using the two NIST measurements bracketing lab *i* is to remove possible change of the aperture during the course of the comparison (artifact effect).

For aperture Apt 11 and Apt 16, the overall NIST mean was used for the ratios.

$$r_{i,j} = \frac{\overline{A}_{i,j}}{\overline{A}_{\mathrm{NIST},j}}$$

2. Uncertainty of the ratio $u(r_{i,j})$

$$u(r_{i,j}) = \left[u_{rel}^2(\overline{A}_{i,j}) + u_{rel}^2(\overline{A}_{\mathrm{NIST},j}) + u_{rel}^2(stability)\right]^{1/2} \qquad (6.2.1)$$

$u_{rel}(\overline{A}_{i,j})$ is the relative combined standard uncertainty of lab *i* area measurement (the mean of uncertainties reported by lab *i*) for aperture *j, i.e., of* $\overline{A}_{i,j}$

$u_{rel}(\overline{A}_{\mathrm{NIST},j})$ is the combined standard uncertainty of the NIST measurements for aperture *j* shown on the fifth column of Table 5.4.

$u_{rel}(stability, j)$ for all apertures except Apt 11 and Apt 16, is the relative combined uncertainty due to changes in the transfer aperture, computed by assuming a rectangular probability distribution.

$$u_{\text{stability},j} = \frac{\left|A_{\text{NIST},j,i}(pre) - A_{NIST,j,i}(post)\right|}{\overline{A}_{\text{NIST},j,i} \cdot 2\sqrt{3}} \tag{6.2.2}$$

$u_{rel}(stability, j)$ for apertures Apt 11 and Apt 16 is the standard deviation of all NIST pilot measurements of aperture *j*.

3. Compute arithmetic mean of the ratios: this is the Reference Value for aperture *j*

$$\bar{r}_j = \frac{\sum_i r_{i,j}}{n_j} \tag{6.3}$$

n_j is the number of labs measuring aperture *j* including NIST.

4. Compute uncertainty, $u(\bar{r}_j)$, of the Reference Value using the propagated uncertainty of the arithmetic mean of the ratios

$$u(\bar{r}_j) = \frac{1}{n_j}\left[\sum_{i=1}^{n_j} u^2(r_{i,j})\right]^{1/2} \tag{6.4}$$

The standard deviation of the mean of all laboratory results for each aperture was also calculated for additional information. This would provide an estimate of uncertainty based on observed spread of the results and not based on reported uncertainties.

5. Compute for each lab *i* the difference from the mean ratio for aperture *j*

$$\Delta_{i,j} = \frac{\left(r_{i,j} - \bar{r}_j\right)}{\bar{r}_j} \tag{6.5}$$

6. Compute the uncertainty of the lab difference from the mean ratio

$$u(\Delta_{i,j}) = \left[\left(1 - \left(\frac{2}{n_j}\right)\right)u^2(r_{i,j}) + u^2\left(\bar{r}_j\right)\right]^{1/2} \tag{6.6}$$

The factor (1-(2/n_j)) corrects for the correlation between $r_{i,j}$ and the Reference Value in the difference of (6.5).

7. Results of the Comparison

7.1. Summarized results of the comparison classified by aperture

The following tables summarize the results of the comparison using the computational steps outlined in the previous section. The first column lists the participant lab, the second presents the mean NIST pilot measurements bracketing lab *i*, the third column contains the mean laboratory *i* measurement results and the fourth column shows the ratio. The succeeding columns show their respective uncertainties. The last row contains the Reference Value for aperture *j* (RV) and its uncertainty, calculated according to (6.4).

Table 7.1.1 Results of the comparison for Apt 01

Lab	$\overline{A}_{\mathrm{NIST}j,i}$	$\overline{A}_{i,j}$	$r_{i,j}$	$u_{rel}(\overline{A}_{\mathrm{NIST},j})$	$u_{rel}(\overline{A}_{i,j})$	$u_{\mathrm{stability},j}$	$u(r_{i,j})$
PTB	550.7551	550.7791	1.000044	0.0025%	0.0023%	0.0005%	0.0034%
NPL	550.7562	550.5900	0.999698	0.0025%	0.0025%	0.0004%	0.0036%
LNE_INM	550.7705	550.8918	1.000220	0.0025%	0.0129%	0.0019%	0.0133%
VNIIOFI	550.7537	550.6220	0.999761	0.0025%	0.0009%	0.0037%	0.0045%
OMH	550.7792	550.6747	0.999810	0.0025%	0.0120%	0.0003%	0.0123%
NIST	550.7717	550.7717	1.000000	0.0025%	0.0025%	0.0000%	0.0035%
RV			**0.999922**				**0.0033%**

Table 7.1.2 Results of the comparison for Apt 04

Lab	$\overline{A}_{\mathrm{NIST}j,i}$	$\overline{A}_{i,j}$	$r_{i,j}$	$u_{rel}(\overline{A}_{\mathrm{NIST},j})$	$u_{rel}(\overline{A}_{i,j})$	$u_{\mathrm{stability},j}$	$u(r_{i,j})$
PTB	34.0237	34.0262	1.000073	0.0045%	0.0091%	0.0018%	0.0103%
NPL	34.0246	34.0189	0.999833	0.0045%	0.0050%	0.0004%	0.0067%
LNE-INM	34.0269	34.0340	1.000210	0.0045%	0.0159%	0.0043%	0.0170%
VNIIOFI	34.0286	33.9905	0.998880	0.0045%	0.0065%	0.0014%	0.0080%
MIKES	34.0276	34.0240	0.999894	0.0045%	0.0426%	0.0003%	0.0429%
BIPM	34.0288	34.0260	0.999918	0.0045%	0.0046%	0.0024%	0.0068%
OMH	34.0331	34.0046	0.999163	0.0045%	0.0526%	0.0088%	0.0536%
NIST	34.0291	34.0291	1.000000	0.0045%	0.0045%	0.0000%	0.0063%
RV			**0.999746**				**0.0091%**

Table 7.1.3 Results of the comparison for Apt 07

Lab	$\overline{A}_{\mathrm{NIST}j,i}$	$\overline{A}_{i,j}$	$r_{i,j}$	$u_{rel}(\overline{A}_{\mathrm{NIST},j})$	$u_{rel}(\overline{A}_{i,j})$	$u_{\mathrm{stability},j}$	$u(r_{i,j})$
PTB	505.0302	505.1476	1.000232	0.0042%	0.0101%	0.0001%	0.0109%
NPL	505.0290	505.1140	1.000168	0.0042%	0.0026%	0.0003%	0.0049%
LNE-INM	505.0388	505.2272	1.000373	0.0042%	0.0081%	0.0014%	0.0092%
VNIIOFI	505.0497	504.8890	0.999682	0.0042%	0.0012%	0.0002%	0.0044%
OMH	505.1159	505.0377	0.999845	0.0042%	0.0174%	0.0030%	0.0181%
NIST	505.0708	505.0708	1.000000	0.0042%	0.0042%	0.0000%	0.0059%
PTB c	505.0302	505.1755	1.000288	0.0042%	0.0016%	0.0001%	0.0045%
NPL c	505.0290	505.1827	1.000304	0.0042%	0.0010%	0.0003%	0.0043%
OMH c	505.1159	505.1665	1.000100	0.0042%	0.0075%	0.0030%	0.0091%
NIST c	505.1421	505.1902	1.000095	0.0042%	0.0005%	0.0000%	0.0042%
NRC c	505.1175	505.1750	1.000114	0.0042%	0.0016%	0.0028%	0.0053%
RV			**1.000109**				**0.0025%**

Table 7.1.4 Results of the comparison for Apt 10/11

Lab	$\overline{A}_{\mathrm{NIST}j,i}$	$\overline{A}_{i,j}$	$r_{i,j}$	$u_{rel}(\overline{A}_{\mathrm{NIST},j})$	$u_{rel}(\overline{A}_{i,j})$	$u_{\mathrm{stability},j}$	$u(r_{i,j})$
PTB 10	23.2793	23.2684	0.999530	0.0029%	0.0468%	0.0014%	0.0470%
NPL	23.2934	23.3131	1.000844	0.0029%	0.0069%	0.0148%	0.0165%
LNE-INM	23.2934	23.3061	1.000543	0.0029%	0.0236%	0.0148%	0.0280%
VNIIOFI	23.2934	23.2870	0.999723	0.0029%	0.0172%	0.0148%	0.0228%
MIKES	23.2934	23.3020	1.000367	0.0029%	0.0451%	0.0148%	0.0475%
BIPM	23.2934	23.3094	1.000685	0.0029%	0.0069%	0.0148%	0.0165%
OMH	23.2934	23.2657	0.998809	0.0029%	0.0688%	0.0148%	0.0704%
NIST	23.2934	23.2934	1.000000	0.0132%	0.0132%	0.0148%	0.0238%
PTB c	23.2793	23.2591	0.999131	0.0029%	0.0365%	0.0014%	0.0367%
NPL c	23.2934	23.3115	1.000775	0.0029%	0.0041%	0.0148%	0.0156%
NIST c	23.2934	23.3141	1.000887	0.0029%	0.0021%	0.0148%	0.0152%
NRC c	23.2934	23.3003	1.000294	0.0029%	0.0092%	0.0148%	0.0176%
RV			1.000132				**0.0098%**

Table 7.1.5 Results of the comparison for Apt 13

Lab	$\overline{A}_{\mathrm{NIST}j,i}$	$\overline{A}_{i,j}$	$r_{i,j}$	$u_{rel}(\overline{A}_{\mathrm{NIST},j})$	$u_{rel}(\overline{A}_{i,j})$	$u_{\mathrm{stability},j}$	$u(r_{i,j})$
PTB*	525.6302	526.2817	1.001239	0.0029%	0.0235%	0.0002%	0.0236%
NPL	525.6279	525.5218	0.999798	0.0029%	0.0025%	0.0000%	0.0038%
LNE-INM	525.6369	525.6808	1.000083	0.0029%	0.0093%	0.0010%	0.0098%
VNIIOFI	525.6333	525.4000	0.999556	0.0029%	0.0021%	0.0014%	0.0038%
OMH	525.6133	525.5362	0.999853	0.0029%	0.0118%	0.0016%	0.0122%
NIST	525.6332	525.6332	1.000000	0.0029%	0.0029%	0.0000%	0.0040%
RV			**0.999858**				**0.0034%**

* The result of PTB for this aperture was excluded in the calculation of RV.

Table 7.1.6 Results of the comparison for Apt 16

Lab	$\overline{A}_{\text{NIST}j,i}$	$\overline{A}_{i,j}$	$r_{i,j}$	$u_{rel}(\overline{A}_{\text{NIST},j})$	$u_{rel}(\overline{A}_{i,j})$	$u_{\text{stability},j}$	$u(r_{i,j})$
PTB*	21.2789	21.3865	1.005058	0.0030%	0.0902%	0.0103%	0.0909%
NPL	21.2789	21.3082	1.001379	0.0030%	0.0113%	0.0103%	0.0155%
LNE-INM	21.2789	21.2887	1.000461	0.0030%	0.0202%	0.0103%	0.0229%
VNIIOFI	21.2789	21.2624	0.999226	0.0030%	0.0042%	0.0103%	0.0115%
MIKES	21.2789	21.2690	0.999536	0.0030%	0.0447%	0.0103%	0.0459%
BIPM	21.2789	21.2786	0.999987	0.0030%	0.0052%	0.0103%	0.0119%
OMH	21.2789	21.2535	0.998807	0.0030%	0.0513%	0.0103%	0.0524%
NIST	21.2789	21.2789	1.000000	0.0000%	0.0000%	0.0103%	0.0103%
RV			0.999914				**0.0111%**

* The result of PTB for this aperture was excluded in the calculation of RV.

Table 7.1.7 Results of the comparison for Apt 19

Lab	$\overline{A}_{\text{NIST}j,i}$	$\overline{A}_{i,j}$	$r_{i,j}$	$u_{rel}(\overline{A}_{\text{NIST},j})$	$u_{rel}(\overline{A}_{i,j})$	$u_{\text{stability},j}$	$u(r_{i,j})$
LNE-INM	518.3143	518.3052	0.999982	0.0048%	0.0081%	0.0094%	0.0133%
VNIIOFI	518.2594	517.8230	0.999158	0.0048%	0.0015%	0.0155%	0.0163%
OMH	518.2704	518.0051	0.999488	0.0048%	0.0212%	0.0033%	0.0219%
NIST	518.2530	518.2530	1.000000	0.0048%	0.0048%	0.0000%	0.0067%
PTB c	518.2310	518.2533	1.000043	0.0048%	0.0058%	0.0004%	0.0076%
OMH c	518.2704	518.2138	0.999891	0.0048%	0.0070%	0.0033%	0.0091%
NIST c	518.3001	518.2163	0.999838	0.0048%	0.0005%	0.0000%	0.0048%
NRC c	518.3004	518.2088	0.999823	0.0048%	0.0016%	0.0000%	0.0050%
RV			**0.999778**				**0.0043%**

Table 7.1.8 Results of the comparison for Apt P21

Lab	$\overline{A}_{\text{NIST}j,i}$	$\overline{A}_{i,j}$	$r_{i,j}$	$u_{rel}(\overline{A}_{\text{NIST},j})$	$u_{rel}(\overline{A}_{i,j})$	$u_{\text{stability},j}$	$u(r_{i,j})$
PTB	314.1094	314.1847	1.000240	0.0054%	0.0097%	0.0005%	0.0111%
NPL	314.1014	314.1180	1.000053	0.0054%	0.0022%	0.0006%	0.0058%
LNE-INM	314.1038	314.1258	1.000070	0.0054%	0.0064%	0.0007%	0.0084%
VNIIOFI	314.1035	313.9440	0.999492	0.0054%	0.0016%	0.0002%	0.0056%
BIPM	314.1126	314.1170	1.000014	0.0054%	0.0104%	0.0000%	0.0117%
OMH	314.1159	314.0771	0.999877	0.0054%	0.0124%	0.0000%	0.0136%
NIST	314.1102	314.1102	1.000000	0.0054%	0.0054%	0.0000%	0.0076%
RV			**0.999964**				**0.0032%**

7.2. Laboratory difference from reference values classified by aperture

The following tables present each participant laboratory's measurement difference from the reference value for aperture j computed according to (6.5), and the computed standard uncertainty of the laboratory difference according to (6.6). The tabulated results are presented in the accompanying charts.

Table 7.2.1 Lab difference from reference value for Apt 01

Lab	Δij(Lab-RV)	u(Δij)
PTB	0.0121%	0.0043%
NPL	-0.0224%	0.0044%
LNE-INM	0.0298%	0.0113%
VNIIOFI	-0.0161%	0.0049%
OMH	-0.0112%	0.0106%
NIST	0.0078%	0.0043%
RV	0.0000%	0.0033%

Table 7.2.2 Lab difference from reference value for Apt 04

Lab	Δij(Lab-RV)	u(Δij)
PTB	0.0326%	0.0127%
NPL	0.0087%	0.0107%
LNE-INM	0.0464%	0.0173%
VNIIOFI	-0.0866%	0.0113%
MIKES	0.0148%	0.0382%
BIPM	0.0171%	0.0108%
OMH	-0.0584%	0.0473%
NIST	0.0254%	0.0105%
RV	0.0000%	0.0091%

Table 7.2.3 Lab difference from reference value for Apt 07

Lab	Δij(Lab-RV)	u(Δij)
PTB	0.0123%	0.0102%
NPL	0.0059%	0.0051%
LNE-INM	0.0264%	0.0087%
VNIIOFI	-0.0427%	0.0047%
OMH	-0.0264%	0.0166%
NIST	-0.0109%	0.0059%
PTBc	0.0178%	0.0048%
NPLc	0.0195%	0.0046%
OMHc	-0.0009%	0.0086%
NISTc	-0.0014%	0.0046%
NRCc	0.0005%	0.0054%
RV	0.0000%	0.0025%

Table 7.2.4 Lab difference from reference value for Apt 11

Lab	Δij(Lab-RV)	u(Δij)
PTB 10	-0.0602%	0.0440%
NPL	0.0711%	0.0180%
LNE-INM	0.0411%	0.0274%
VNIIOFI	-0.0409%	0.0230%
MIKES	0.0235%	0.0445%
BIPM	0.0552%	0.0180%
OMH	-0.1323%	0.0650%
NIST	-0.0132%	0.0239%
PTB c	-0.1001%	0.0349%
NPL c	0.0643%	0.0173%
NIST c	0.0754%	0.0170%
NRC c	0.0162%	0.0189%
RV	0.0000%	0.0098%

Table 7.2.5 Lab difference from reference value for Apt 13

Lab	Δij(Lab-RV)	u(Δij)
PTB*	0.1381%	0.0196%
NPL	-0.0060%	0.0046%
LNE-INM	0.0225%	0.0087%
VNIIOFI	-0.0302%	0.0046%
OMH	-0.0005%	0.0106%
NIST	0.0142%	0.0048%
RV	0.0000%	0.0034%

*The RV excludes the PTB value

Table 7.2.6 Lab difference from reference value for Apt 16

Lab	Δij(Lab-RV)	u(Δij)
PTB*	0.5144%	0.0750%
NPL	0.1465%	0.0168%
LNE-INM	0.0548%	0.0217%
VNIIOFI	-0.0688%	0.0145%
MIKES	-0.0378%	0.0391%
BIPM	0.0073%	0.0147%
OMH	-0.1106%	0.0442%
NIST	0.0086%	0.0139%
RV	0.0000%	0.0111%

*The RV excludes the PTB value

Table 7.2.7 Lab difference from reference value for Apt 19

Lab	Δij(Lab-RV)	u(Δij)
LNE-INM	0.0204%	0.0122%
VNIIOFI	-0.0620%	0.0147%
OMH	-0.0290%	0.0194%
NIST	0.0222%	0.0070%
PTBc	0.0265%	0.0077%
OMHc	0.0113%	0.0088%
NISTc	0.0060%	0.0058%
NRCc	0.0045%	0.0059%
RV	0.0000%	0.0042%

Table 7.2.8 Lab difference from reference value for Apt P21

Lab	Δij(Lab-RV)	u(Δij)
PTB	0.0276%	0.0100%
NPL	0.0089%	0.0061%
LNE-INM	0.0106%	0.0079%
VNIIOFI	-0.0471%	0.0059%
BIPM	0.0050%	0.0106%
OMH	-0.0087%	0.0120%
NIST	0.0036%	0.0073%
RV	0.0000%	0.0036%

The following charts, Figs. 7.2.1 to Fig. 7.2.8 show the percent difference of each lab's measurement of Apt *j* from the reference value. The error bar on the reference value, $u(\bar{r}_j)$, is the uncertainty computed according to (6.4), which is the propagated uncertainty. The error bar on each participant's difference from the reference value, $u(\Delta_{i,j})$, is computed according to (6.6). The dotted lines bracketing the reference value represent the standard deviation of the mean of the relative differences.

The plots of PTB data for apertures 13 and 16 in these figures use the original values reported, but the reference values exclude the PTB data. The results of the comparison using the corrected results of these apertures are shown in Appendix D.

Figure 7.2.1 Lab difference from reference value for Apt 01

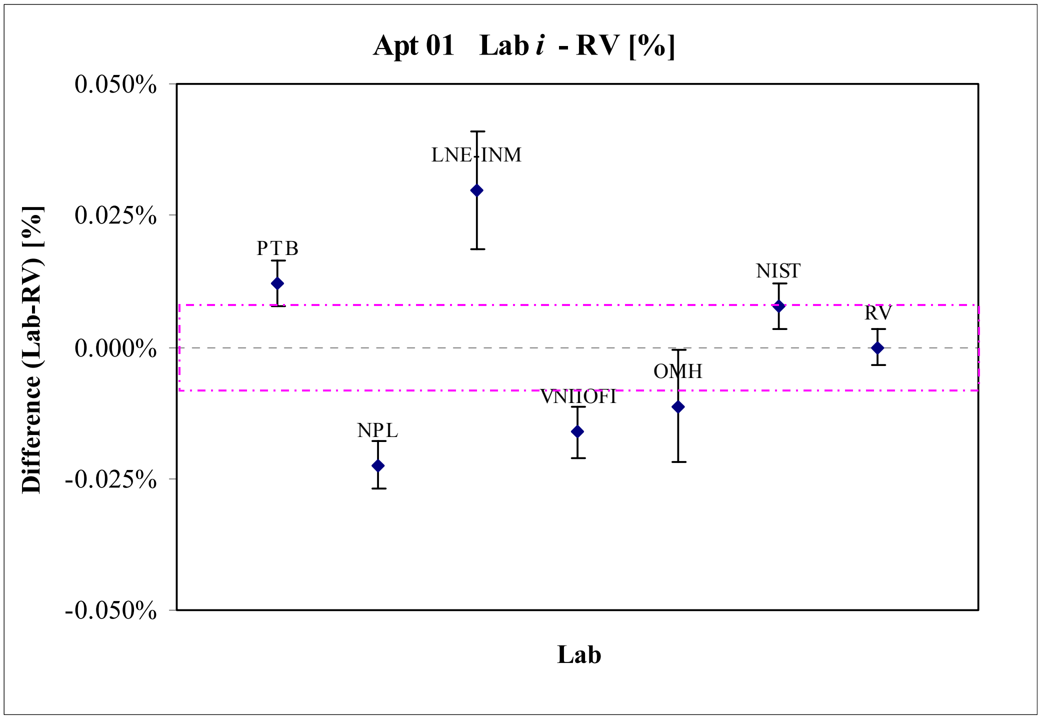

Figure 7.2.2 Lab difference from reference value for Apt 04

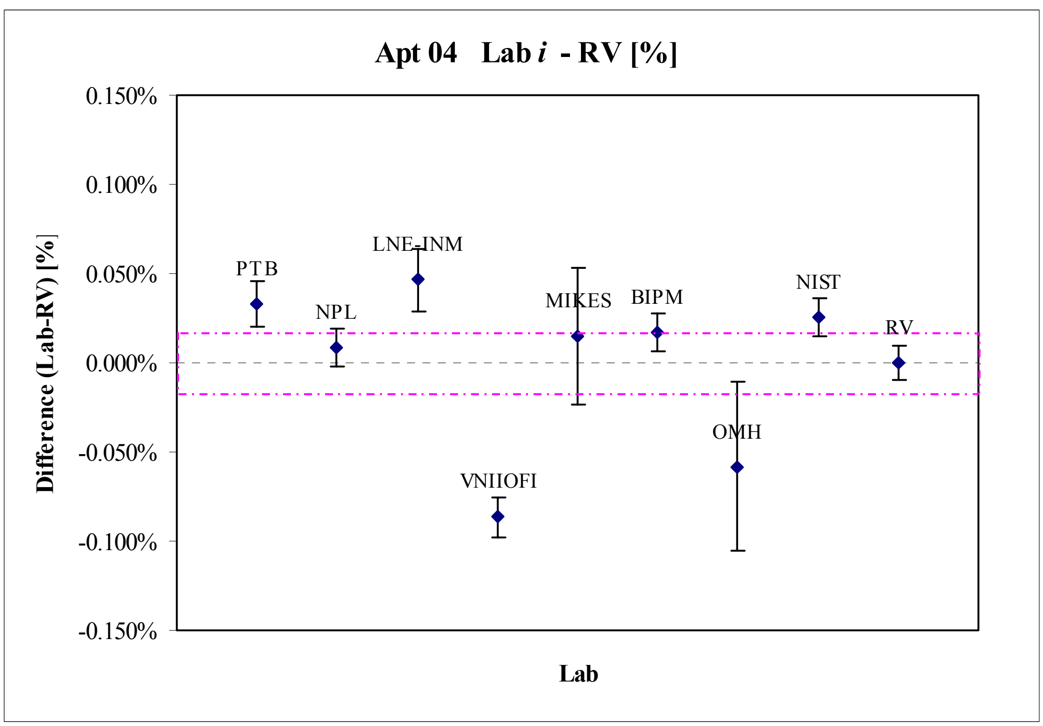

Figure 7.2.3 Lab difference from reference value for Apt 07

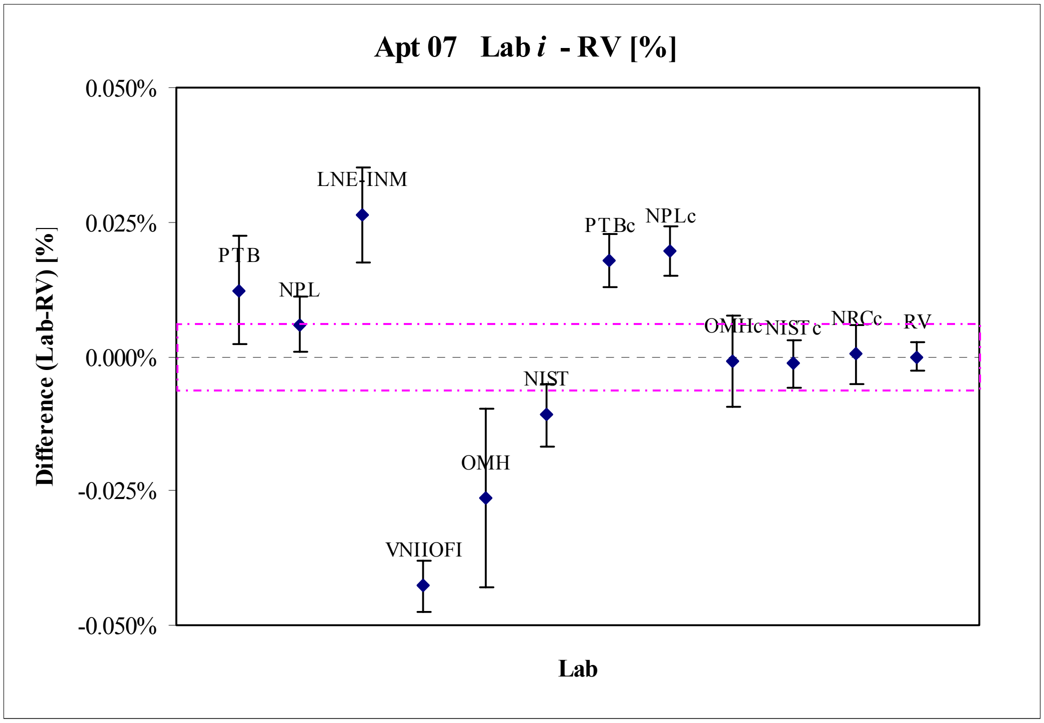

Figure 7.2.4 Lab difference from reference value for Apt 11

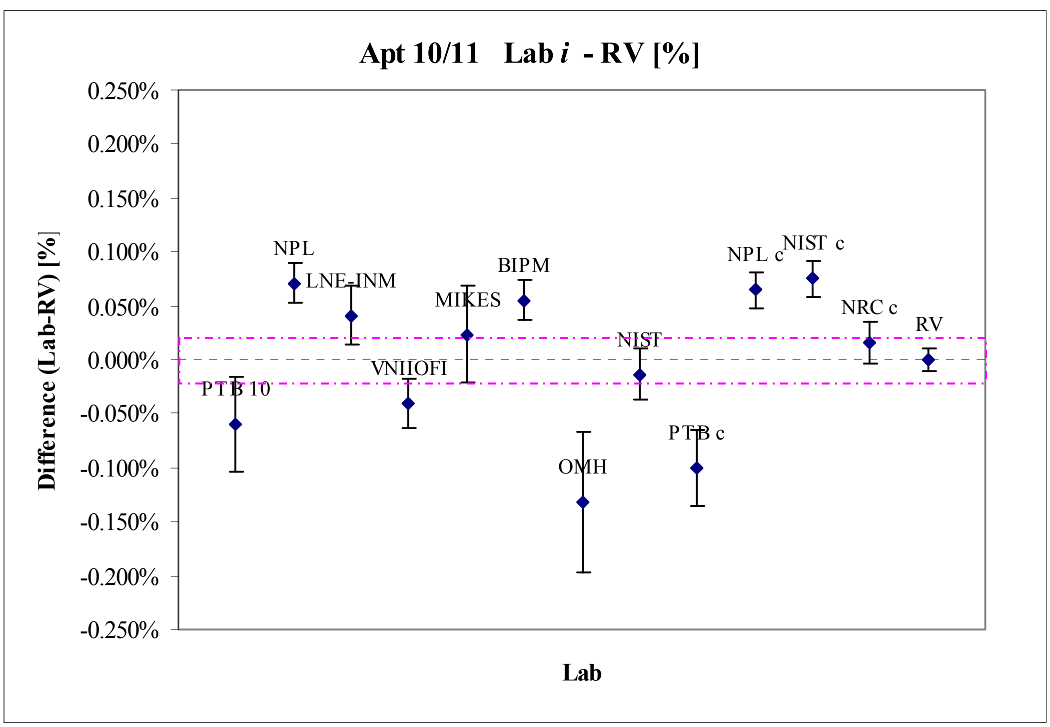

Figure 7.2.5 Lab difference from reference value for Apt 13

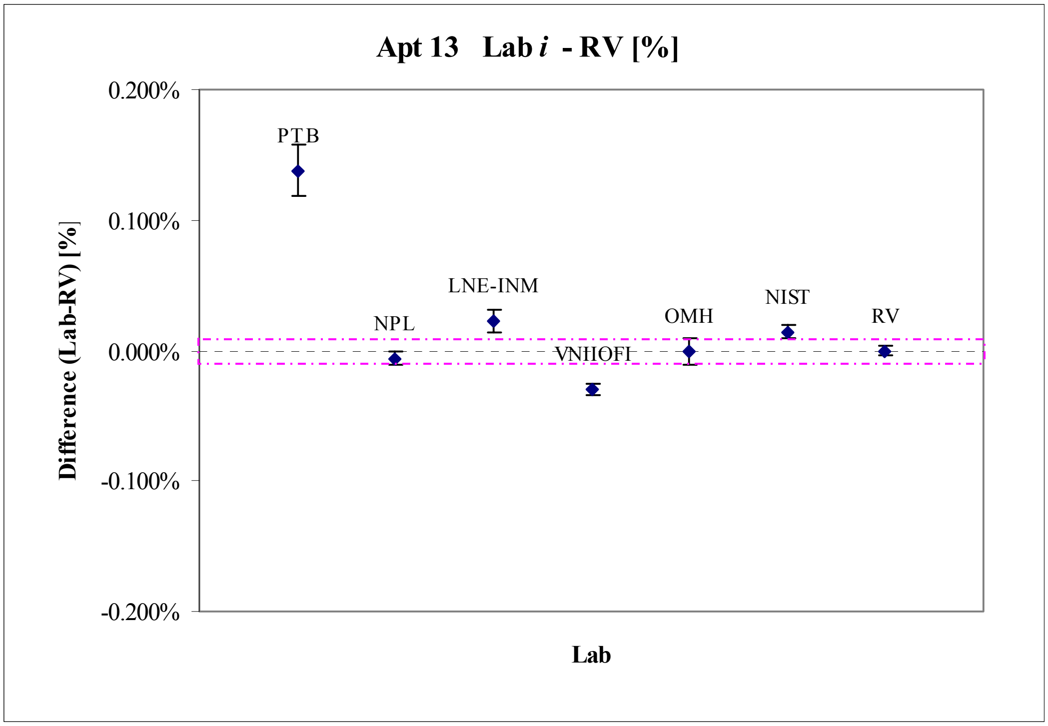

Figure 7.2.6 Lab difference from reference value for Apt 16

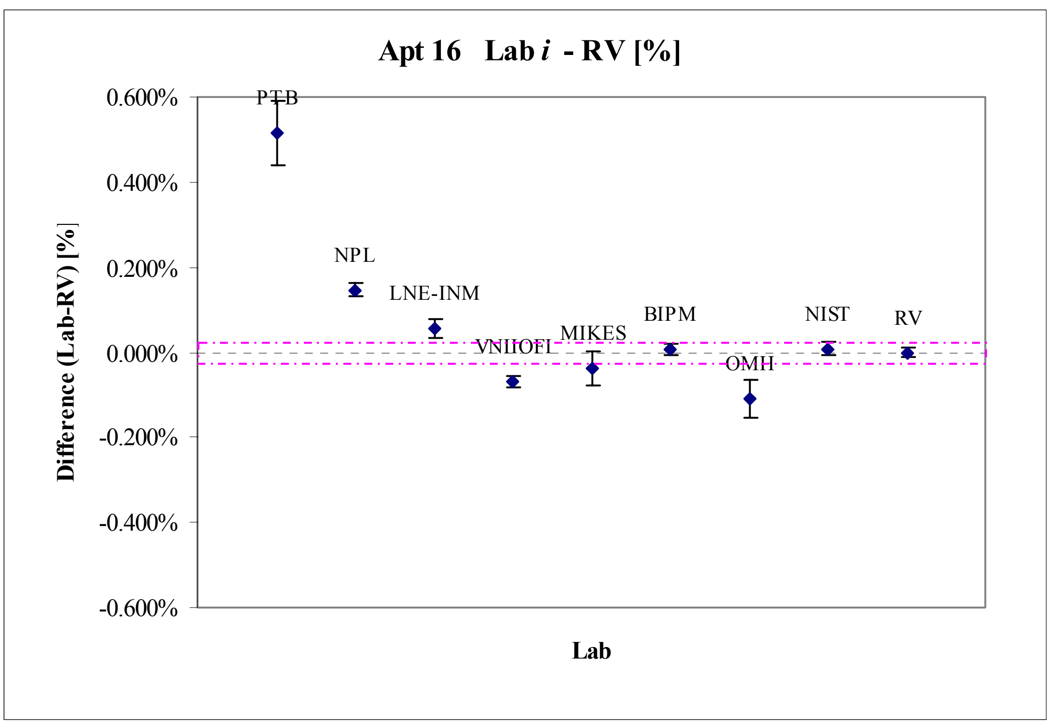

Figure 7.2.7 Lab difference from reference value for Apt 19

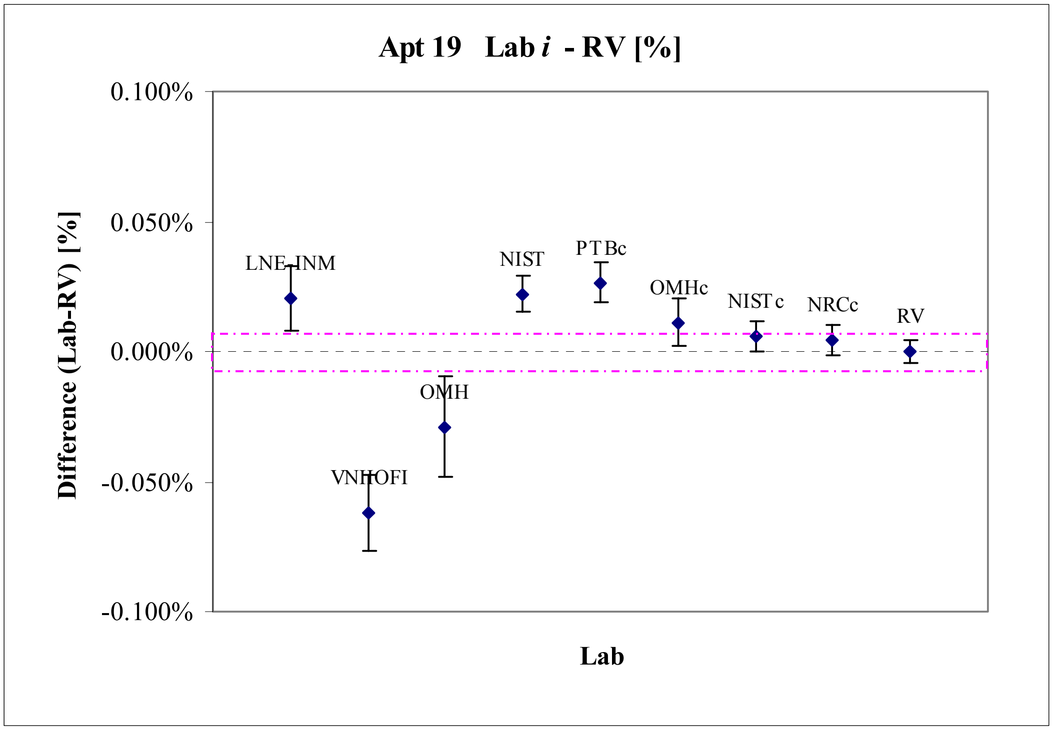

Figure 7.2.8 Lab difference from reference value for Apt 21

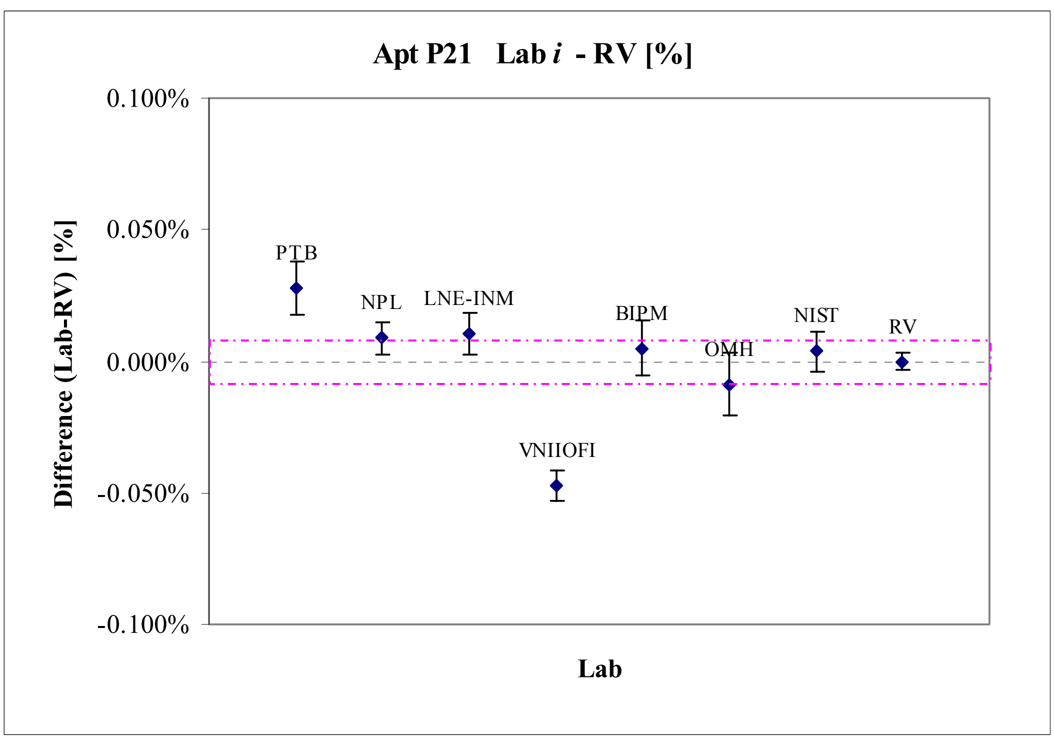

7.3. Laboratory difference from reference value classified by laboratory

The laboratory differences for each participant laboratory's measurement of apertures from the reference values for each aperture are presented in the following charts. Both non-contact and contact measurement results are presented in the same chart for laboratories that used both methods.

Figure 7.3.1 PTB Lab differences from reference values of apertures measured

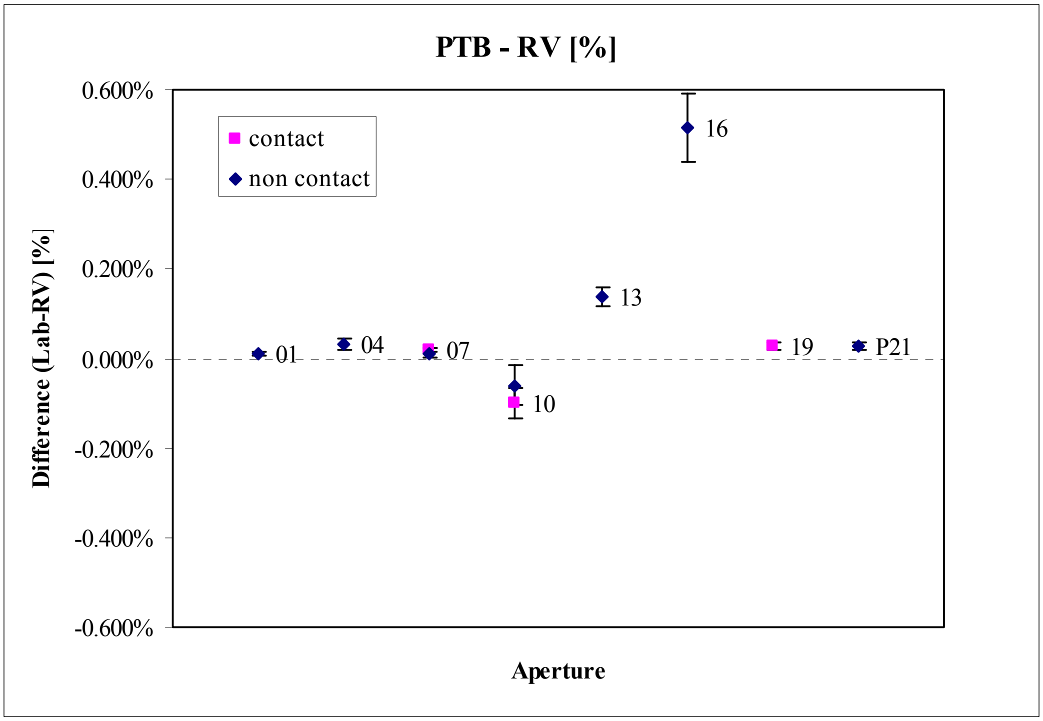

* Figure including corrected results of Apt. 13 and 16 are shown in Appendix D.

Figure 7.3.2 NPL Lab differences from reference values of apertures measured

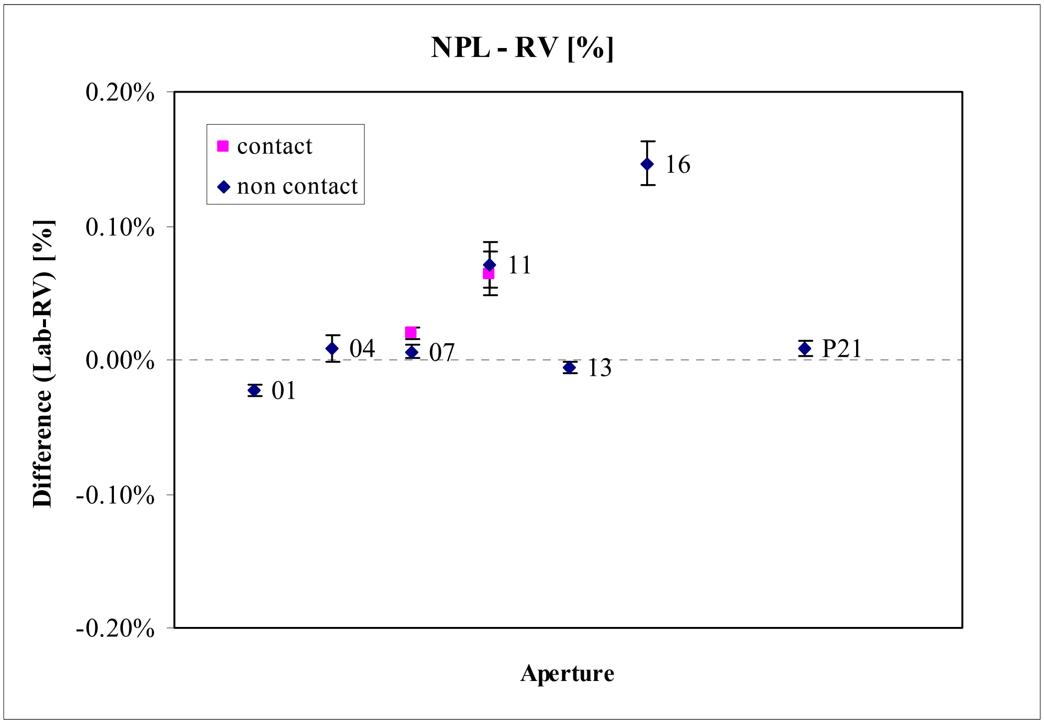

Figure 7.3.3 LNE-INM Lab differences from reference values of apertures measured

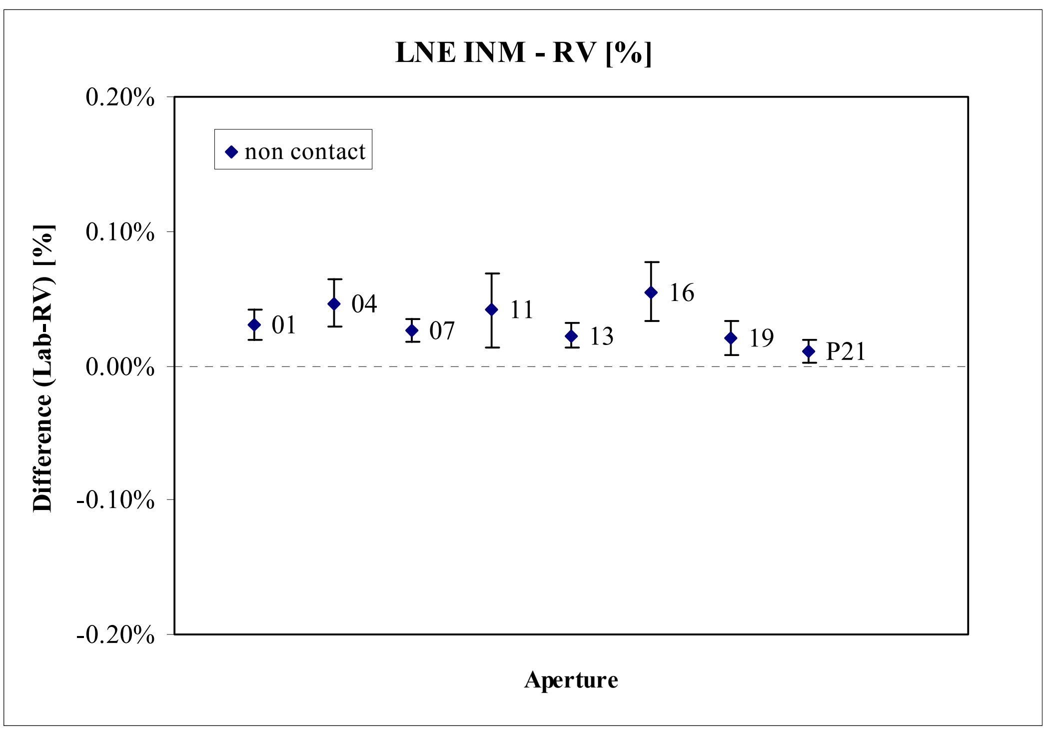

Figure 7.3.4 VNIIOFI Lab differences from reference values of apertures measured

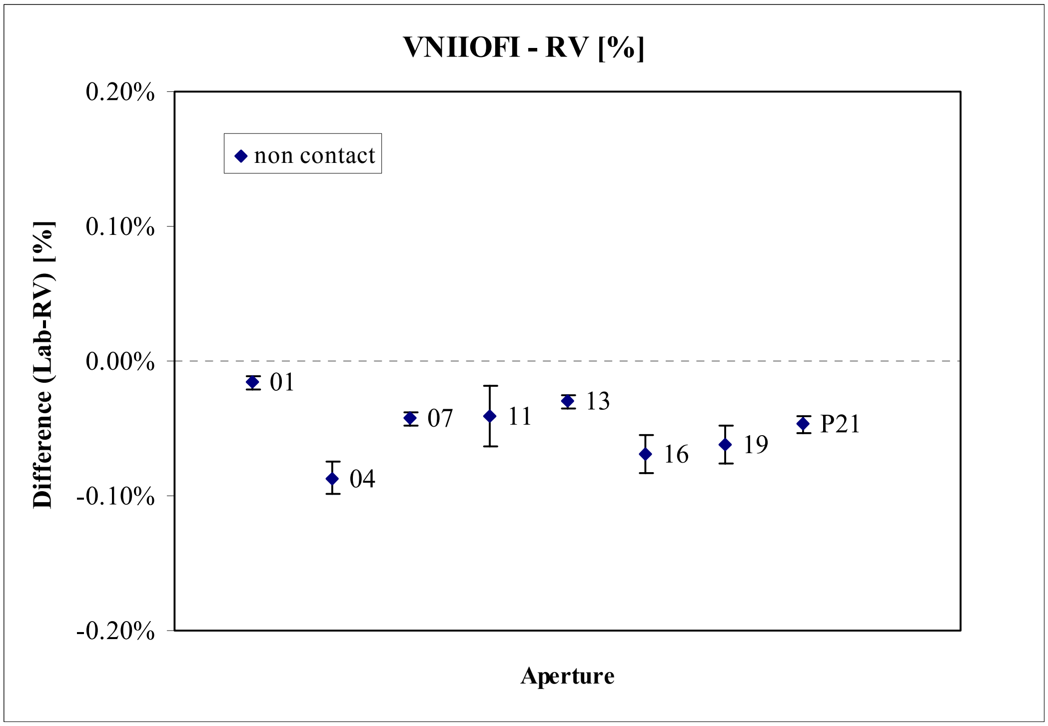

Figure 7.3.5 MIKES Lab differences from reference values of apertures measured

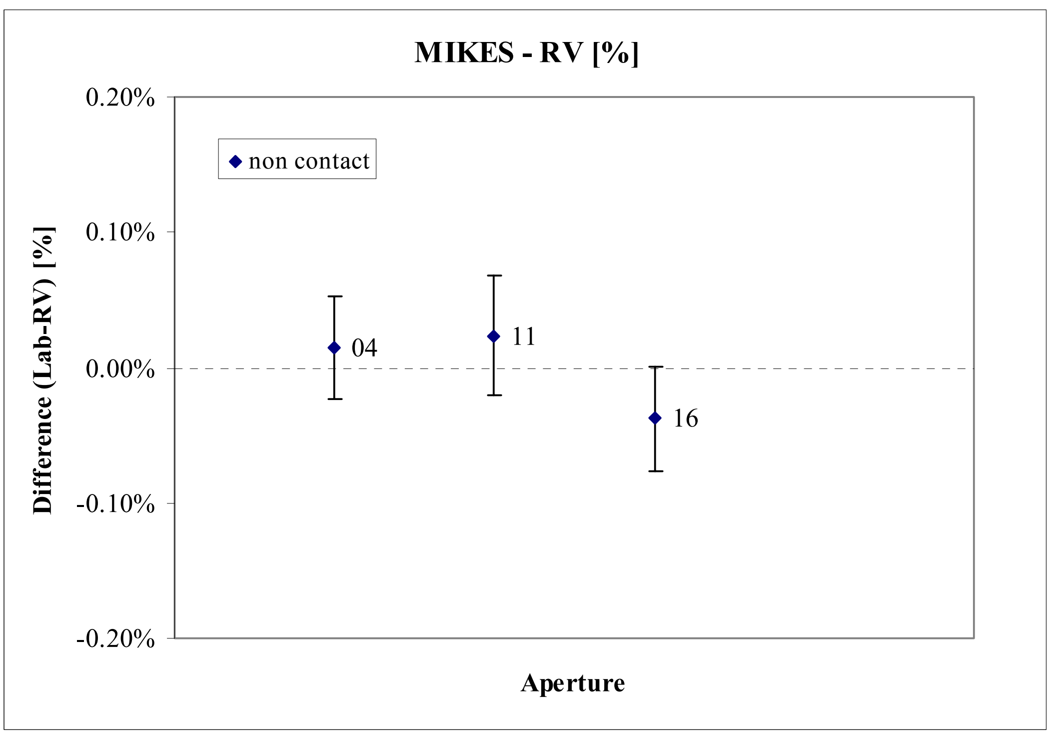

Figure 7.3.6 BIPM Lab differences from reference values of apertures measured

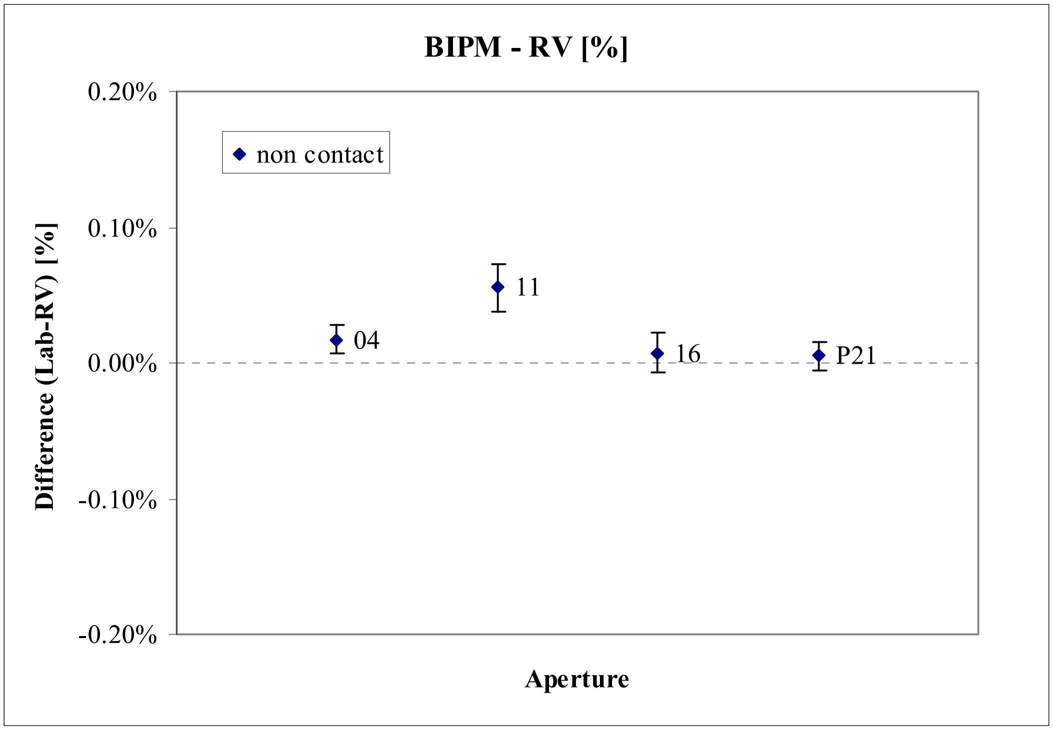

Figure 7.3.7 OMH Lab differences from reference values of apertures measured

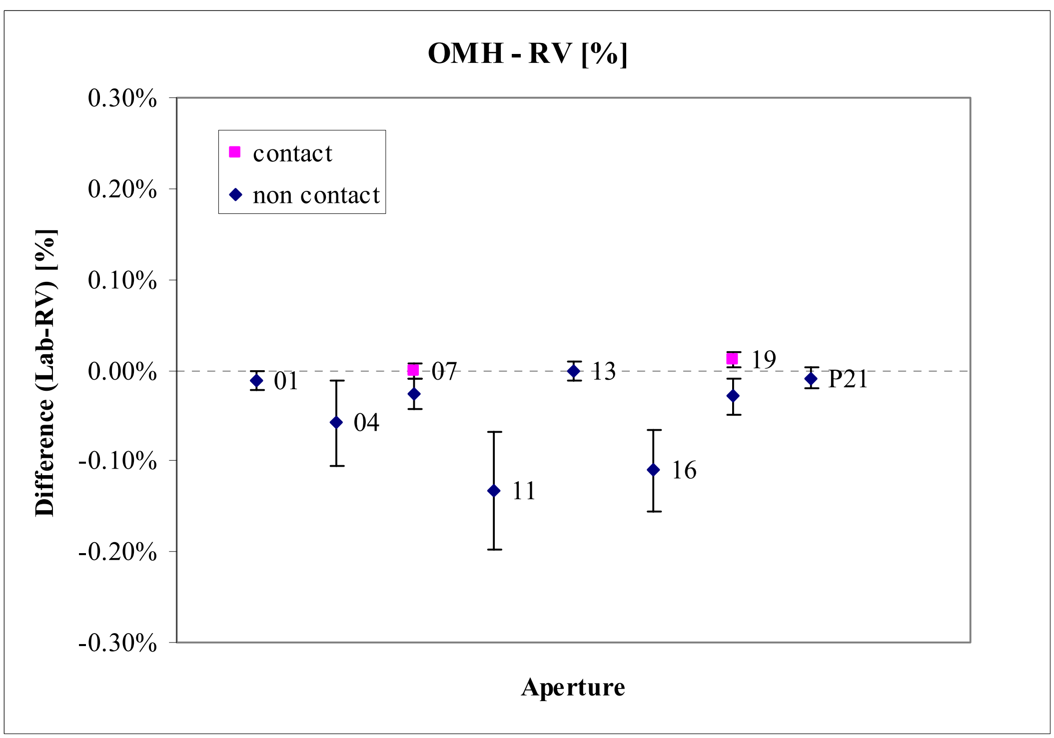

Figure 7.3.8 NRC Lab differences from reference values of apertures measured

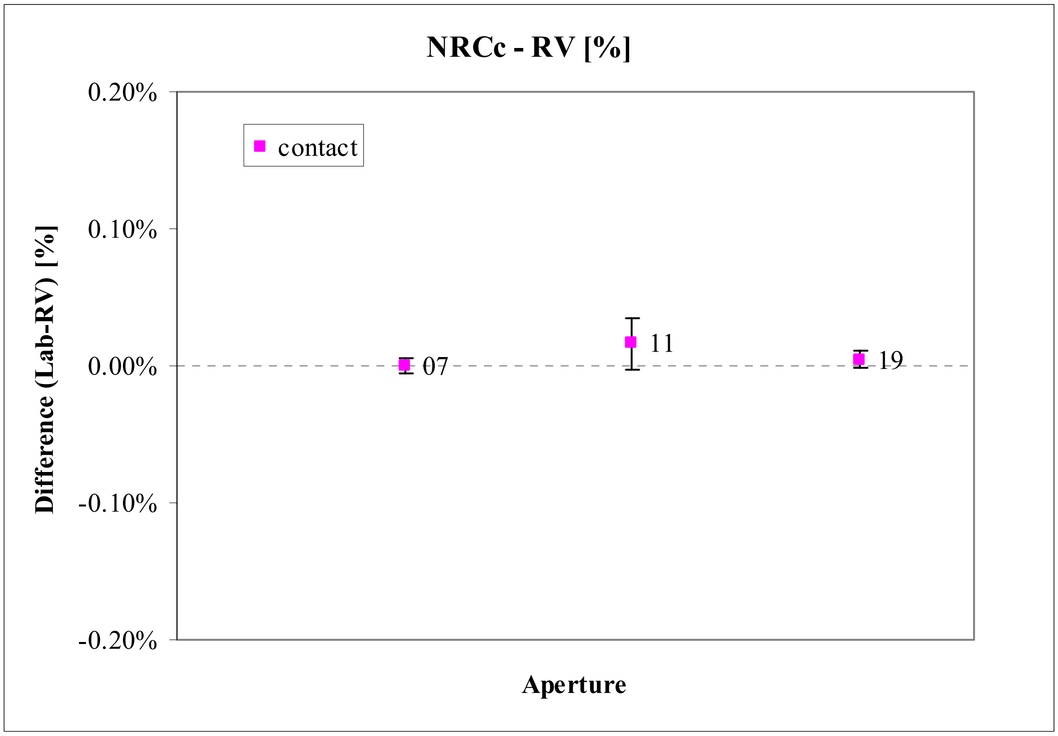

Figure 7.3.9 NIST Lab differences from reference values of apertures measured

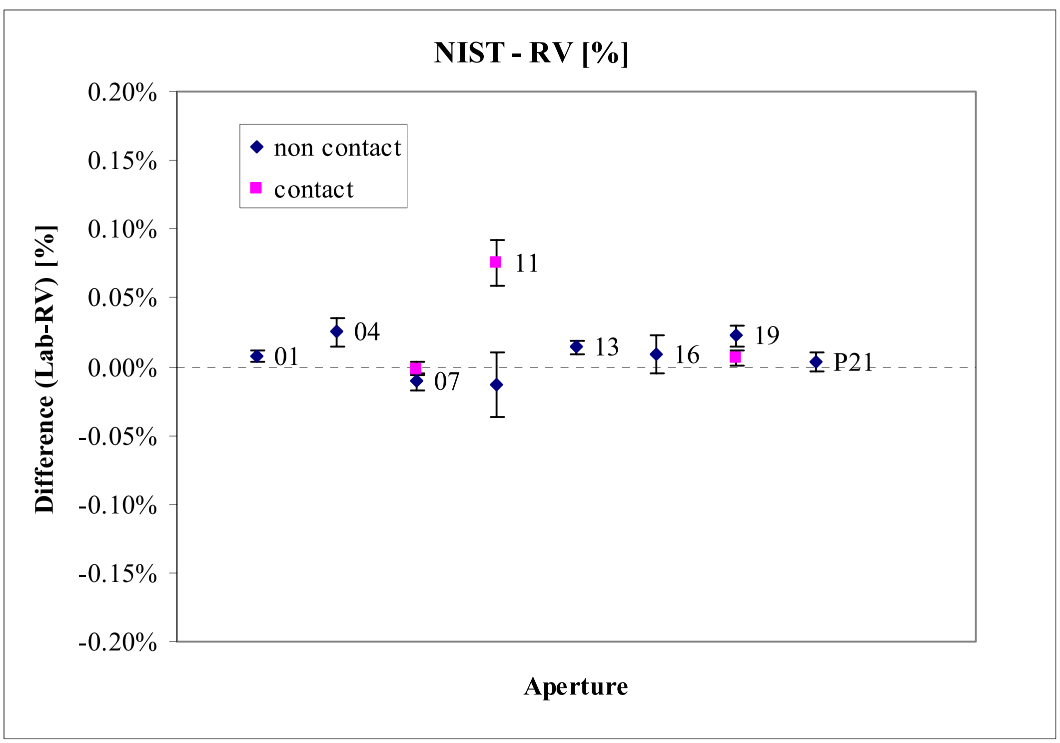

8. Summary and Conclusions

1. A total of eight transfer apertures were circulated in a star pattern among nine different laboratories. Four of the laboratories (PTB,NPL, OMH and NIST) measured the cylindrical apertures using both non-contact and contact methods. One (NRC) measured the cylindrical apertures using contact method only. Two (MIKES, BIPM) of the eight labs using the optical method did so by measuring the radiometric area, compared to using the optical method to measure geometric area.
2. The control apertures measured at NIST did not show appreciable drift. The variances of the transfer apertures were about the same as the control or larger.
3. The measurement results from the contact method are more consistent than the non-contact method, as shown in the charts in Sec 7.2 for Apt 07, 11 and 19. The analysis of variance box plots in Appendix C further illustrate this difference. It should be noted that the contact probe method has been used more extensively in metrology than the optical methods used here, and some laboratories have participated in previous inter-laboratory comparisons.
4. It is apparent from the figures in Section 7 that most of the participant laboratories underestimate their measurement uncertainties.
5. The smaller apertures (6mm) appear to sustain larger relative deviations in area over the course of the comparison in contrast to the larger 25 mm diameter apertures regardless of the material. However, as charts 5.1.9 through 5.1.16 show, the absolute change in area is comparable to those of the larger apertures.
6. Scanning electron micrographs of the edges (Appendix B) show many defects, even for the diamond-turned knife edges. These are scattering centers, and contributions to the measurement uncertainty vary with the technique. This needs to be addressed by each laboratory.
7. Some laboratories showed a consistent bias in the measurements.

9. References

1. Fowler, J., and Litorja, M., " Geometric Area Measurements of Circular Radiometric Apertures at NIST", *Metrologia*, 40, S9-S12, (2002)
2. Bevington, P.R. and Robinson, D.K. "Data Reduction and Error Analysis for the Physical Sciences" 2^{nd} ed. McGrawHill (1992)
3. Ruhkin, A.L. and Vangel, M.G. "Estimation of a Common Mean and Weighted Means Statistics" Jour. of the American Statistical Assn. Vol. 93, 441, 1(1998)

10. Acknowledgements

The authors wish to thank Adriana Hornikova and Stefan Leigh of the Statistical Engineering Division for running calculations using the Maximum Likelihood Estimator for the data from this comparison, which served as a check of our results, and for the analysis of variance charts used in Appendix C. We also wish to thank Dr. Yoshi Ohno and Dr. Gerald Fraser for technical guidance in preparing this document.

A. Appendix A: Uncertainty Tables for Aperture Measurement of CCPR-S2 Participating Laboratories

This appendix includes a brief description of the method employed by each participant in aperture area measurement, as well as relevant references the participant included in their report.

A.1 PTB

Contact: **Dr. Jurgen Hartmann**
Email: **Dr.j.hartmann@ptb.de**

Non-Contact Method

The location of the edge is detected by monitoring the reflected light of a focused laser beam. The laser beam (wavelength 790 nm) is emitted by a diode laser and focused on the aperture surface. A movable lens is used to keep the surface of the aperture in the focus of the laser beam. The reflected radiant power is collected by a photodiode and recorded as a function of the aperture position. A perfect edge is detected when the reflected radiant power reaches half the maximum value. In case of circular apertures the mean of the measured diameters (at least 150 diameters) is used to calculate the aperture area.

References:
J. Fischer, M. Stock: A non-contact measurement of radiometric apertures with an optical microtopography sensor, *Meas. Sci. Technol.* (1992) **3** pp. 693-698
J. Hartmann, J. Fischer, J. Seidel: Improved accuracy in measurement of radiometric apertures with a non-contact technique, *Metrologia* , (2000) **37** pp637-640

Table A1.1 Uncertainty budget of the PTB non contact technique (coverage factor k=1).

	5 mm nominal diameter		25 mm nominal diameter		
Source of uncertainty	Correction of d /µm	u /µm	Correction of d /µm	u /µm	Type
Air temperature		0.001		0.005	B
Atmospheric pressure		0.001		0.005	B
Humidity		0.002		0.010	B
Abbe error, vertical	-0.050	0.010	-0.090	0.050	B
Abbe error, horizontal		0.010		0.010	B
Angle error	0.001	0.001	0.005	0.005	B
Cosine error	0.0003	0.0002	0.0015	0.001	B
Centering error	0.0001	0.0001	0.0001	0.0001	B
Laser wavelength		0.0001		0.0001	B
1 dim approximation	0.050	0.050			B
Partial fitting error*	-0.250	0.030	-0.250	0.030	B
Random uncertainty*		0.080		0.080	B
Fitting error*		0.050		0.050	A
Sum	-0.249	0.112	-0.333	0.112	

* The value for the random uncertainty and the fitting error were averaged, the uncertainties actually used were determined separately for every measurement.

The uncertainties of Table A.1.1 are valid in case of ideal aperture edges. As real apertures do not have infinitely steep edges, a so-called bevel uncertainty has to be added. For the nearly ideal apertures we used the value of 0.3 µm. This value we have found to be sufficient for other higher quality apertures we have frequently used for the thermodynamic temperature measurements. Additional uncertainties and corrections were introduced for the non-contact measurements of other apertures. The additional contributions due to the non-ideal edges have to be added to the original ones inherently connected to our experiment. The final corrections and uncertainties of the measured aperture diameters resulting from these two contributions are included in the results.

Contact Technique

The apertures with non-fragile edges, the non-knife-edged ones, were measured using a contact technique, with the Abbe-type laser comparator, described in the following references:

M. Negebauer: the uncertainty of diameter calibrations with the comparator for diameter and form, *Meas. Sci, Technol.* (1998) **9**, pp. 1053-1058.
M. Negebauer, F. Ludicke, D. Bastam, H. Bosse, H. Reimann, C. Topperwien: A new comparator for measurement of diameter and form of cylinders spheres and cubes under clean-room conditions, *Meas. Sci. Technol.* (1997) **8**, pp. 849-856

Table A.1.2 Uncertainty budget for diameter measurements with the laser comparator

		5 mm nominal diameter		25 mm nominal diameter	
Source of Uncertainty	Relative Uncertainty	Uncertainty Contribution / µm		Uncertainty Contribution/ µm	
Laser interferometer value		0.006		0.006	
Vacuum wavelength	$2x10^{-9}$	0		0	
Refractive index of air	$1.4x10^{-7}$	0.001		0.004	
Probing System measurement		0.005		0.005	
Abbe arrangement		0.002		0.002	
Maximum diameter		0.001		0.001	
Optics		0.001		0.001	
Measurement object		0.001		0.001	
Correction to 20 ºC	$5x10^{-7}$	0.003		0.013	
Drift of metrological frames		0.01		0.01	
Drift of probing systems		0.002		0.002	
Elastic deformation		0.001		0.001	
Cleaning		0.002		0.002	
Fixing		0		0	
Contacting spheres diameter		0.025		0.025	
Contribution of comparator		0.03	0.03	0.03	0.03
Experimental standard deviation*		1.0	0.75	0.75	0.2
Total standard uncertainty		1.0	0.75	0.75	0.2

- for various setting, adjusting and fixing of the measurement objects (coverage factor k=1)
- the influence of the form deviations of the measurements objects is the dominating uncertainty contribution.

A.2 NPL

Contact: **Dr. Nigel Fox**
Email: **nigel.fox@npl.co.uk**

Non-Contact Technique

Each aperture is scanned across a focused laser beam, using a computer-controlled high-precision translation stage. The light reflected from the surface of the aperture is detected by a photodiode. The edge of the aperture is located by adjusting the aperture position until only 50% of the incident light is reflected back onto the detector. Movements of the aperture in the x and z directions are measured by an interferometer. Two diameters are measured, one along the x-axis and one along the z-axis. The average of the two diameters is then used to calculate the geometric area of the aperture.

Apparatus

The apparatus used consists of three parts - a HeNe laser probe beam with an associated detector, a laser interferometer and a pair of translation stages with controller. These are described individually in more detail below. Control of the stages and processing of the outputs from the stages, interferometer and detector are all dealt with via a PC.

(i) HeNe Laser Probe Beam
An intensity-stabilised 15mW HeNe laser (λ=632 nm) is used as the optical 'stylus' or probe. A Pockels cell is placed immediately in front of the laser. This will form part of the stabilisation control. The output beam is then passed through a spatial filter, then collimated by a single f=100 mm lens. A variable aperture is then used to extract the central part of the diffracted beam. After passing through a polariser, a fraction of the beam is diverted to a photodiode. The signal thus generated provides feedback to the Pockels cell and so controls the laser power. The beam then passes through another variable aperture (to reduce scatter).

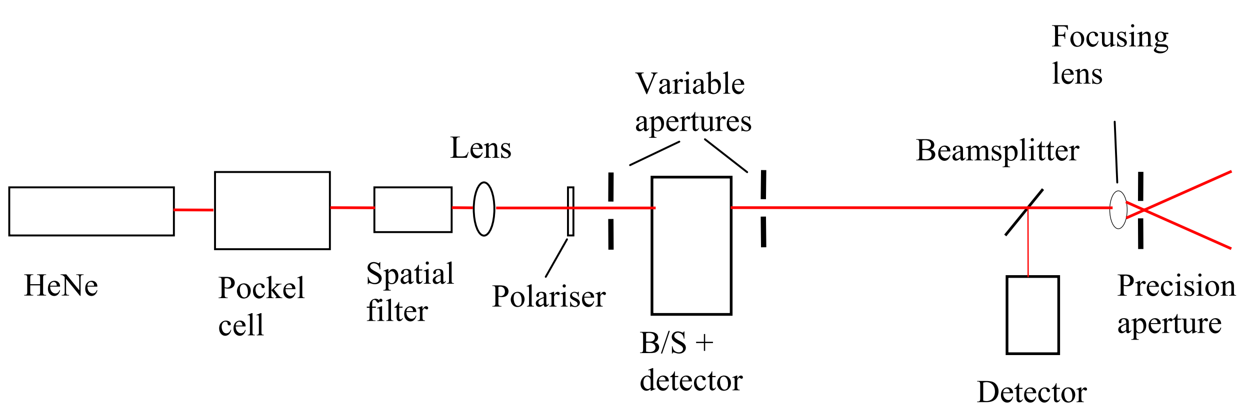

Figure (1): Optical Arrangement for HeNe Probe Beam

The beam passes through a pellicle beam splitter before being focused by a x60 microscope objective. The pellicle beamsplitter provides a return path for the light reflected from the surface of the aperture, and deflects it onto a photodiode detector.
The overall beam path measures approximately 2.0 m (from the laser to the precision aperture) therefore reducing uncertainties due to misalignment of the beam.

(ii) Interferometer
The interferometer used is produced by Hewlett Packard and consists of a HP 5519A laser head combined with a HP 10887P interferometer board and a HP 10886A compensation board. The latter allows for variations in measured length, due to non-standard values of temperature, pressure and humidity, to be compensated for.

(iii) Translation Stages
A pair of motorised translation stages (manufactured by Time and Precision) are combined to give movement in the *x* and *z* planes.

It is important to ensure that the aperture is oriented such that the plane of the aperture coincides with the plane of movement of the two stages. Furthermore, the HeNe probe beam should be normal to both of these planes.
Firstly, the HeNe probe beam is oriented such that it is normal to the base of the z-axis stage, by using a plane mirror to produce a back-reflection.
It is also important to ensure that the movement of the aperture is along the arms of the interferometer. This is achieved by aligning the interferometer input beam parallel to the incident HeNe probe beam (using the back reflection from the aperture). The interferometer beam is thus orthogonal to the aperture. A 45^{o} prism is then used to turn the interferometer beam through 90^{o} and thus parallel to the plane of movement of the aperture.
The beam-splitting cube is aligned normal to the beam using the reflected light from the front surface and each of the retroreflectors placed at the correct height. The 45^{o} prism is then replaced with a plane mirror, set at 45^{o}. The two retroreflectors (one for each arm) are then aligned by rotating, until both beams pass back to the front of the interferometer without clipping.

Method

The technique used to measure the diameter of an aperture is as follows.
Firstly, an algorithm was developed which can find the position which corresponds to the location of an edge (see below). This algorithm is then applied to first measure a chord of the aperture. The midpoint of this chord is found and then the edges vertically above and below this midpoint are located. This separation corresponds to the first measurement of diameter. The midpoint of this first measurement is then used to measure the diameter horizontally

<u>Algorithm to Locate Aperture Edge</u>

(1) Find dark level (beam inside aperture)

- Take photodiode signal at 10 points, separated by 10microns
- Average $\Rightarrow$ dark signal

(2) Find light level (beam on aperture)

- Take photodiode signal at 10 points, separated by 10microns
- Average ⇒ light signal
- $I_{50\%}$ = (Light+Dark)/2

(3) Repeat loop until signal = $I_{50\%}$ or step size <0.1μm.

- Measure photodiode signal (averaged over 10 readings)
- Reduce step size by factor 1.2
- Move in either positive or negative direction depending on photodiode signal

(4) Take interferometer reading

- Use 2s time delay to allow stage to settle
- Read interferometer (averaged over 100 readings)

Measurements

Five measurements were taken for each aperture. Before each measurement, the alignment of the aperture was checked by firstly removing the focusing lens and ensuring that the reflection from the aperture surface was aligned with the incident beam. Secondly, the lens was re-positioned such that the back reflection was again aligned with the incident beam.
For each measurement, a correction was made for the expansion of the aperture due to temperature. The values of temperature recorded in the laboratory before (T_1) and after (T_2) each measurement set and the values of expansion coefficient used are listed in the table below the tables of results.

Analysis of Type B Uncertainties

a) Interferometer Drift: Over the period between consecutive edge measurements (~2 mins) the interferometer was observed to typically drift by 0.02 μm.
b) Interferometer Alignment: The maximum angular misalignment of the interferometer is estimated to be 1/400 rad. A misalignment will lead to an increase in the displacement measured, the size of which will depend on the nominal diameter of the aperture.
c) Laser stability: Long term drifts will cause the edge position to move to compensate for a change in laser power. If the drift occurs in a single direction (which is likely) then all readings in a set will be similarly affected. During the period between consecutive edge measurements, the laser could be observed to drift in power to give an uncertainty in displacement of 0.04 μm.
d) Environmental Conditions: These will affect the interferometer readings and are compensated for by recording values for temperature, pressure and humidity and using supplied algorithms to give a correction.
e) Resolution: In this case, the limiting factor is the movement of the stage. The smallest step is 0.07 revolutions, which corresponds to 0.06 μm. The resolution of the interferometer (given by $\lambda/64$, where λ=632.99 nm) makes only a small contribution to the overall resolution.

Table A.2.1 Uncertainty budget for NPL non-contact method

Source of Uncertainty	Value (μm)	Value/√3 (μm)
Interferometer drift	±0.02	±0.012
Inteferometer alignment	±0.03 (5 mm ϕ)	±0.017
	±0.12 (20 mm ϕ)	±0.069
	±0.15 (25 mm ϕ)	±0.087
Laser stability	±0.04	±0.023
Environmental conditions	**	**
Resolution	±0.06	±0.035
Combined uncertainty		
Nominal 5 mm ϕ	±0.11	±0.05
Nominal 20 mm ϕ	±0.16	±0.08
Nominal 25 mm ϕ	±0.19	±0.10

Analysis of Type A Uncertainties
The measurements are repeated five times in an attempt to remove random uncertainties. The resulting values for repeatability are given for each of the individual aperture result tables. Components of uncertainty which will contribute to the values for repeatability are as follows:

a) Laser stability: The measurement process relies on the laser power being constant. The 50% value is measured at the start of the measurement proves; subsequent edges are locating using the same value. Low-frequency noise will cause an apparent shift of the edge position. High frequency noise will be averaged out during the measurements.
b) Surface defects: The 50% value is determined from the reflected signal at the first edge. Subsequent edges may produce a different value for the high signal (due to surface defects/variations in reflectance, etc) and therefore an uncertainty in the true edge position.
c) Alignment of Aperture: The initial alignment of the system ensured that the aperture was orthogonal to the probe laser beam. Prior to each measurement for each aperture, this alignment was checked.

Contact method

Diametral measurements were made on each aperture on a machine employing laser interferometry. Measurements were made in two orthogonal planes, that plane passing through the lines marked on the top surface being designated 0 and the axis of measurement being parallel with the end face furthest from the bore. Contact with the bore surface was made using a 2.00 mm diameter ball-ended stylus.

Each aperture was assessed for roundness. Departure from roundness is defined as the difference in radii of two coplanar concentric circles, the annular space between which just contains the profile of the surface examined.

Uncertainties

The Type A and Type B contributions are combined using the methods detailed in the ISO Guide to the Expression of Uncertainty in Measurement. The following documents are also of use:

NIS 80 Guide to the Expression of Uncertainties in Testing,
M 3003 The Expression of Uncertainty and Confidence in Measurement.

The total uncertainty is estimated at a 95% confidence level (k = 2) and is the quadratic sum of the uncertainty contributions. The Type B components are calculated by the software. An example full calculation for DIAMETER is given in the following section.

The expanded uncertainties are given in Table A2.2 each being based on a standard uncertainty multiplied by the coverage factor k shown.

Table A.2.2. Sources of uncertainty for the NPL contact method

Parameter	Aperture/plane	ν_{eff}	k	Expanded unc. [mm]
Diameter	APT XX/0	25.3	2.11	0.00012
	APT XX/90	14.2	2.20	0.00014
	APTYY/0	6.5	2.47	0.00022
	APTYY/90	18.5	2.15	0.00012
Roundness	Apt XX	11.0	2.26	0.00019
	AptYY	10,123	2.00	0.00008

Notes
a) A value for the coefficient of linear thermal expansion for aluminum bronze of 18.9 ppm/°C has been used to correct diameters to 20°C.
b) The temperature of the apertures during the measurements varied between 20.16 °C and 20.33°C
c) When making allowance for elastic compression a V value for aluminum bronze of 2.45×10^{-8} gf/mm^2 has been used, where V is defined as $(1-\sigma^2)/\pi E$ where Poisson's ratio (σ) was taken to be 0.320 and Young's modulus (E) was taken to be 11.73×10^6 gf/mm^2 (115 GPa). These values were supplied by NIST.
d) The results and uncertainties refer to on-the-day values and make no allowance for subsequent drift.

Example for Uncertainty Calculation

Contributions for coverage factor k = 1 (D is in mm):

A) Alignment of the traverse of the table with the diameter of the ring:

$$\frac{0.05}{\sqrt{3}}\,\mu m = 0.029\,\mu m$$

Note:
Below is a table which shows the distance the work table would have to move normal to the measurement direction to give an error in diameter of 0.1 µm and 0.01 µm.

$$Error = 2r - (r + \sqrt{r^2 - y^2})$$

$$\therefore y = \sqrt{r^2 - (error - r)^2}$$

where r = radius of ring
e = diameter error
y = table displacement

Ring diameter	Table displacement (mm) for error in diameter of 0.1 um	Table displacement (mm) for error in diameter of 0.01 um
3	0.17	0.005
5	0.022	0.007
10	0.032	0.010
20	0.045	0.014
30	0.055	0.017
40	0.063	0.020
50	0.071	0.022
100	0.100	0.032
150	0.122	0.039
200	0.141	0.045
250	0.158	0.050
300	0.173	0.055

The straightness of the worktable motion was measured when the machine was originally commissioned and was found to be 2.5 µm over 300 mm. The squareness of the mechanism for finding a reversal to the main motion was measured to be 1.27 µm in 7.6 mm i.e 0.167 µm per mm.

Combining these two contributions gives the total table displacement during traverse of a ring as (D x 0.167 + 2.5) µm in the worst case. The likely error due to coming off diameter is therefore less than 0.01 µm for all sizes of ring. In fact a greater source of error is how well one can set on diameter in the first place (probably no better than 0.04 µm) hence the value of 0.05 µm above.

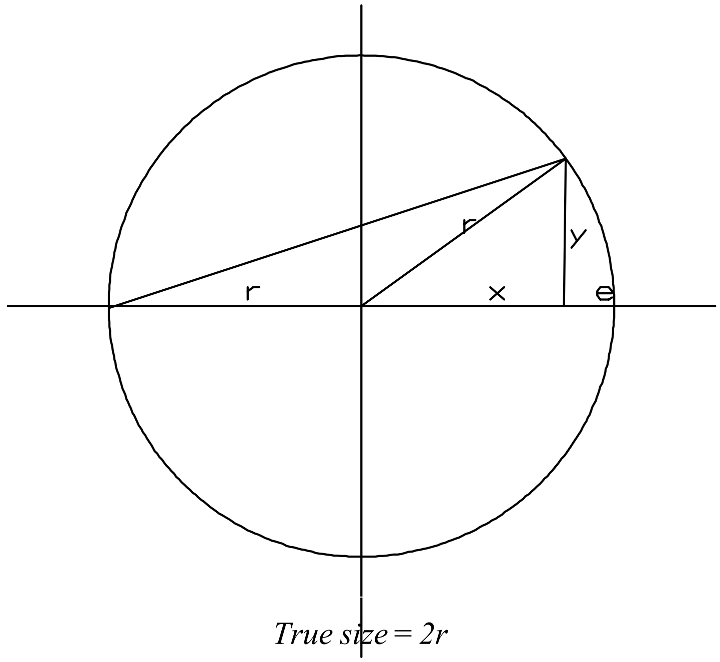

$$True\ size = 2r$$

$$Measured\ size = r + x = r + \sqrt{r^2 - y^2}$$

$$Error\ Error = 2r - r + \sqrt{r^2 - y^2} = r + \sqrt{r^2 - y^2}$$

$$error = r + \sqrt{r^2 - y^2}$$

$$\therefore (error - r)^2 = r^2 - y^2$$

$$y^2 = r^2 - (error - r)^2$$

$$y = \sqrt{r^2 - (error - r)^2}$$

B) Effect of the vertical movement of the worktable during its traverse:

$$0.000\,02\ D\ \mu m$$

C) Resolution and accuracy of the laser interferometer system (assume a rectangular distribution)

$$\pm \frac{0.005 + 0.0001D}{\sqrt{3}}\ \mu m$$

D) Alignment of the interferometer with machine motion

$$\frac{0.0005\ D}{\sqrt{3}}\ \mu m = \pm 0.000\,3\ D$$

E) Interferometric measurement of the silica box standard. The uncertainty in this measurement is 0.04 µm at a 95% confidence level. The contribution is therefore

0.020 µm. This is an example only. The current uncertainty in the measurement should be obtained from the latest calibration of the box standard.

F) The standard deviation s_{n-1} of the stylus constant determinations can be up to 0.03 µm for four determinations

$$\frac{0.030}{\sqrt{4}} = 0.015\ \mu m$$

G) Each applied compression correction has an uncertainty of 10%. This correction typically has a value of 0.10 µm. The contribution, assuming a rectangular distribution is therefore

$$\sqrt{2\left(\frac{0.01}{\sqrt{3}}\right)^2} = 0.008\,\mu m$$

H) Uncertainty in the expansion coefficient of the ring material. If for this example we assume an excursion from 20 °C of 0.25 °C and a 1ppm/°C uncertainty in the expansion coefficient we have a contribution of

$$\frac{0.25 x 1 x 10^{-6} x D}{\sqrt{3}} = 1.4 x 10^{-7} D\ mm$$

= 0.000 14 D µm

I) The uncertainty in the temperature measuring system is ± 0.01 °C at a 95% confidence level. For a steel ring (a = 11.7 x 10^{-6}) this contribution amounts to

$$\frac{0.01}{2} x 11.7 x 10^{-6} x D = 5.85 x 10^{-8} D$$

= 0.000 06 D µm

J) Results are rounded to the nearest 0.05 µm and this introduces an uncertainty of up to 0.02 µm. This contribution is distributed rectangularly and is

$$\pm \frac{0.02}{\sqrt{3}} = 0.012\ \mu m$$

K) Uncertainty in the calculation of the V.O.L. compensation factor is 0.000 1 D µm. This has been derived as follows and takes into account the errors in the sensors and in the Edlen equation.

Temperature: Assuming an uncertainty in the measurement of air temperature of 0.1 °C, this equates to an error in V.O.L compensation factor of 0.000 000 10.

Pressure: The uncertainty in the generated pressures used to calibrate the digital pressure indicator is 0.03 mbar (k = 1). The calibrations with rising and falling pressure agree to 0.09 mbar. If we assume an uncertainty in pressure measurement of 0.1 mbar, this equates to an error in V.O.L compensation factor of 0.000 00 03.

Humidity: The uncertainty in the applied humidity used to calibrate the humidity sensor is 0.5% rh (k = 1). Taking into account interpolation between calibration points and the fact that we only make a point measurement we will assume an uncertainty of 5% rh. This equates to an error in V.O.L of 0.000 000 04.

Edlen: The edlen equation has an inherent error in the calculation of the V.O.L compensation factor of 0.000 000 01.

Combining these terms, expressed in parts per million, gives

$$\sqrt{0.10^2 + 0.04^2 + 0.03^2 + 0.01^2} = 0.11\ ppm$$

which in terms of length is 0.000 1 D µm.

Note: The following table shows the information from which the above values have been derived. Pressure is in mbar and temperature in degrees Celcius. The V.O.L is expressed in ppm e.g 0.999732086 is expressed as 732.086.

45 % rh			50% rh			55% rh		
P	T	V.O.L	P	T	V.O.L	P	T	V.O.L
999.9	19.9	732.071	999.9	19.9	732.113	999.9	19.9	732.155
999.9	20.0	732.165	999.9	20.0	732.207	999.9	20.0	732.250
999.9	20.1	732.259	999.9	20.1	732.302	999.9	20.1	732.344
1000.0	19.9	732.044	1000.0	19.9	732.086	1000.0	19.9	732.128
1000.0	20.0	732.138	1000.0	20.0	732.180	1000.0	20.0	732.223
1000.0	20.1	732.232	1000.0	20.1	732.275	1000.0	20.1	732.317
1000.1	19.9	732.017	1000.1	19.9	732.059	1000.1	19.9	732.101
1000.1	20.0	732.111	1000.1	20.0	732.154	1000.1	20.0	732.196
1000.1	20.1	732.205	1000.1	20.1	732.248	1000.1	20.1	732.291

L) The Type A contribution when measuring a plain setting ring is typically (for n = 4)

10 mm s = 0.025 µm 0.025/2 = 0.013 µm
150 mm s = 0.10 µm 0.10/2 = 0.050 µm

250 mm s = 0.10 µm 0.10/2 = 0.050 µm

The combined standard uncertainty is the square root of the sums of the squares of contributions A to L. The software calculates the combined standard uncertainties of the non random contributions. To calculate the total uncertainty this value is squared and added to the squares of the random contributions. The square root is then found and the result multiplied by a coverage factor, usually 2, to obtain the expanded uncertainty. Below is a derivation of a typical uncertainty formula and the formula for the best measurement capability. However uncertainties are always calculated on a case by case basis using the value on the computer printout and the actual variations in the measurements.

The combined standard uncertainty is given by the expression

$$\sqrt{A^2 + B^2 + C^2 + D^2 + E^2 + F^2 + G^2 + H^2 + I^2 + J^2 + K^2 + L^2}$$

collecting terms and using the values given above for A to L

$$\begin{aligned} & A^2 + E^2 + F^2 + G^2 + J^2 \\ & = 0.029^2 + 0.020^2 + 0.015^2 + 0.008^2 + 0.012^2 \\ & = 0.0017\ \mu m^2 \end{aligned}$$

$$\begin{aligned} & B^2 + D^2 + H^2 + I^2 + K^2 \\ & = (0.00002D)^2 + (0.0003D)^2 + (0.00014D)^2 + (0.00006D)^2 + (0.0001D)^2 \\ & = 1.236 \times 10^{-7} D^2\ \mu m^2 \end{aligned}$$

Combining these two values and introducing terms C and L gives:

$$\sqrt{0.0017 + 1.236x\,10^{-7} D^2 + \left(\frac{0.005 + 0.0001D}{\sqrt{3}}\right)^2 + L^2}$$

$$= \sqrt{0.0017 + 1.269x\,10^{-7} D^2 + 3.33x\,10^{-7} D + L^2}$$

Using this formula with values of 10 mm, 150 mm and 250 mm gives the following values:

10 mm:	Combined standard uncertainty	= ± 0.044 µm
	Expanded uncertainty (k = 2)	= ± 0.088 µm
150 mm:	Combined standard uncertainty	= ± 0.084 µm
	Expanded uncertainty (k = 2)	= ± 0.169 µm
250 mm:	Combined standard uncertainty	= ± 0.111 µm
	Expanded uncertainty (k = 2)	= ± 0.221 µm

Fitting a line to the expanded uncertainty values gives an expression for the typical uncertainty when measuring a ring of

$$\pm(0.085 + 0.00054D)\ \mu m$$

Note: For rings that exhibit a large non-uniformity of diameter it may be necessary to increase the uncertainty to take into account the uncertainties in height setting. If a ring showed a uniformity of diameter of 0.000 30 mm over the central 2 mm and it is estimated that height settings can be made to no better than ± 0.25 mm then the additional term equals 0.000 04 mm. This term should be added in quadrature at the same time as the random contributions.

A.3 BIPM

Contact: **Dr. Michael Stock**
Email: **mstock@bipm.org**

Experimental Set-up

At the BIPM, the scanning-beam technique is applied for the measurement of aperture areas. The measurement principle is described in detail elsewhere [3.3.1,3.3.2, 3.3.3] and is only described briefly here. If an aperture is irradiated by a known uniform irradiance *E*, its area *A* can be determined from a measurement of the transmitted flux Φ according to $A = \Phi/E$. A uniform field can be produced by a superposition of laser beams regularly arranged in two dimensions. In the scanning beam technique, instead of simultaneously superimposing many beams in the aperture plane, the aperture is scanned across a single laser beam with steps Δx and Δy in two orthogonal directions perpendicular to the beam. The throughputs Φ_{ij} for all positions (x_i, y_j) are measured and from this the area A is calculated as

$$A = \Delta x \Delta y \sum_{i,j} \frac{\Phi_{i,j}}{\Phi_L}$$

where Φ_L is the total flux in the beam. No absolute power measurement is required since only the ratios of measured powers are needed.

The following figure shows schematically our set-up.

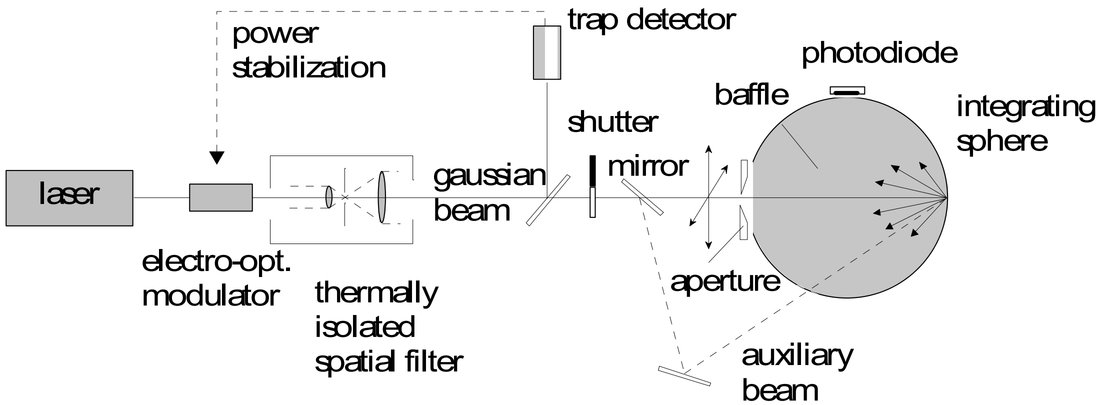

The optical arrangement with the He-Ne laser provides an intensity-stabilised and spatially-filtered beam with a power of about 2 mW. The beam shape is very close to a perfect Gaussian. The input port of our integrating sphere has a diameter of 50 mm, allowing apertures with diameters up to about 25 mm to be measured. Due to additional limitations from some mechanical parts, the upper limit for the diameter is, however, actually about 20 mm. The translation stages for the displacement of the aperture are mechanically coupled with length gauges equipped with optical encoders with uncertainties of the order of 0.1 µm. An auxiliary beam can be introduced into the sphere by a second port to measure the changes of the sphere response related to the changing position of the aperture which forms a part of the sphere wall.

To avoid erroneous results, special care is given to the following points:

- The profile of the laser beam must be close to gaussian.
- The power of the laser beam must be stable during the measurement to within several parts in 10^5.
- The position of the laser beam in the aperture plane needs to be stable to about 0.1 µm during a measurement.
- Reflecting apertures must be inclined to avoid direct back-reflections.
- Light reflected by the aperture and light leaving the sphere must be absorbed to avoid that it returns into the sphere.
- The beam for measurement and the auxiliary beam should hit the sphere wall at nearly the same position.
- The steps Δx and Δy have to be sufficiently small, so that the sum of all signals Φ_{ij} corresponds to a measurement made in a sufficiently uniform field.
- The photodiode must be very linear.
- The aperture must be clean.

A typical measurement consists of 5 to 10 individual scans of the aperture to reduce the effect of random variations. The relative experimental standard deviation of the individual results is typically 6 x 10^{-5}.

Uncertainty Budget

The following table shows the uncertainty budget for the four apertures that were measured. The estimated uncertainties are aperture-dependent since some contributions depend on the aperture diameter and the thickness of its land. Only the larger contributions will be discussed here.

Correction for tilt angle
Reflecting apertures have to be tilted by a small angle (0.6˚) to avoid a perturbation of the power stabilization by the back-reflected beam. A correction is applied which takes into account the reduction of the surface scanned by the laser beam due to the cosine-effect and the obstruction of a part of the clear opening by the land. The latter effect is predominant for apertures with relatively thick lands. The corresponding uncertainty results from incomplete knowledge of the angle, the thickness of the land and the reflection coefficient of the land.

Temperature correction
A correction is applied for the small temperature deviation from the reference temperature of 20 °C. The temperature variation during the measurements was typically only 0.03 °C, which is insignificant for the area measurements. Since we measure not directly the temperature of the aperture, but the temperature at a position close to it, we assume an uncertainty of 0.2°C.

Change of sphere-response with position of aperture:
The rear of the aperture forms a part of the sphere wall, so that the response of the sphere will change when an aperture is displaced. This effect is measured by displacing the aperture while an auxiliary beam enters the sphere by the second input port. From this a correction is calculated for each aperture, the repeatability of which is taken as its uncertainty, *i.e.,* 2×10^{-5} for the smaller apertures and 1×10^{-4} for larger apertures. It was verified that after applying this correction, the response of the sphere with the larger at its input port is in fact uniform to better than 10^{-4}.

Non-uniformity of sphere response:
The effect of a non-ideal behavior of the sphere is difficult to quantify. For the future we plan to make a Monte-Carlo simulation. At the moment we estimate this effect to be very small, since at least for high quality apertures, at any position (x_i,y_j) of the aperture nearly all the flux of the laser beam is confined to a very small angular range. A rough estimation results in the values shown in the table.

Table A.3. Sources of uncertainty for BIPM method

Contribution to combined uncertainty	10^5 x relative standard uncertainty (Δ/A)
Accuracy of optical encoders (glass scales):	
Proportional error	0.2
Residual error	1.6
Correction for tilt angle (0.6˚)	4.8
Temperature correction	0.8
Aperture transmission (clipping of beam)	1
Non-uniformity of sphere response	2.3
Change of sphere response with position of aperture	2

Orthogonality of laser beam and translation axes	0.2
Stray light	0.1
Experimental standard deviation of the mean for n=5 (temporal stability of laser flux, positioning tolerance…)	3
Combined Standard Uncertainty	6.8

The experimental standard deviation of a series of repeated measurements is typically 6×10^{-5}. Contributions to this are the stability of the laser power, the tolerance of 0.1 µm allowed for the positioning of the aperture and the pointing stability of the laser beam. In most cases, the measurements reported here consist of 3 to 10 individual aperture scans. If we take n=5 as representative, the standard deviation of the mean is 3×10^{-5}.

References:
Lassila A., Toivanen P., Ikonen E., *Meas. Sci. Technol.,* 1997, **8**, 973-377.
Ikonen E., Toivanen P., Lassila A., *Metrologia*, 1998, **35**, 369-372.
Stock M., Goebel R., *Metrologia*, 2000, **37**, 633-636.

A.4 LNE-INM

Contact: **Dr. Annick Razet**
Email: **razet@cnam.fr**

The aperture dimensions were measured using a 60X magnification microscope with an eyepiece equipped with a reticule. A micrometric two-axis XY translation stage was used to move the diaphragm under the microscope.

Calibration of the apparatus
Before measuring the aperture, the two-axis translation stage was calibrated by means of a glass scale graduated with a step of 0,1 mm on a 50 mm length, this glass scale itself being calibrated by an interferometric method. The two-axis XY translation stage was calibrated over a length of 30 mm to evaluate the ratio between the values read from the translation stage on those given by the glass scale. Relative standard uncertainties on these corrective factors are respectively 5.10^{-5} for X-axis and 6.10^{-5} for Y-axis. They are estimated from a score of calibration curves made in a few days.

Measurements

The method by which the areas of aperture are determined is that of measuring the co-ordinates x_i and y_i of the periphery of the aperture for 37 positions spaced by about 10°. We fix one value of the position x_i (or y_i), and then shift the Y-axis (or X-axis) of the translation stage until the crosswire of the microscope coincide with an intersection with the aperture. From these pairs (x_i, y_i), we can use our least-squares method to estimate the radius R_0 and the area of the aperture.

Uncertainties of the estimated radius R_0

The sources of errors in the result of the estimated radius R_0 come from the acquisition of values x_i and y_i, the temperature, the flatness of the translation stage and the “perpendicularity” of axes of the translation stage.

Acquisition of values x_i and y_i

The standard uncertainties in the values x_i and y_i were estimated respectively to be 1,3 µm and 1,8 µm, taking into consideration both the dispersion of the measurements (conditions of repeatability) (0,8 µm for x_i and 1,3 µm for y_i), the uncertainty coming from the resolution of the thumb screws (0,3 µm) and the uncertainties in the calibration of the translation stage (1 µm for X-axis and 1,2 µm for Y-axis).

Uncertainty in the estimated radius R_0 is calculated from those on x_i and y_i [4.4.1]. For each diaphragm, we carried out five series of measurements for different positions of the aperture on the translation stage (conditions of reproducibility). The dispersion associated with these results is larger than that obtained under conditions of repeatability. In the final uncertainty budget, the reproducibility uncertainty is retained.

Temperature

Temperature measurements are made before and after each series of acquisitions. The values of the radii are given to a temperature of 20°C. The standard uncertainty $u(T)$ associated with this temperature gives a standard uncertainty $u(R)$ in the radius of the aperture whose the expression is given by:

$u(R_0) = R_0 \cdot \alpha \cdot u(T)$

where α is the thermal expansion coefficient of the aperture.

Flatness of the translation stage

The flatness of the translation stage was given with an inductive sensor with axial movement TESA. The study showed that this translation stage had a variation of flatness of 26 µm with a standard uncertainty estimated at 5 µm over a 72,111 mm length given with a standard uncertainty of 2 µm. From these results, the angle θ between the translation stage and the horizontal one could be deduced, $tg(\theta) \approx \theta \approx 3,6.10^{-4}$ rad with a standard uncertainty $u(\theta)$ of 7.10^{-5} rad (fig. 1).

Figure A.4.1 : No flatness of the translation stage

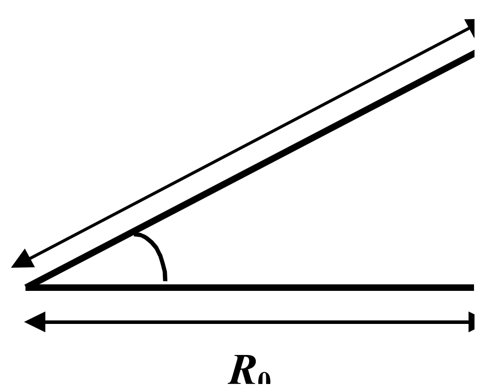

The correction c applied, deduced from figure 1, is given by the following expression:

$$c = R - R_0 = \frac{R_0}{cos(\theta)} - R_0 = R_0\left(\frac{1}{cos(\theta)} - 1\right)$$

The angle θ being small, the term cos(θ) was replaced by $1-\frac{\theta^2}{2}$ in the previous expression, consequently the expression of the correction becomes:

$$c = R_0\left(\frac{1}{cos(\theta)} - 1\right) = R_0\left(\left(1-\frac{\theta^2}{2}\right)^{-1} - 1\right)$$
$$\approx R_0\left(1+\frac{\theta^2}{2} - 1\right) = R_0\frac{\theta^2}{2}$$

The relative standard uncertainty associated this correction C is given by:

$$\frac{u(c)}{c} = \frac{2.u(\theta)}{\theta} \approx 0{,}4$$

And we can deduce the standard uncertainty in the correction:

$$u(c) = \frac{2.c.u(\theta)}{2.\theta} = \frac{2.R_0.\theta^2.u(\theta)}{2.\theta} = R_0.\theta.u(\theta)$$

The corrections c applied to the radii of the apertures of the inter comparison are negligible, of the order of 0,9 nm for the aperture of larger radius ($R_0 \approx 13{,}24$ mm)
"Perpendicularity" of axes of the translation stage

Not being able to check in experiments the perpendicularity of X and Y axes, a computer program of simulation was used, making it possible to quantify it. The influence of an angle ± β (fig. 2) between the Y-axis and the Y'-axis on the values of radii obtained at the exit of the program "circles of least squares" was studied.

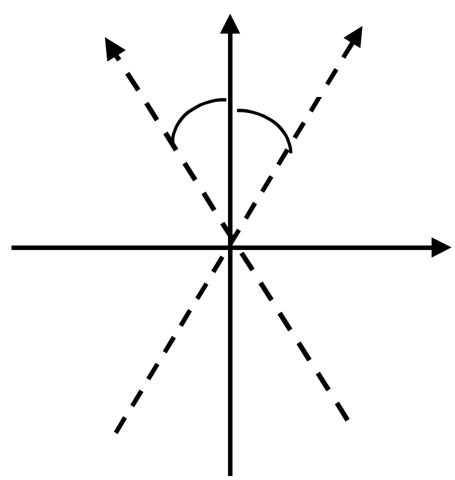

Figure A.4.2 : No perpendicularity of the axes

The retained value β is that for which experimental standard uncertainty of the radii is of the same order of magnitude as that resulting from the simulation program. The stop of this test supposes that one assigns to experimental uncertainty standard, the only effect of no perpendicularity of the axes, which actually is not the case. The estimated values of β, equal to ± 0,5 mrad, is taken as a maximum value. For the angles β = ± 0,5 mrad, we determined the variations ± Δ between the theoretical radius and that resulting from the calculation of least squares.

The assumption of a random variable associated this variation, distributed uniformly between the values ± Δ, with a zero expectation was retained. The associated standard uncertainty is given by the expression:

$$u(\mathrm{P}) = \frac{\Delta}{\sqrt{3}}$$

Table A.4. Components of uncertainty for the LNE-INM method

Component	Standard uncertainty	Sensitivity coefficient	Standard uncertainty contribution (µm)
Reproducibility	u_{repro} = 0,51 µm	1	0,51 µm
Temperature	$u(T)$ = 0,3 °C	2,4. 10^{-1} µm.K^{-1}	0,072 µm
Flatness of the translation stage	$u(\theta)$ = 7 . 10^{-5} rad	4,57 µm	0,000 32 µm
"Perpendicularity" of axes of the translation stage	$u(P)$ = 0,03 µm	1	0,03 µm

The combined standard uncertainty $u(R_0)$ = 0,52 µm

The expression of area of diaphragm is given by : $S = \pi R_0^2$

The standard uncertainty in the area is given by **:** $u(S) = \sqrt{\left(\frac{\partial S}{\partial R_0}\right)^2 . u^2(R_0)}$ = 0, 041 mm^2.

References

A.Razet, « Analytical resolution of least-squares applications for the circle in interferometry and radiometry », *Metrologia*, 1998, 35, 143-149

A. Razet, J. Bastie, « Etalonnage de diamètres de diaphragmes pour des mesures radiométriques » (« Aperture area calibration for radiometric measurements ») , *Bulletin du LNE-INM*, 120, 2001-2, 27-33

A.5 VNIIOFI

Contact: **Dr. Boris Khlevnoy**
Email: **khlevnoy-m4@vniiofi.ru**

The measurements were carried out in cooperation with another Russian institute VNIIM. VNIIM's standard facility for calibrations of internal and external diameters was used.

Type of the equipment used

The laser interferometer LIY-200 for calibrations of internal and external diameter standards.

Description of the equipment

The 1D laser interference instrument is used for absolute non-contact measurements with a stabilized He-Ne laser $\lambda = 633$ nm.

The laser interferometer has a photoelectric microscope with a scanning slit as an edge detector. The refractive index of air is measured by a laser refractometer with an uncertainty no more then $5 * 10^{-8}$.

Resolution of laser interferometer is 0,01 mcm.

Table A.5. Uncertainty Budget of the VNIIOFI method for the apertures measured

Sources of Uncertainty	Contribution / m
Wavelength	$1x10^{-8}$
Refractive index	$5x10^{-8}$
Temperature	$2x10^{-8}$
Fix an edge	$8x10^{-8}$
Repeatability and non-circularity	7-19 $x10^{-8}$
Total Diameter uncertainty (k=1) µm	0.10-0.45
Total Area uncertainty (k=1) mm^2	0.0009-0.011

A.6 MIKES

Contact: **Dr. Erkki Ikonen**
Email: **erkki.ikonen@MIKES.fi**

The calibration was carried out by the aperture-area-measurement system of the Helsinki University of Technology (Lassila et al. 1997 and Ikonen et al. 1998). The measurement system consists of a power-stabilised laser, a spatial filter, a monitor detector, an aperture holder, a high-precision xy translation stage, an interferometer and an integrating sphere detector. An aperture under calibration is attached to the holder. The intensity profile of the laser beam is purified by using the spatial filter. A known, uniform irradiance is generated by moving the aperture between equally spaced positions in relation ot the laser beam by using the xy translation stage. The plane of movement is perpendicular to the laser beam. The length scale of the translation stage is calibrated by the interferometer. For each position of the aperture, the optical power penetrated through the aperture is recorded with the integrating sphere detector immediately behind the aperture. The area of the aperture A is calculated using the formula:

$$A = \frac{\Delta x^2 P_{summed}}{P_{beam}}$$

Where P_{beam} is the power of the laser beam, P_{summed} is the total radiant flux passed through the aperture and the Δx is the step length of the *xy* translation stage.

First the aperture under calibration was attached to the *xy* translation stage and aligned in 0.3° angles in respect to the laser beam. The cosine and land errors in the aperture area caused by the tilting angle were corrected to the results after measurements. Before each measurement, the power passing through the aperture was measured by a trap detector. The aperture was moved aside, and the trap detector measured the power of the laser beam again. The ratio of these measurements was used as a transmission correction. Typically the transmission correction was $5x10^{-5}$-$2.5x10^{-4}$.

For the aperture area measurements, the trap detector was replaced by an integrating sphere detector. The aperture was moved within a rectangular area in a way that the center of the aperture divided the area to small squares. The power penetrating through the aperture was recorded in each position of the aperture and summed. During the measurements, the power of the laser beam was monitored by using a beam splitter and a trap detector. The dark current of the integrating sphere detector and the monitor detector was measured before and after each scan. The average dark current was subtracted from the measured power value in each position. In one measurement, the scan was repeated approximately sixteen times. For each aperture, the measurement was repeated five times with different alignment.

Table 6. Uncertainty budget for the MIKES aperture area measurement. Uncertainty values on the table are relative standard uncertainties at a level of 10^{-4}.

Table A.6 Uncertainty budget for MIKES aperture area measurement

Component	APT
Repeatability (std. dev of mean n=16)	0.8
Length scale	4.4
Cosine error	0.3
Land correction	0.3
Transmission loss	0.5
Detector non-linearity	0.6
Non-uniformity of integrating sphere	0.2
Non-uniformity of aperture holder	0.2
Stray light	0.5
Combined Standard uncertainty/10^{-4}	4.6
Expanded uncertainty (k=2)/10^{-4}	9.2

References:
Lassila, P. Toivanen and E. Ikonen, "An optical method for direct determination of the radiometric aperture area at high accuracy", *Meas. Sci. Technol*. **8**, 973-977 (1997).
E. Ikonen, P. toivanen, and A. Lassila, "A new optical method for high-accuracy determination of aperture area," *Metrologia* **35**, 369-372 (1998).

A.7 OMH

Contact: **Dr. M. Machacs**
Email: **M. Machacs@omh.hu**

Non-Contact Method

The area of the aperture was calculated from its diameter. The diameter measurements were c arried out on a universal measuring microscope equipped by a HP displacement laser interferometer adjusted along one of the axis. We used lower illumination and 50 times magnification. The targeting of the edges of the aperture was carried out visually. The average diameter of the aperture was calculated from several diameter measurements taken along different diameters.

Equation of measurement for 20°C (measurement model):

$A = L_a^2\pi/4$ $\quad\quad$ $L_a = L_e + \delta L_{ap} + \delta L_l + \delta L_{ta} + \delta L_d - L(\bar{\alpha} * \delta t + \delta\alpha * \Delta\bar{t})$

$\mathbf{L_a}$	diameter of the aperture on ambient temperature
$\mathbf{L_e}$	readings of the standard (laser interferometer)
$\mathbf{\delta L_{ap}}$	correction due to the improper horizontal adjustment of the aperture, estimate zero
$\mathbf{\delta L_l}$	correction due to the improper adjustment of the laser, estimate zero
$\mathbf{\delta L_{ta}}$	correction due to the targeting of the aperture edge, estimate zero
$\mathbf{\delta L_d}$	correction due to other mechanical problems
L	nominal diameter
$\bar{\alpha} = (\alpha_{ap} + \alpha_e) / 2$	average thermal expansion coefficients of the aperture and of the standard
$\delta t = (t_{ap} - t_e)$	temperature difference between the aperture and the standard
$\delta\alpha = (\alpha_{ap} - \alpha_e)$	difference in the thermal expansion coefficients between the aperture and the standard
$\Delta\bar{t} = (t_{ap} + t_e) / 2 - t_0$	deviation of the average temperature of the aperture and of the standard from the reference temperature
α_{ap}	temperature coefficient of the aperture
α_e	temperature coefficient of the standard
Δt_a	temperature deviation of the aperture from the reference (maximum 0,6 °C, estimate)
Δt_e	temperature deviation of the standard from the reference (maximum 0,6 °C, estimate)

Table A7.1.1 Sources of uncertainty for the OMH non contact method

Source	Estimate	Uncertainty	Probability distribution	Sensibility coefficient (L in µm)	Uncertainty component (µm)
Standard	L µm	0,2/2 µm	normal	1	0,1
δL_{ap}	0 µm	0,3/√3 µm	rectangular	1	0,3/√3
δL_{l}	0 µm	0,2/√3 µm	rectangular	1	0,2/√3
δL_{ta}	0 µm	1/√3 µm	rectangular	1	1/√3
δL_{d}	0 µm	0,7/√3 µm	rectangular	1	0,7/√3
δt	0°C	0,1/√3 °C	rectangular	$-18,9*10^{-6}*L$	$-18,9*10^{-6}*0,1/\sqrt{3}*L$
$\delta\alpha * \Delta\bar{t}$	0	$(0,566*10^{-6})$	rectangular	-L	$-0,566\ 10^{-6}*L$
Repeatability of the measurement process	0 µm	s	normal	1	s
Combined uncertainty					

Table A.7.1.2 OMH Example of uncertainty estimates for a particular aperture

Source	Estimate	Uncertainty	Probability distribution	Sensibility coefficient (L in µm)	Uncertainty component (µm)
Standard	L µm	0,2/2 µm	normal	1	0,1
δL_{ap}	0 µm	0,3/√3 µm	rectangular	1	0,173
δL_{l}	0 µm	0,2/√3 µm	rectangular	1	0,115
δL_{ta}	0 µm	1/√3 µm	rectangular	1	0,577
δL_{d}	0 µm	0,7/√3 µm	rectangular	1	0,404
δt	0°C	0,1/√3 °C	rectangular	$-18,9*10^{-6}*L$	-0,006
$\delta\alpha * \Delta\bar{t}$	0	$(0,566*10^{-6})$	rectangular	-L	-0,003
Repeatability of the measurement process	0 µm	1,2	normal	1	1,2
Combined uncertainty					1,411
Expanded uncertainty (k = 2):					**2,8**

$$\mathbf{U_{La} = 2,8\ \mu m} \quad (k=2)$$

Contact Method

The standards used:

Co-ordinate measuring machine
Producer: SIP, Switzerland
Type: CMM5
.. Id. no: 502
Measuring range: (700 x 700 x 550) mm
Resolution: 0,1 μm

Standard setting ring
Producer: Microtool
Id. no.: 0726
Traceable to METAS

The measuring procedure:

The apertures were placed onto a steel block with the dimensions of (400 x 100 x 20) mm and carefully fixed. A stylus with a nominal diameter of 3 mm was used, the applied measuring force was 0,05 N.

The following procedure was used for each aperture:
The upper surface was probed with 10 points, spatial alignment with the normal vector of the calculated plane (z axis). Circles were probed in x-y plane in different heights and the diameters of the circles were calculated. A set of 240 points was taken for every circle.
The temperature of the steel block was measured with 2 sensors (PT100) belonging to the CMM.
The standard ring of a nominal diameter of 25 mm was used as a reference. The results were reported for the reference temperature corrected with the given linear expansion coefficient.

The results were reported for the actual material temperature with a linear expansion coefficient equal to zero.

Uncertainty evaluation:

The uncertainty calculation was based on the equation of:

$$\mathbf{u = \sqrt{(u_c^2 + u_p^2 + u_w^2)} + abs(E)}$$

where
- $\mathbf{u_c}$: uncertainty from the standard used (from the certificate)
- $\mathbf{u_p}$: uncertainty from the measuring process
  - probing
  - difference of elastic deformations of the standard and the object
  - repeatability of the measurement

- **u_w**: uncertainty from the object to be measured
  - form deviation
  - linear exp. coefficient
  - temperature drift during the measurement of the object

- **abs(E)**: systematic error calculated from the measured and the certified value of the standard that includes:
  - temperature drift during the measurement of the standard
  - error of the thermometers' readings
  - unc. distribution of the linear exp. coeff.

Table A.7.2 Uncertainty table for the OMH contact method

Source	u (x_i)	distribution	c_i	$u_i(y)$ /µm/
Standard ring	0,05 µm	normal	1	0,05
Probing process	0,2/√3 µm	rectangular	1	0,12
Diff. of elastic. def.	0,1/√3 µm	rectangular	1	0,06
Repeatibility (stdev.)	0,4 µm	normal	1	0,4
Form dev. of the object	0,1/√3 µm	rectangular	1	0,06
Linear exp. coeff.	$2*10^{-6}$/√3 1/°C	rectangular	$25*10^{3}*0,2$ µm °C	0,006
Temp. drift during the measurement	0,1/√3 °C	rectangular	$25*10^{3}*19*10^{-6}$ µm/°C	0,03
SQR root of the quadratic sum:				0,43
Abs(E)	0,3			0,3
$u= \sqrt{(u_c^2 + u_p^2 + u_w^2)}$ + abs(E)				0,73
U (k=2)				**1,6**

A.8 NIST

Contact: **Dr. Maritoni Litorja**
Email: litorja@nist.gov

Non-Contact Method

The aperture area was determined using non-contact video microscopy. An interferometrically-controlled XY stage translates the test sample, and a microscope with a CCD camera locates the edge points. To perform the measurements, the aperture was mounted on a custom-made mounting ring, with the beveled side facing the illumination source.

Four edge points are initially located to circumscribe the inner-aperture circumference to accelerate the measurements. Apertures were measured using 360 points, at 1° interval. Five measurements were performed for each aperture. Replicate runs provide a measure of the reproducibility of the measurements and allow an assessment of the uncertainty due to defects in the edges. The Cartesian coordinates of the edge points are used in a circle- and ellipse-fitting routine to determine the geometric area of the aperture.

In the circle and ellipse-fitting routines, the bootstrap method is utilized to determine the standard "random plus form" uncertainty.[8.1.2.3] This is a repeated Monte Carlo resampling from a single data set to generate a standard deviation of the fitted radii. Table 8.1 presents the sources of uncertainty and their nominal contributions to the total relative uncertainty in area for the non-contact method.

Uncertainty in Measurement Results

The present analysis yields the radius and area of the circle from the set of measurands, the coordinates of the edge points. The uncertainty in the radius and area thus require an understanding of the uncertainty in the measured edge-point coordinates. The coordinates of an edge point, (x,y), are determined from the positional readings of the stage, (X,Y), and from a subpixel length correction, C, associated with the edge-detection method,

$$x(y)_{coordinate} = X(Y)_{\text{stage}} \pm C \, .$$

The random plus form component (u_i) is the pooled standard deviation of the 5 × N total measurements of the aperture radius, and because of the large number of measurements is dominated by the form component, which specifies the non-circularity of the aperture. The Type A uncertainty (k = 1) on a single x or y measurement is less than 25 nm, and contributes significantly less to the overall uncertainty due to the large number of coordinate measurements performed. The systematic uncertainties from the stage readings ($u_{j(stage)}$) and from the image ($u_{j(image)}$) are estimated. For a more detailed discussion of these instrumental uncertainties, please refer to the first reference listed below. Uncertainty ($u_{j(t)}$) is due to the variation of the temperature over the course of the measurement. The highest temperature variation in the replicate runs was used to estimate the uncertainty in dimension due to thermal variation. There is uncertainty due to the geometry ($u_{j(g)}$) of the sample with respect to the instrument. This can be attributed to the non-planarity of the aperture edges upon mounting. The optimal focal positions of the microscope, the z-axis positions, provide information on the location of the edges with respect to the XY (stage) plane. The Δz quantity is the maximum difference of two opposite edge points, and thus provides an estimate of the general tilt of the aperture with respect to the XY stage.

The combined uncertainty in the radius is the root-sum-of-squares of the various components.[8.1.2.4] The factor 4 in the calculation is due to the fact that two points are sampled to determine a radius.

$$u^2(R) = [u_i^2 + 4u_{j(stage)}^2 + 4u_{j(image)}^2 + u_{j(t)}^2 + u_{j(g)}^2]$$

Table A.8.1 Sources of uncertainty for the NIST non contact method

	TYPE	Sources of Uncertainty	Estimate Value/ *nm*	*R*=5 mm *u(A)/A*	*R*=25 mm *u(A)/A*
u_i	A	Random (A) plus form	50	$2.0\text{x}10^{-5}$	$4.0\text{x}10^{-6}$
$u_{i(stage)}$	B	Stage,systematic(B)	2.6x2R	$1.0\text{x}10^{-6}$	$1.0\text{x}10^{-5}$
$u_{j(image)}$	B	Image, systematic(B)	4		
	B	*p* pixel fraction			
	A	focus		$2.4\text{x}10^{-8}$	$4.8\text{x}10^{-9}$
	B	coherence factor		$1.3\text{x}10^{-6}$	$2.7\text{x}10^{-7}$
	B	off-axis thresholding		$2.3\text{x}10^{-7}$	$4.7\text{x}10^{-8}$
	B	*L* pixel length		$3.8\text{x}10^{-10}$	$7.6\text{x}10^{-11}$
	A	β stage/CCD angle		$8.9\text{x}10^{-16}$	$1.8\text{x}10^{-16}$
	A	*M* magnification		$4.5\text{x}10^{-9}$	$9.0\text{x}10^{-10}$
$u_{j(t)}$	B	Thermal Change	8x*R*	$1.7\text{x}10^{-5}$	$1.7\text{x}10^{-5}$
$u_{j(g)}$	B	Artifact geometry	0.08°	$2.0\text{x}10^{-6}$	$2.0\text{x}10^{-6}$
		Total *u(A)/A* (k=1)		$4.4\text{x}10^{-5}$	$2.8\text{x}10^{-5}$

References:

Fowler, J., and Litorja, M., " Geometric Area Measurements of Circular Radiometric Apertures at NIST", *Metrologia*, 40, S9-S12, (2002)

Shakarji, C., "l2cir2d Matlab version 1.0", NIST Manufacturing and Engineering Laboratories, (2000); Litorja, M and Leonov, I. "Circle, ellipse fitting and determination of random uncertainty by the bootstrap method, in LabView", NIST Physics Laboratory (2002)

Efron, B and Tibshirani, R., "An Introduction to the Bootstrap" *Chapman and Hall* (1993)

Taylor, B.N., and Kuyatt, C.E., "Guidelines for Evaluating and Expressing the Uncertainty of NIST Measurement Results," *NIST Technical Note* **1297**, (1994)

Contact method

The apertures were measured using an error-mapped coordinate measuring machine. The CMM is housed in a constant humidity measurement environment where temperature is controlled to 20.00 °C 0.05 °C. The measurement process employs several parts. The artifacts are measured multiple times to generate short-term repeatability data and to sample artifact geometry and surface finish effects. NIST control standards are measured concurrently to develop statistical long-term reproducibility data for the measurement system. The apertures were fixed using small amount of epoxy and laid on a precision straight edge. No restrictive or clamping devices were used. The average diameter and form results are measured for each aperture using 12, 24, and 48 equidistant measurement points collected at a distance of 50 µm below the level of the top surface. The area is calculated using the data from the 48-point measurement data

Table A.8.2 Sources of uncertainty for the NIST contact method

Source	μm	ppm
Machine scale uncertainty	0.04	
Temperature difference in beam paths during calibration		0.01
Laser frequency difference		0.02
Measurement Reproducibility	0.04	0.04
Edlen Equation		0.03
Index of Refraction-Air Temperature		0.01
Index of Refraction –Air Pressure		0.04
Index of Refraction – Humidity		0.03
Thermal Expansion		0.05
Coefficient of Thermal Expansion		0.05
Contact Deformation	0.002	
Gage Surface Geometry	0.004	
Gage Form Estimation Technique	0.005-0.100	
U (um) = 0.11 μm +0.20x10^{-6} L (k=2) best		

A.9 NRC

Contact: **Mr. Kostadin Doytchinov**
Email: **Kostadin.Doytchinov@nrc-cnrc.gc.ca**

Contact Method

Set-Up**:** A special jig was made to secure each aperture, distortion-free, one-at-a-time, with its aperture plane parallel to the x-y plane of the NRC CMM (Mitutoyo Legex Model 707, with MPP300 probe head). A calibrated step gauge aligned to the x-axis was fixed to the CMM table near the aperture jig, and likewise a similar step-gauge made parallel to the y-axis. Temperature sensors were attached to the aperture and to the step gauges. A CMM probe stylus sphere diameter of 4 mm was used for all measurements.

Measurement**:** For each aperture set-up, routine probe calibration and alignment to define the CMM measurement coordinate system to that of the aperture disk was made. The probe sphere bottom located the top surface of the aperture disk, and the CMM program moved the probe over the centre of the aperture hole, and descended by half the probe diameter plus half the height of the land (nominal 100 μm) formed at the edge defining the perimeter of the aperture hole, thereby ensuring that during each programmed radial approach at this elevation, the probe would contact the aperture in the mid-region of the land. Starting at this elevation, a series of 180 points was measured at 2° intervals in a clock-wise direction around the 360° circle perimeter of the aperture opening, all taken with radial approaches to the land at this elevation. Once the circle was measured, the measurement program then made measurements of the step-intervals on each of the two step gauges, to confirm the scale of x and y measurements in the data run as well as reveal possible bi-directional probing error. Several circle & step-gauge data runs were made with each set-up, to test the repeatability of the measurements. After measuring a given aperture, a master cylinder of size similar to that of the aperture, and with calibrated small roundness, was substituted into the position of the aperture jig, and the circle & step-gauge measurements were run several times as before, to test the repeatability on a ‘perfect’ part. Each aperture was measured in two orientations with respect to the CMM x-axis (0° and then rotated in-plane by 90°), which allowed any x vs. y CMM effects to be revealed and compensated. The original plan was to make at least three measurement runs for each of the two orientations (with new set-up between), to test the repeatability and reproducibility of the method, but project timing required the artifacts to be returned to the Pilot before our detailed analysis, and the subsequent analysis showed some runs to be spoiled, and thus were eliminated from the reported results. For this reason, there are sometimes only 4 or 5 runs reported for each aperture, instead of 6.

Analysis: The step-gauge measurements confirmed that x-y scale readings were correct and traceable to the definition of the metre. A least-square (LS) circle was fitted to each circle data sequence, and the residuals of the measured points about the fitted circle made a radial profile for each data run. The profile of the points measured on the master cylinder exhibited a small systematic departure from roundness that was attributed to the residual CMM carriage-probe characteristic, normally this is applied as a correction to the data taken for each aperture. In this case due to the magnitude of the described contaminations this compensation was small and was not applied. The profile for each aperture showed 1, 2 or 3 reproducible 'bumps' that are usually characteristic of dirt or some other contaminating particles (as opposed to 'dents' in the material due to tooling pits or scratches). The bumps were not typical of clean lathe-turned profiles, and careful re-cleaning reduced but did not eliminate their occurrence. Thus it was decided to manually 'smooth' the profile through each bump occurrence, and base the aperture diameter/area on the smoothed profile. This multi-step processing was applied to each run in each orientation, and the individual results are listed in the table that follows. The within-orientation and between-orientation variability are similar, and contribute dominant components to the reported uncertainty.

Table A.9 Sources of uncertainty for the NRC contact method measurement

Contributor	Unit	Distribution	u_{ix}	u_{iy}	Remark
CMM repeatability on LS diameter measurements on NRC standards	μm	Normal	0.022	0.022	Same measurement condition, number of points, probe, etc as the apertures. This is an uncertainty of the mean
CMM repeatability on LS diameter measurements on the apertures - after outlier removal	μm	Normal	0.09	0.09	This is an uncertainty of the mean
Uncertainty of the NRC standards	μm		0.025	0.025	
Uncertainty of the length transfer	μm	Normal	0.05	0.05	
Uncertainty of the temperature compensation	μm	Rectangular	0.005	0.002	The mean temperature was 20.03°C with a range of 0.03°C
Uncertainty of the diameter due to non-removed contaminations	μm	Rectangular	0.2	0.2	Expert judgment
Combined standard uncertainty for the diameter measurement				0.25	
U, Expanded uncertainty for the diameter measurement, k=2				0.50	

B. Appendix B: Electron microscope pictures of some CCPR S2 transfer apertures

Prepared by: Jürgen Hartmann, PTB

In this document electron microscope pictures obtained of some of the apertures circulated within the CCPR S2 are presented. The photos have been made during the measurements at PTB from April to June 1999.

The specifications of the eight apertures as given by the NIST are summarized in Table B.1.

Table B.1: Specification of the apertures supplied by NIST

Aperture	**APT01**	**APT04**	**APT07**	**APT10**	**APT13**	**APT16**	**APT19**	**APT22**
land	Knife edge	Knife edge	Cylin-drical	Cylin-drical	Knife edge	Knife edge	Cylin-drical	Cylin-drical
fabrication	Diamond turned	Diamond turned	Diamond turned	Diamond turned	Conven-tional	Conven-tional	Conven-tional	Conven-tional
Diameter / mm	25	5	25	5	25	5	25	5
material	ofhc copper	ofhc copper	Al-Bronze	Al-Bronze	Al-Bronze	Al-Bronze	Al-Bronze	Al-Bronze
Thermal expansion coefficient	.0000166 K^{-1}	.0000166 K^{-1}	.0000189 K^{-1}	.0000189 K^{-1}	.0000189 K^{-1}	.0000189 K^{-1}	.0000189 K^{-1}	.0000189 K^{-1}
Measuring technique	Non-contact	Non-contact	Non-contact, contact	Non-contact, contact	Non-contact	Non-contact	Contact	Contact

NIST and PTB decided to also include three diamond turned apertures manufactured by Rodenstock and supplied by the PTB. The specifications of these apertures are summarized in Table 1 b).

Table B.2: Specifications of the apertures manufactured by Rodenstock and supplied by PTB

Aperture	**P21**	**P23**	**P24**
Land	Cylindrical, ≈15 µm	Cylindrical, ≈15 µm	Cylindrical, ≈15 µm
Fabrication	Diamond turned	Diamond turned	Diamond turned
Diameter / mm	20	20	20
Material	Al	Al	Al
Thermal expansion coefficient	.0000238K^{-1}	.0000238K^{-1}	.0000238K^{-1}
Measuring technique	Non-contact	Non-contact	Non-contact

In the following the obtained pictures are presented for information without any comment. The length scale is given in the lower right corner of the pictures.

Figure B.1 APT 04 SE micrographs

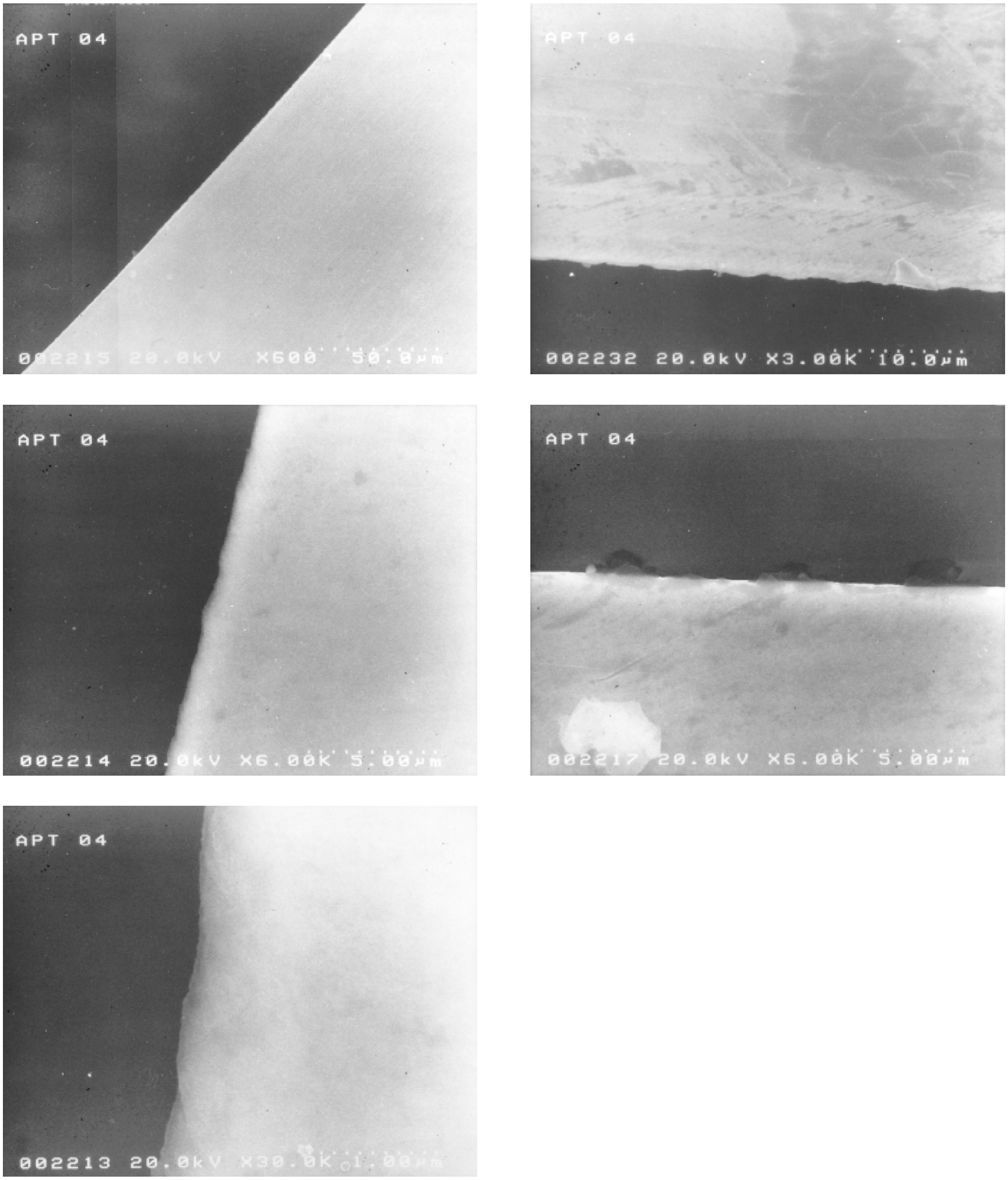

Pictures of aperture APT04 before re-shaping by NIST

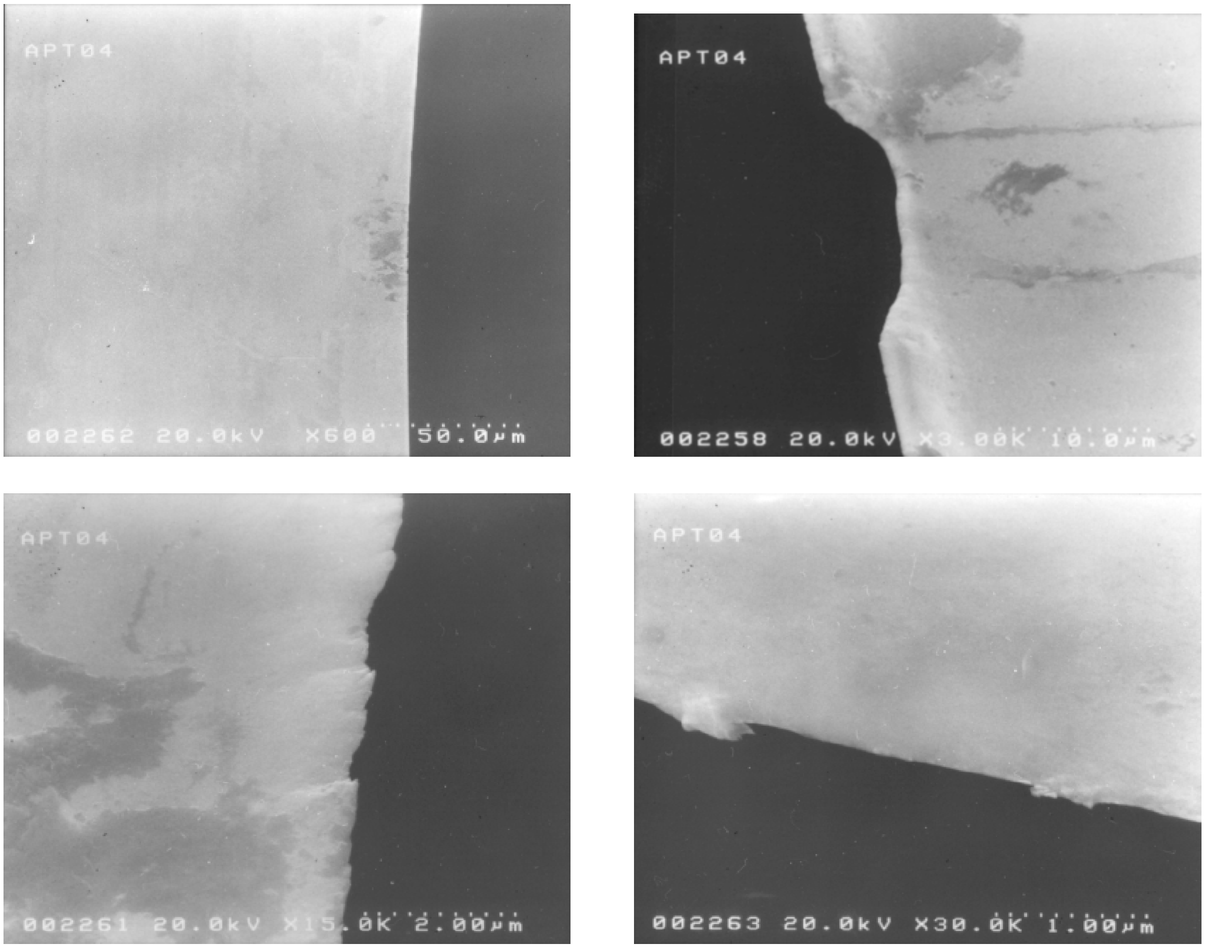

Pictures of APT 04 after re-shaping by NIST

All pictures of aperture APT 04 are showing a view on the top of the aperture edge

Figure B.2 APT 10 SE micrographs

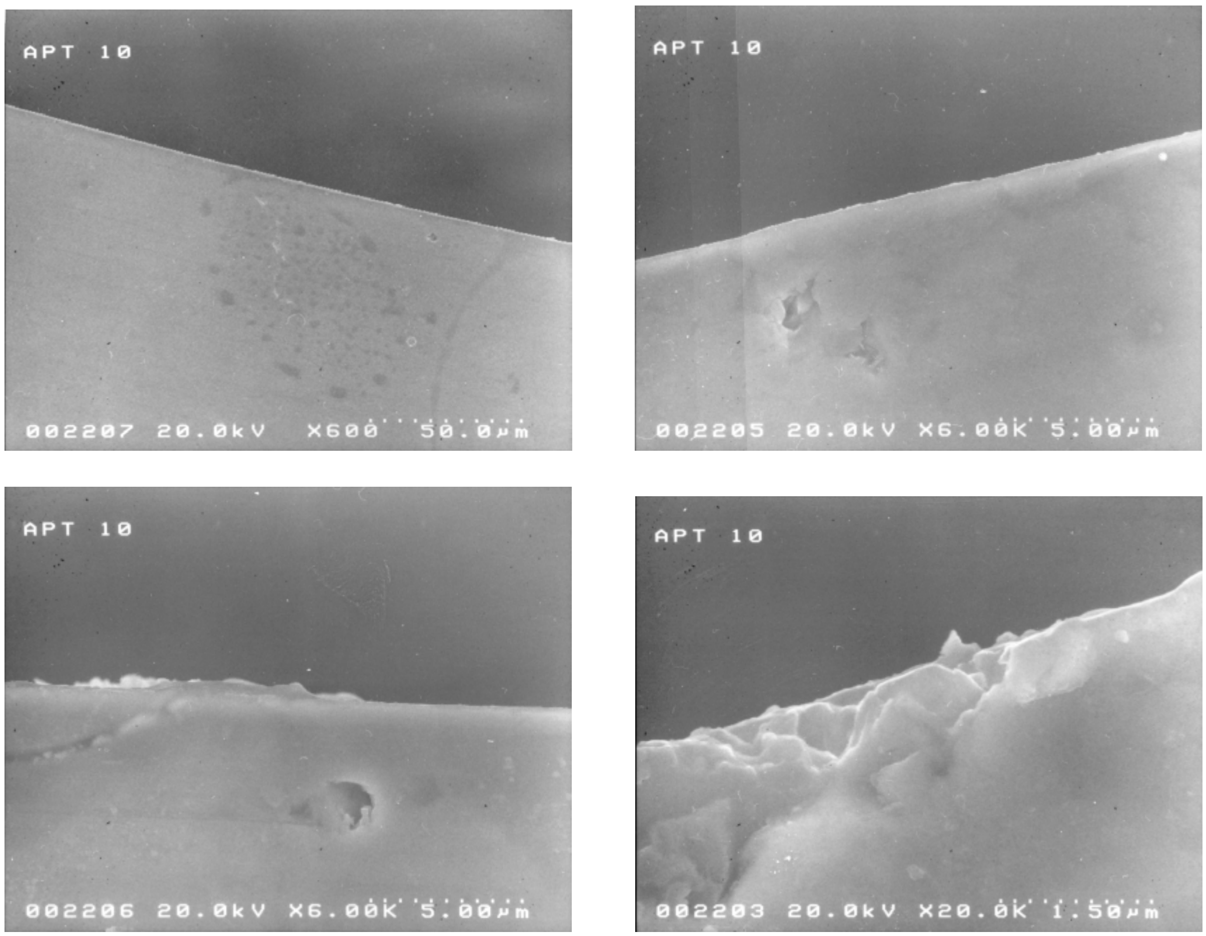

All pictures of aperture APT 10 are showing a view on the top of the aperture edge

Figure B.3 APT 16 SE micrographs

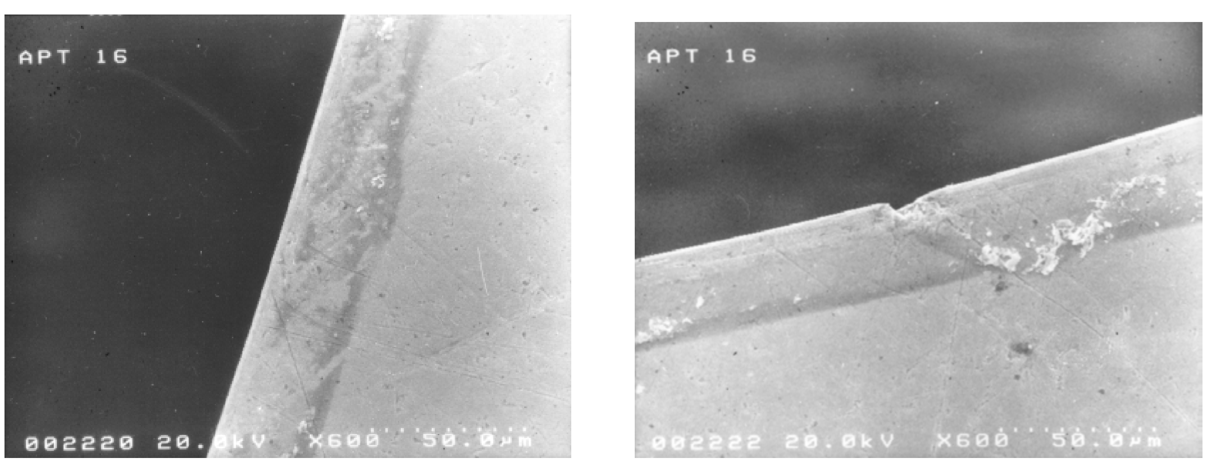

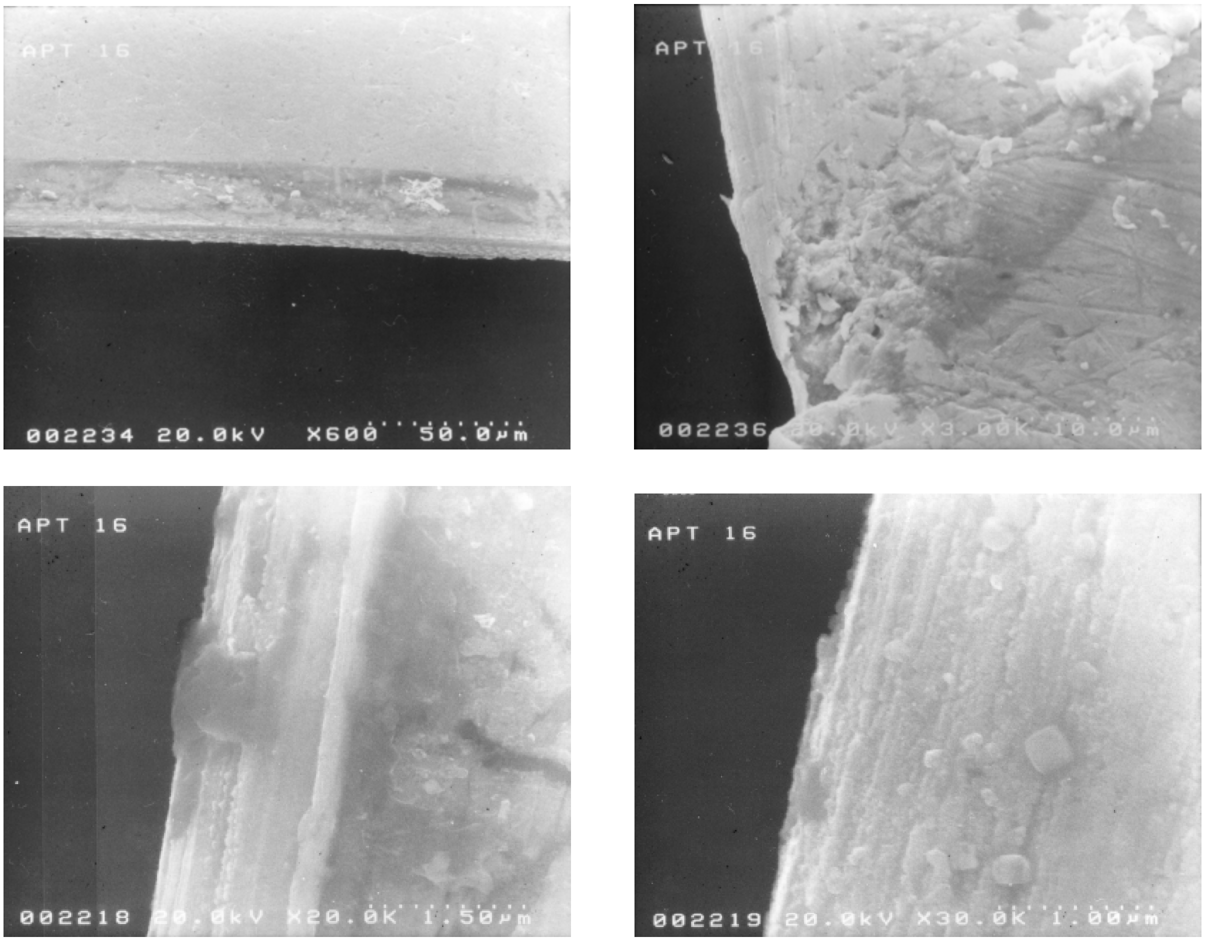

All pictures of aperture APT 16 are showing a view on the top of the aperture edge

Figure B.4 APT 22 SE micrographs

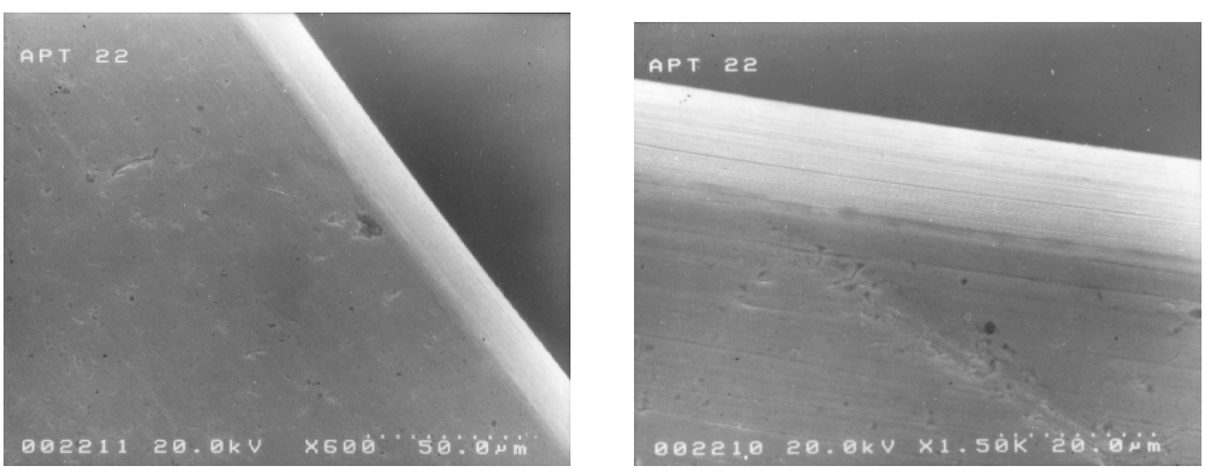

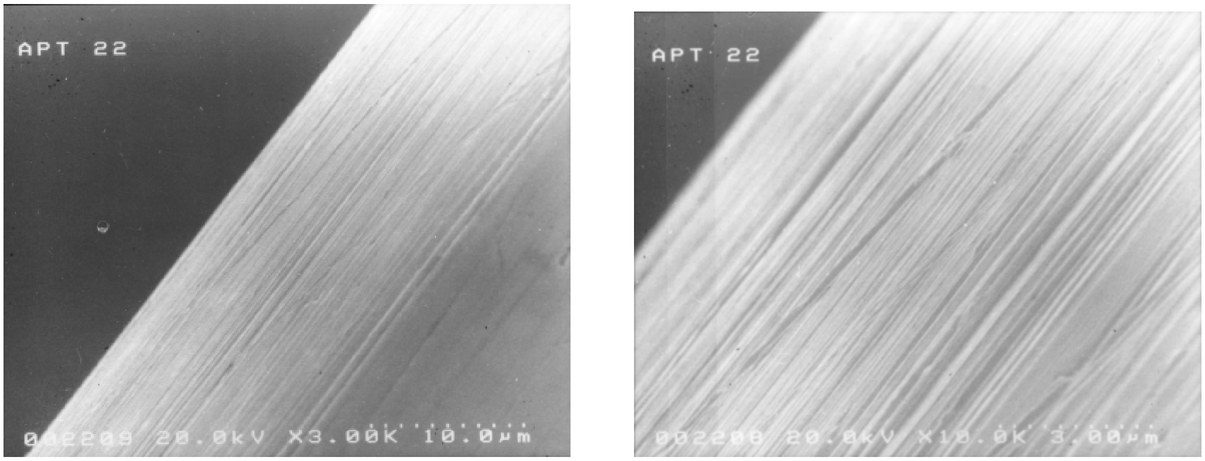

All pictures of aperture APT 22 are showing a view on the top of the aperture edge

Figure B.5 P20 SE micrographs

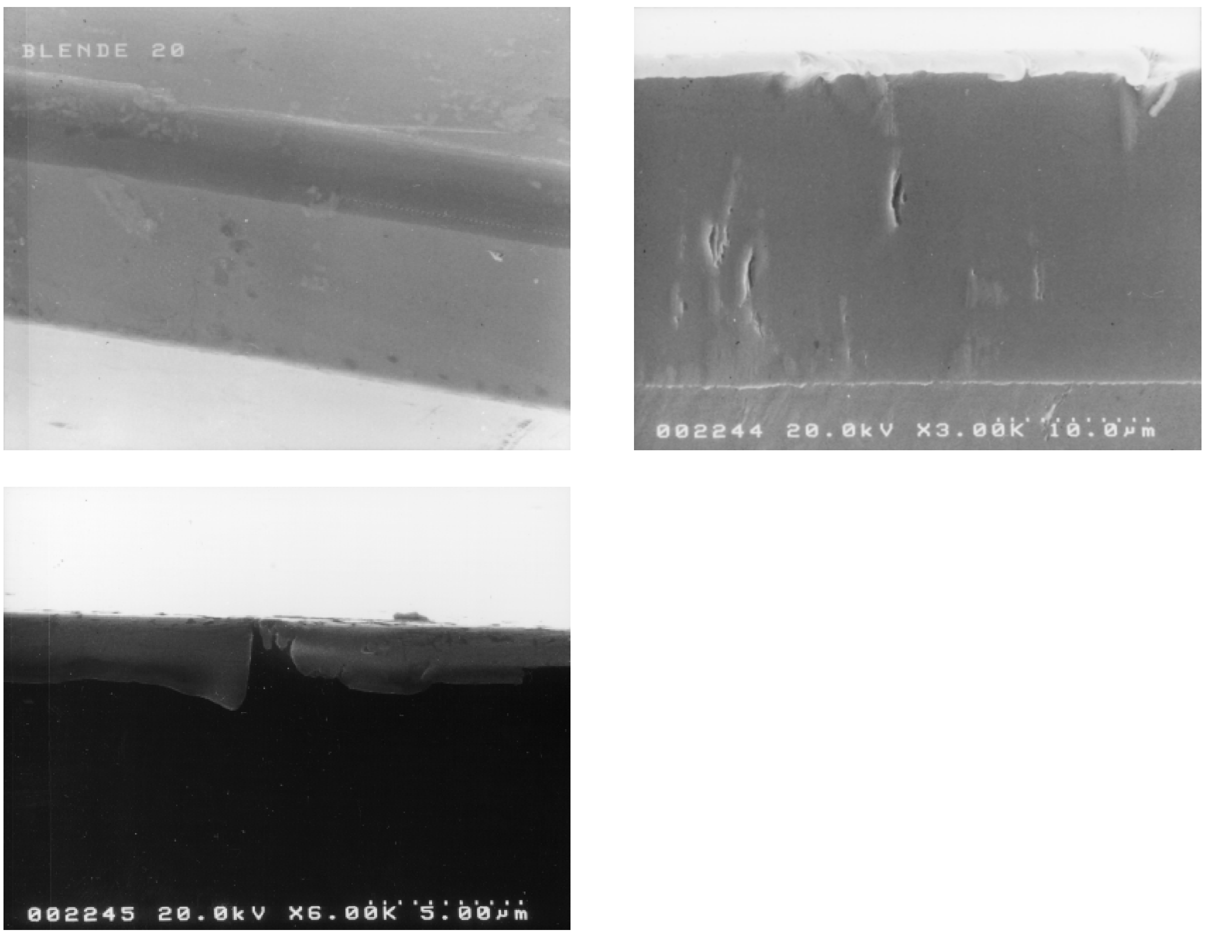

View of P20 of the "land" of the tilted aperture. On top is the front side of the aperture on the bottom the slanted backside - the cone .- can be seen. Aperture P20 is from the same batch as apertures P21, P23, and P24.

Figure B.6 P21 SE micrographs

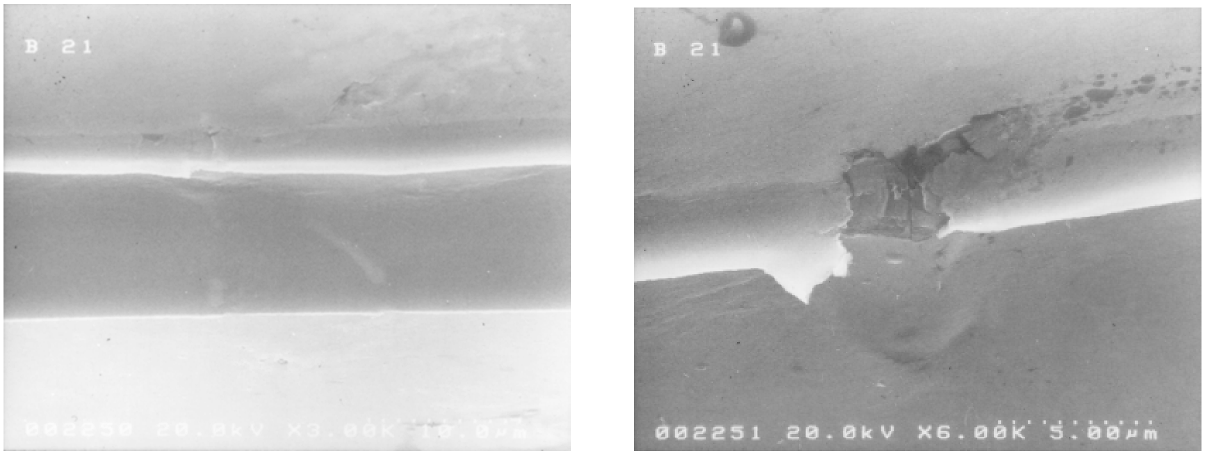

View of P21 of the "land" of the tilted aperture. On top is the front side of the aperture on the bottom the slanted backside - the cone .- can be seen

Acknowledgement:
The pictures were taken by Ms. Cornelia Assmann and electronically processed by Ms. Monika Korte

C. Appendix C: Analysis of variance for apertures with a land

Several laboratories were able to measure three of the apertures, Apt 07, Apt 11 and Apt 19 using both non-contact and contact methods. This presented an opportunity to examine the effect of the measurement method in the comparison. An analysis of variance on the method variable was applied on the data sets.[4]

The tables and graphs show the data sets on the three apertures. The ordinate axis is the measured area in [mm^2], while in the abscissa are labels for the method used. The height of the box represents the measurement values from the middle 50% of the distribution while the high and low bars indicate the minimum and maximum results.

In all three apertures, the measured areas by the contact method generally register higher than the non-contact method. The contact method values also exhibit a much tighter variation pattern. All three apertures have a cylindrical edge (land).

[4] A general reference on analysis of variance:
Hoaglin, D.C., Mosteller, F., Tukey, J.W. "Fundamentals Of Exploratory Analysis Of Variance", New York: John Wiley, 1991

Table.C.1 Measurement data for Apt 07 Methods 1 and 2

Apt 07 Area	u(i)
Method 1	**Non Contact**
505.1476	0.05090
505.1140	0.01300
505.2272	0.04100
504.8890	0.00600
505.0377	0.08770
505.0708	0.02120
Method 2	**Contact**
505.1755	0.00800
505.1827	0.00470
505.1665	0.03780
505.1902	0.01000
505.1750	0.00800

Figure C.1 Box plot for non-contact and contact measurements of Apt 07

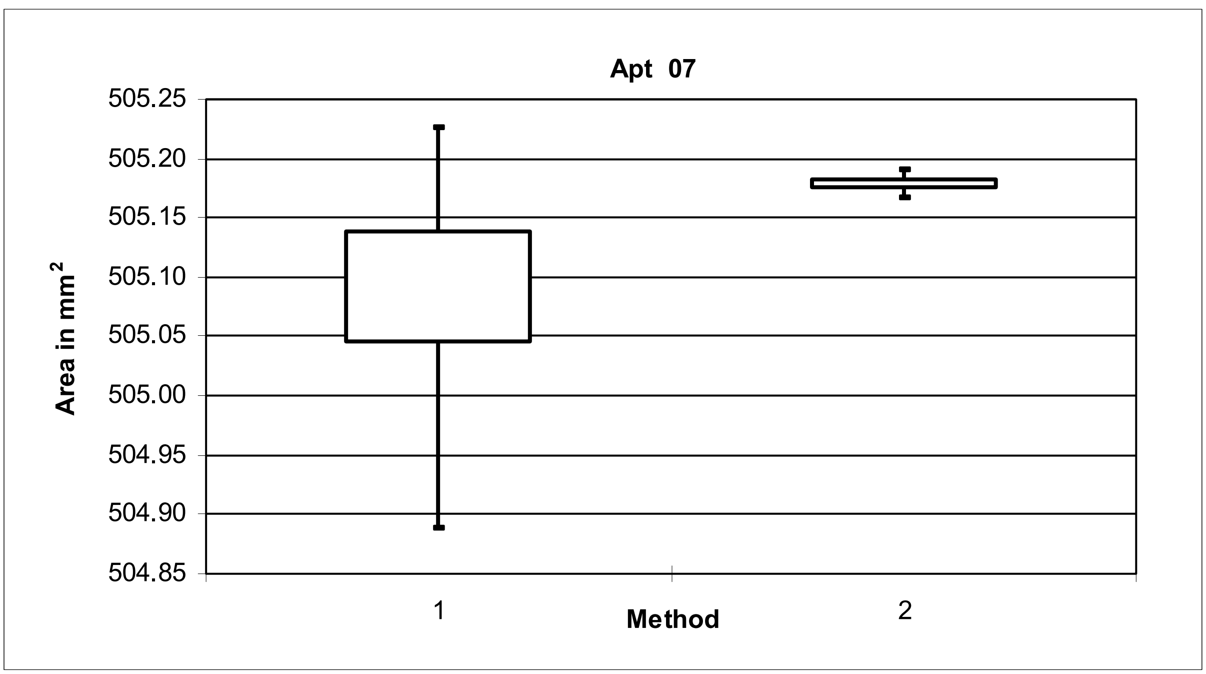

Table C.2 Measurement data sets for Apt 11, methods 1 and 2

Apt 11 Area	U(j)
Method 1	**Non contact**
23.3131	0.00160
23.3061	0.00550
23.2870	0.00400
23.3020	0.01050
23.3094	0.00160
23.2657	0.01600
23.2934	0.00075
Method 2	**Contact**
23.3115	0.00096
23.3141	0.00049
23.3003	0.00214

Figure C.2 Box plot for non-contact and contact measurements of Apt 11

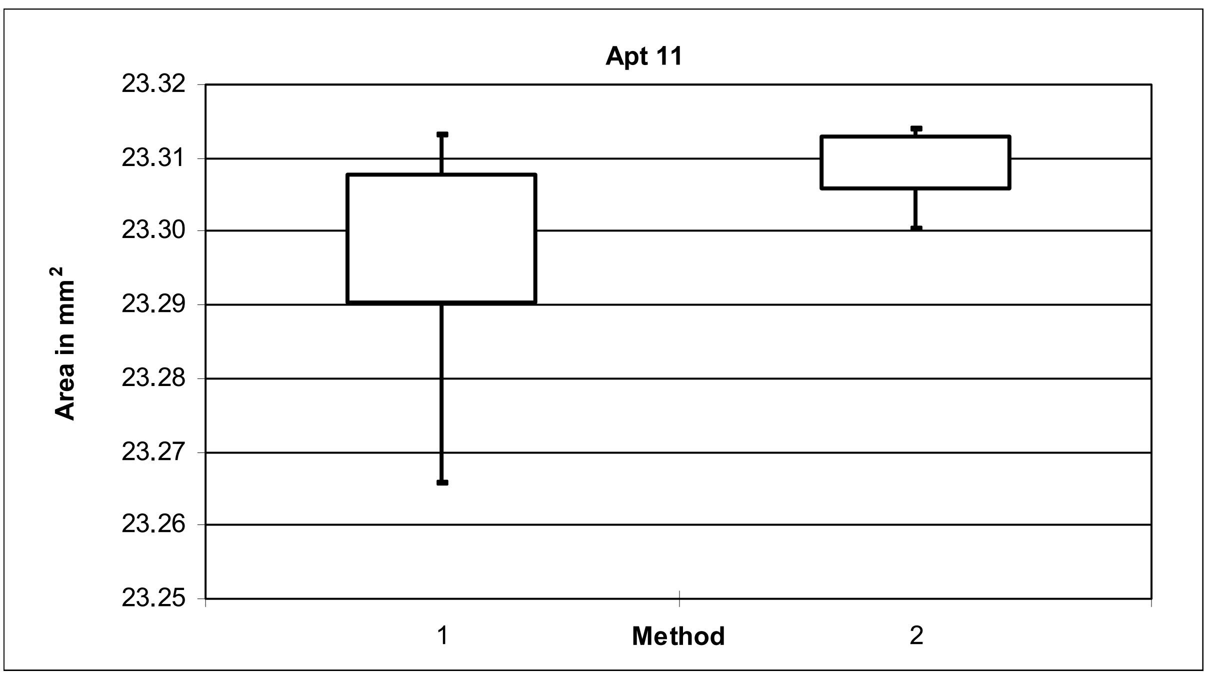

Table C.3 Measurement data sets for Apt 19, methods 1 and 2

Apt 19	U(j)
Method 1	**Non contact**
518.3052	0.04200
517.8230	0.00800
518.0051	0.10960
518.2530	0.01203
Method 2	**Contact**
518.2533	0.03030
518.2138	0.03630
518.2163	0.00240
518.2088	0.00807

Figure C.3 Box plot for non-contact and contact measurements of Apt 19

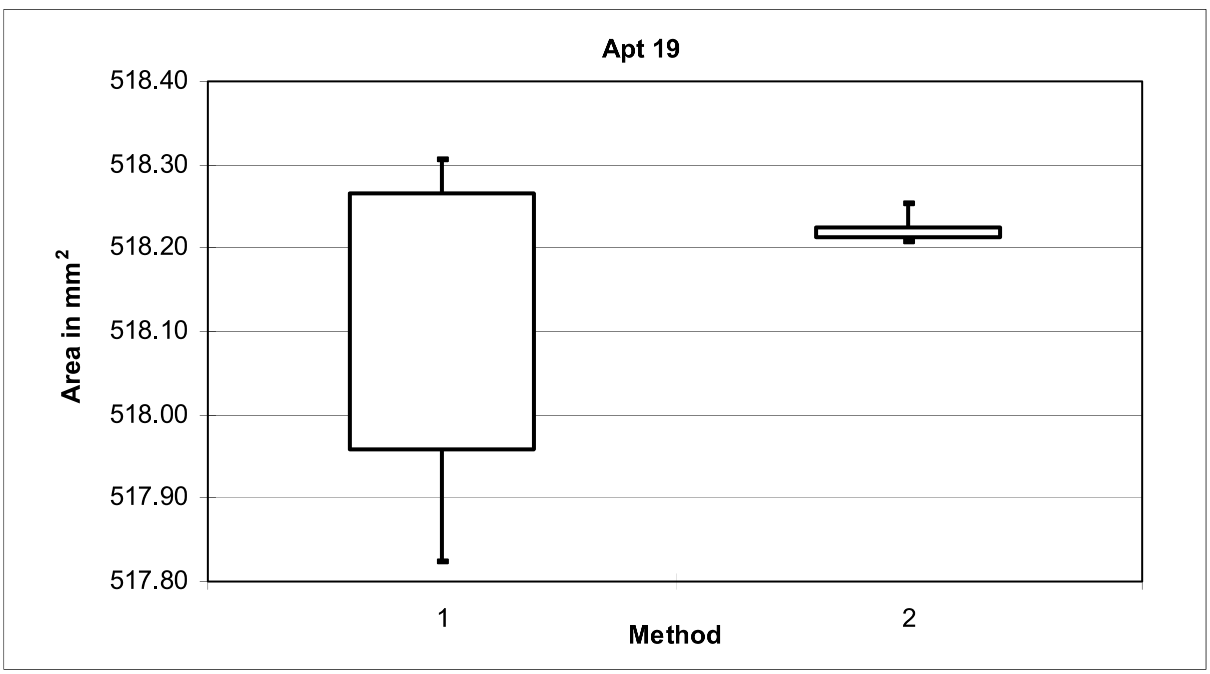

D. Appendix D: Corrections to Reported Data

The PTB discovered transcription errors to their reported data for Apt 13 and Apt 16 after Draft A was distributed. Table D.1 shows the reported measurement results for all apertures measured by the PTB, with the corrected values for Apt 13 and Apt 16.

Table D.1 Mean area measurements by the PTB non-contact method (corrected Table 4.1.1)

Aperture	Area (A) [mm^2]	$u(A)$ [mm^2]
Apt 1	550.7791	0.0126
Apt 4	34.0262	0.0031
Apt 7	505.1476	0.0509
Apt 10	23.2684	0.0109
Apt 13	526.0117	0.1235
Apt 16	21.3321	0.0193
Apt 21	314.1847	0.0273

The following tables and figures are the results of the comparison including the corrected values for the PTB for Apt 13 and Apt 16, and the attendant changes to the values for lab differences. PTB results are included in the calculation of RV in these tables.

Table D.2 Results of the comparison for Apt 13 including PTB correction (corrected Table 7.1.5)

Lab	$\overline{A}_{\mathrm{NIST}j,i}$	$\overline{A}_{i,j}$	$r_{i,j}$	$u_{rel}(\overline{A}_{\mathrm{NIST},j})$	$u_{rel}(\overline{A}_{i,j})$	$u_{\mathrm{stability},j}$	$u(r_{i,j})$
PTB	525.6302	526.0117	1.000726	0.0029%	0.0235%	0.0002%	0.0237%
NPL	525.6279	525.5218	0.999798	0.0029%	0.0025%	0.0000%	0.0038%
LNE-INM	525.6369	525.6808	1.000083	0.0029%	0.0093%	0.0010%	0.0098%
VNIIOFI	525.6333	525.4000	0.999556	0.0029%	0.0021%	0.0014%	0.0038%
OMH	525.6133	525.5362	0.999853	0.0029%	0.0118%	0.0016%	0.0122%
NIST	525.6332	525.6332	1.000000	0.0000%	0.0000%	0.0000%	0.0000%
RV			**1.000003**				0.0048%

Table D.3 Results of the comparison for Apt 16 including PTB correction (corrected Table 7.1.6)

Lab	$\overline{A}_{\text{NIST}j,i}$	$\overline{A}_{i,j}$	$r_{i,j}$	$u_{rel}(\overline{A}_{\text{NIST},j})$	$u_{rel}(\overline{A}_{i,j})$	$u_{\text{stability},j}$	$u(r_{i,j})$
PTB	21.2789	21.3321	1.002501	0.0030%	0.0900%	0.0340%	0.0963%
NPL	21.2789	21.3082	1.001379	0.0030%	0.0113%	0.0340%	0.0360%
LNE-INM	21.2789	21.2887	1.000461	0.0030%	0.0202%	0.0340%	0.0397%
VNIIOFI	21.2789	21.2624	0.999226	0.0030%	0.0042%	0.0340%	0.0344%
MIKES	21.2789	21.2690	0.999536	0.0030%	0.0447%	0.0340%	0.0562%
BIPM	21.2789	21.2786	0.999987	0.0030%	0.0052%	0.0340%	0.0345%
OMH	21.2789	21.2535	0.998807	0.0030%	0.0513%	0.0340%	0.0616%
NIST	21.2789	21.2789	1.000000	0.0000%	0.0000%	0.0340%	0.0340%
RV			**1.000237**				0.0188%

Table D.4 Lab difference from reference value for Apt 13 including PTB (corrected Table 7.2.5)

Lab	Δij(Lab-RV)	u(Δij)
PTB	0.0723%	0.0199%
NPL	-0.0205%	0.0057%
LNE-INM	0.0081%	0.0093%
VNIIOFI	-0.0447%	0.0057%
OMH	-0.0149%	0.0111%
NIST	-0.0003%	0.0048%
RV	0.0000%	0.0048%

Table D.5 Lab difference from reference value for Apt 16 including PTB (corrected Table 7.2.6)

Lab	Δij(Lab-RV)	u(Δij)
PTB	0.2263%	0.0855%
NPL	0.1141%	0.0364%
LNE-INM	0.0224%	0.0392%
VNIIOFI	-0.1011%	0.0352%
MIKES	-0.0701%	0.0522%
BIPM	-0.0250%	0.0353%
OMH	-0.1429%	0.0566%
NIST	-0.0237%	0.0349%
RV	0.0000%	0.0188%

Figure D.1 Lab difference from reference value for Apt 13 including the PTB (corrected Fig. 7.2.5)

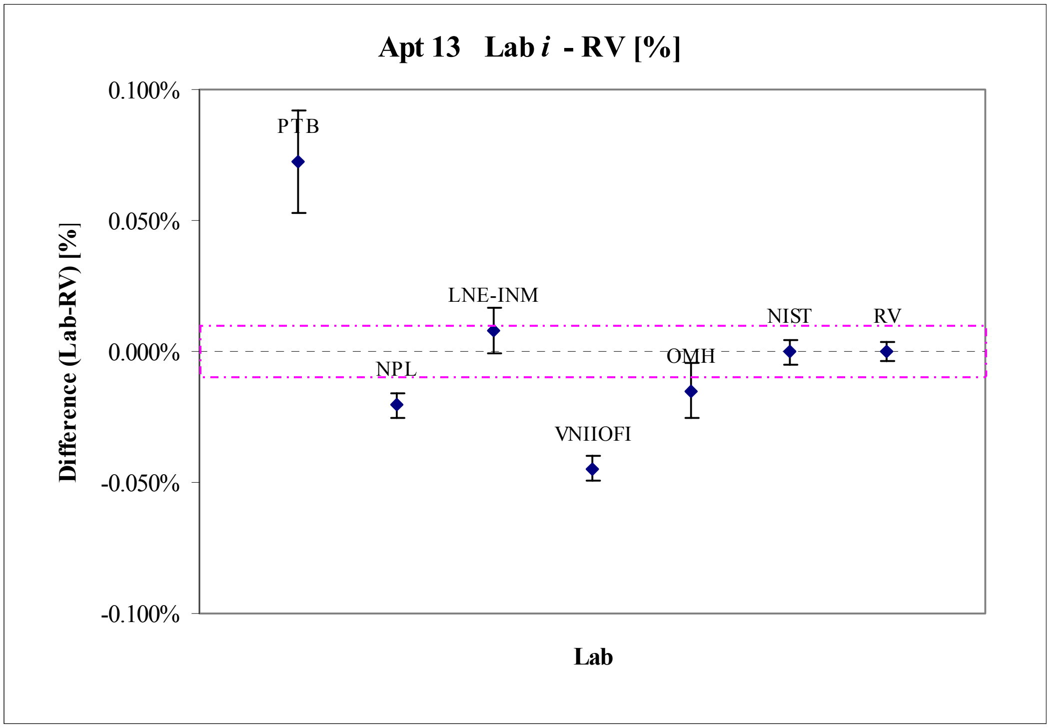

Figure D.2 Lab difference from reference value for Apt 16 including the PTB (corrected Fig. 7.2.6)

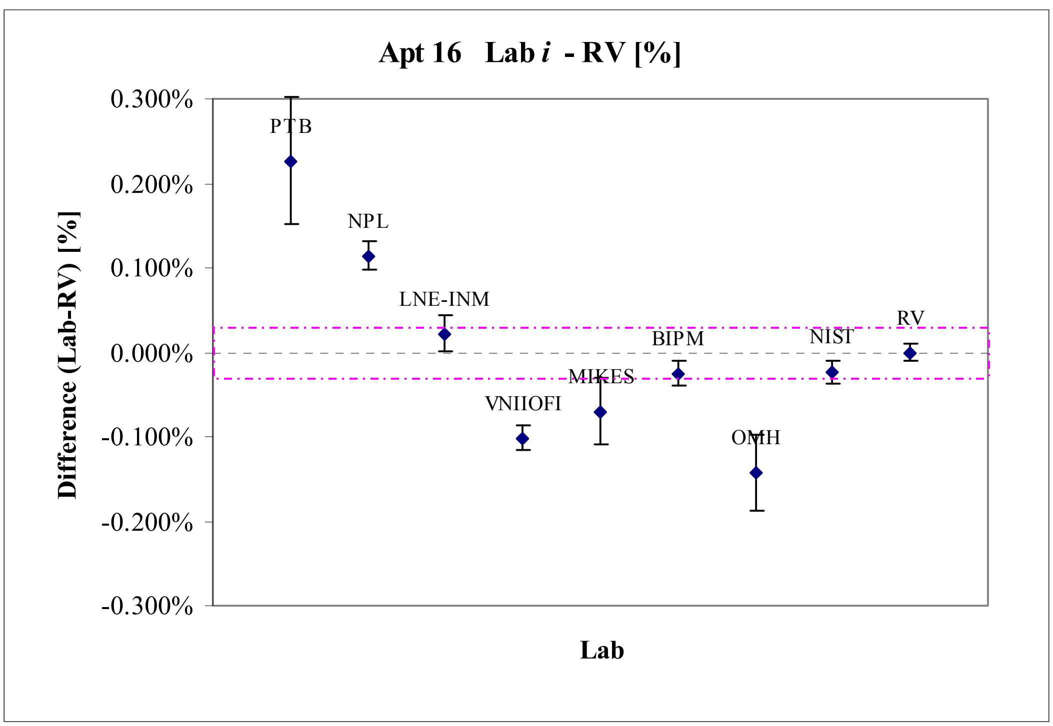

Figure D.3 PTB Lab differences from RV of apertures measured using revised values

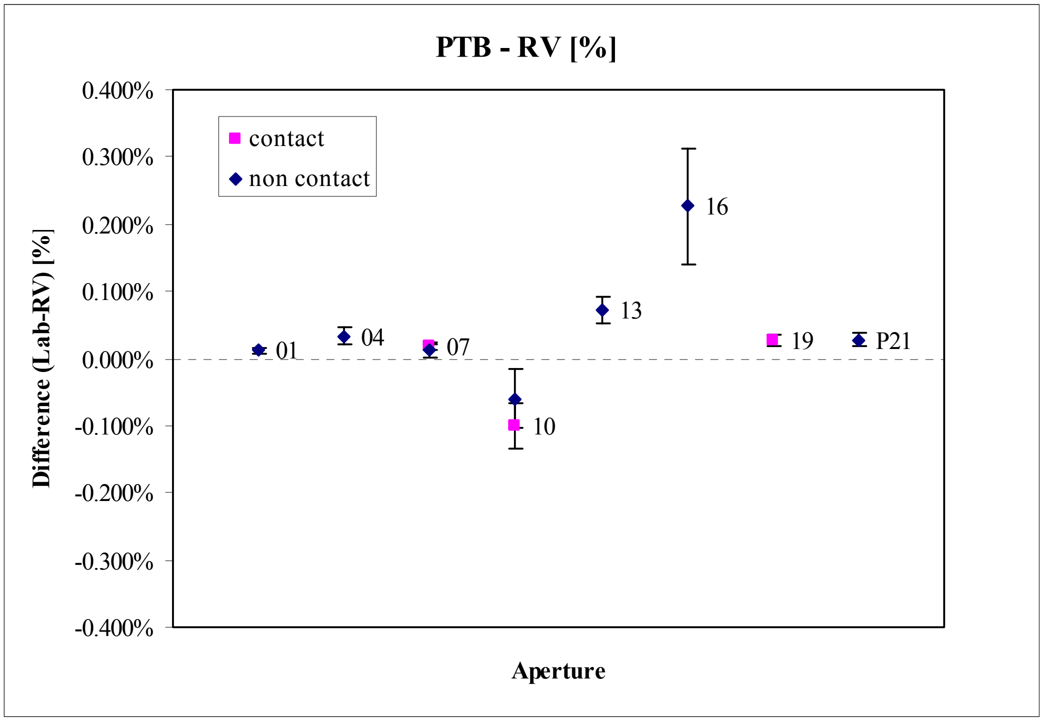

Figure D.4 NPL Lab differences from RV of apertures measured using revised values

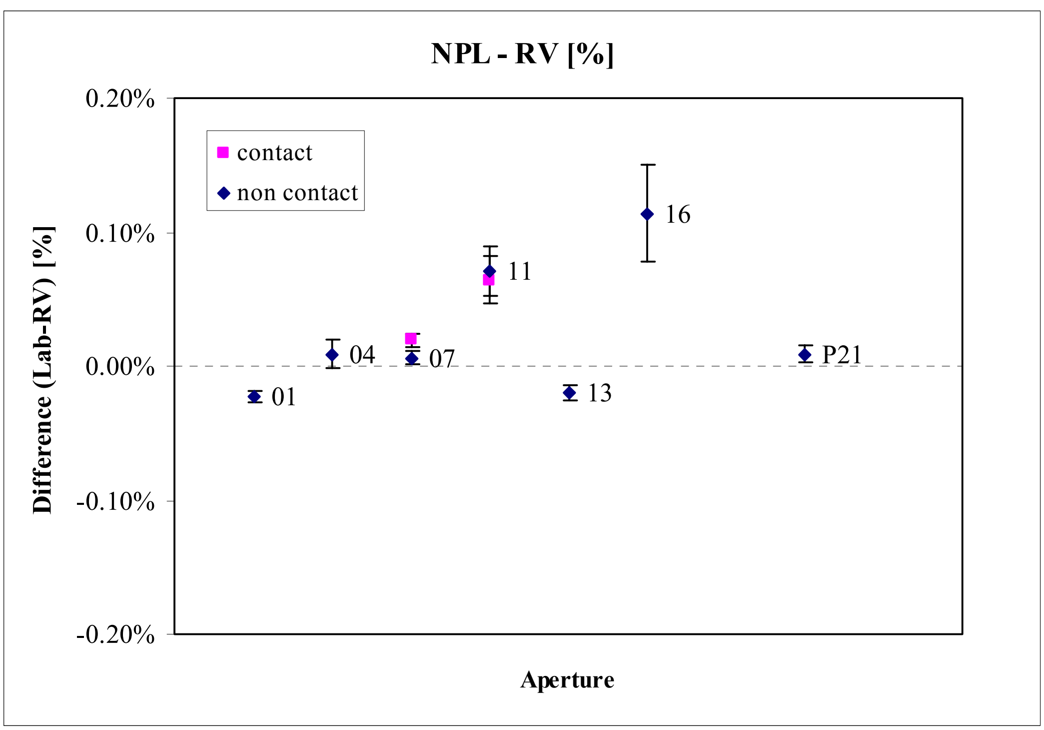

Figure D.5 LNE-INM Lab differences from RV of apertures measured using revised values

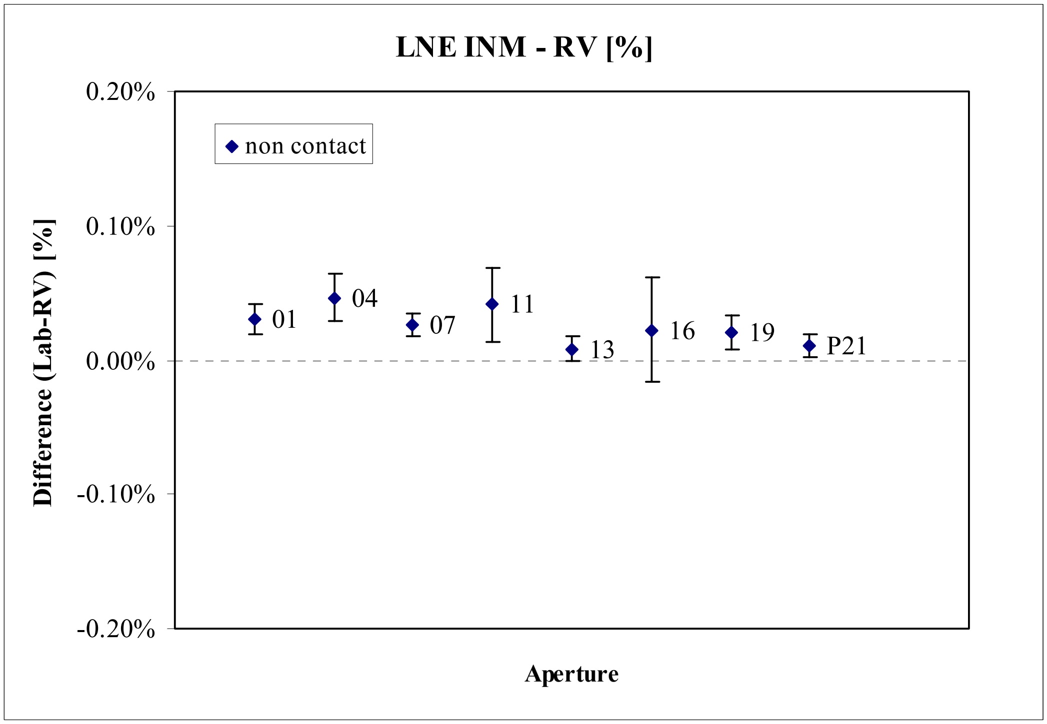

Figure D.6 VNIIOFI Lab differences from RV of apertures measured using revised values

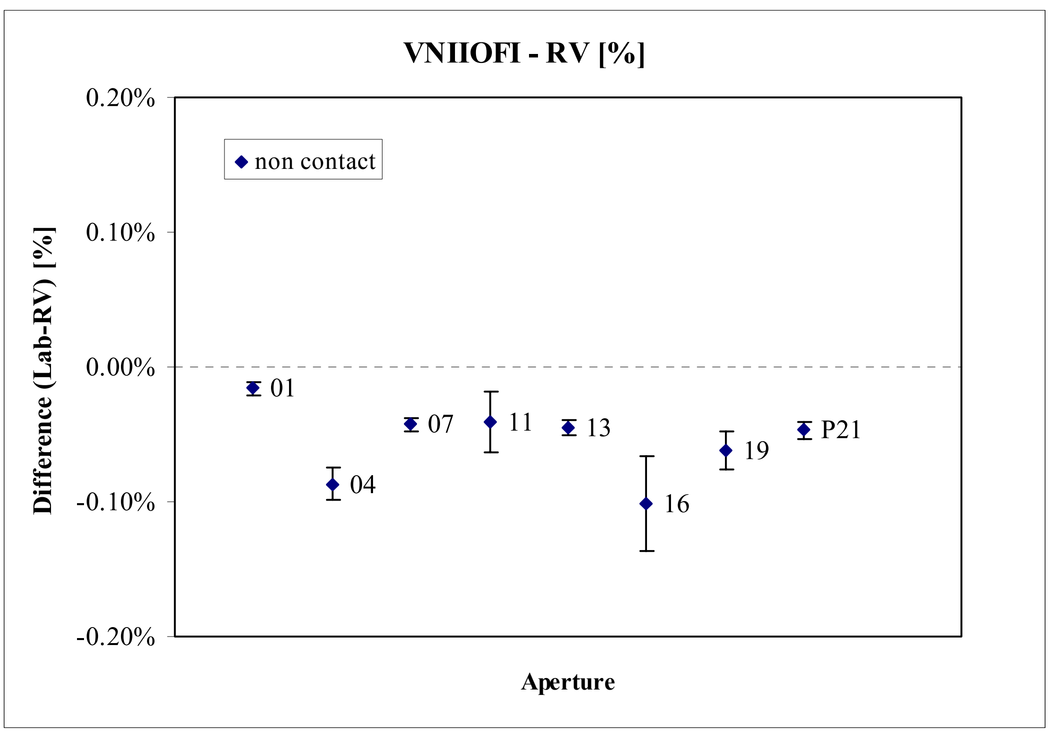

Figure D.7 MIKES Lab differences from RV of apertures measured using revised values

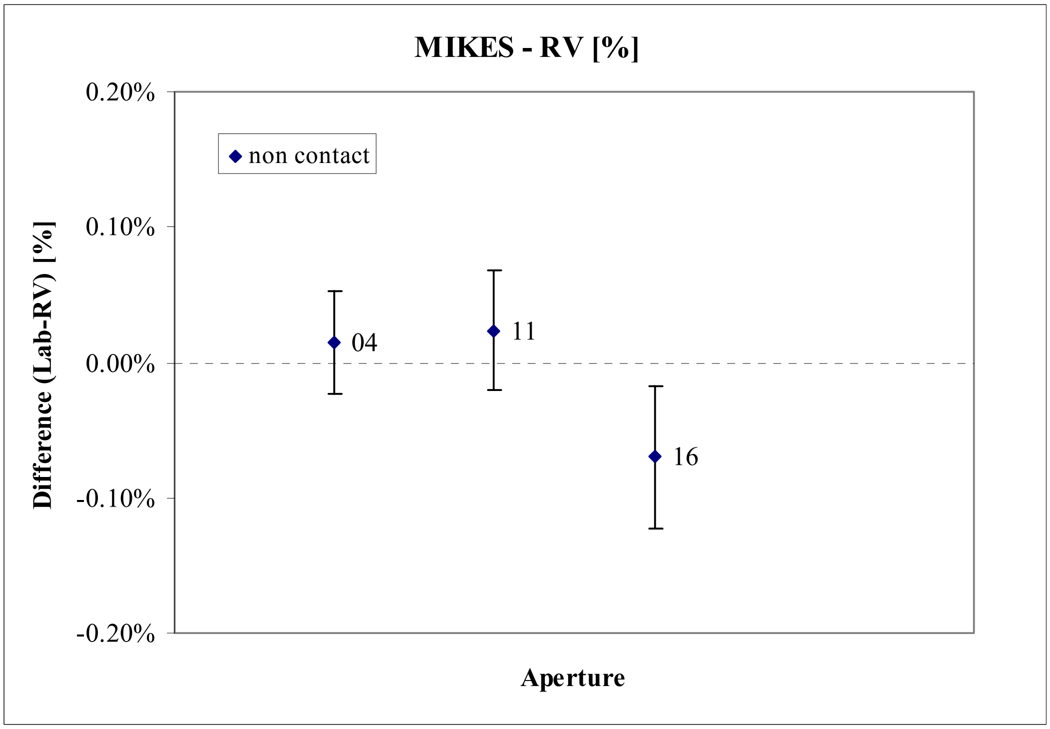

Figure D.8 BIPM Lab differences from RV of apertures measured using revised values

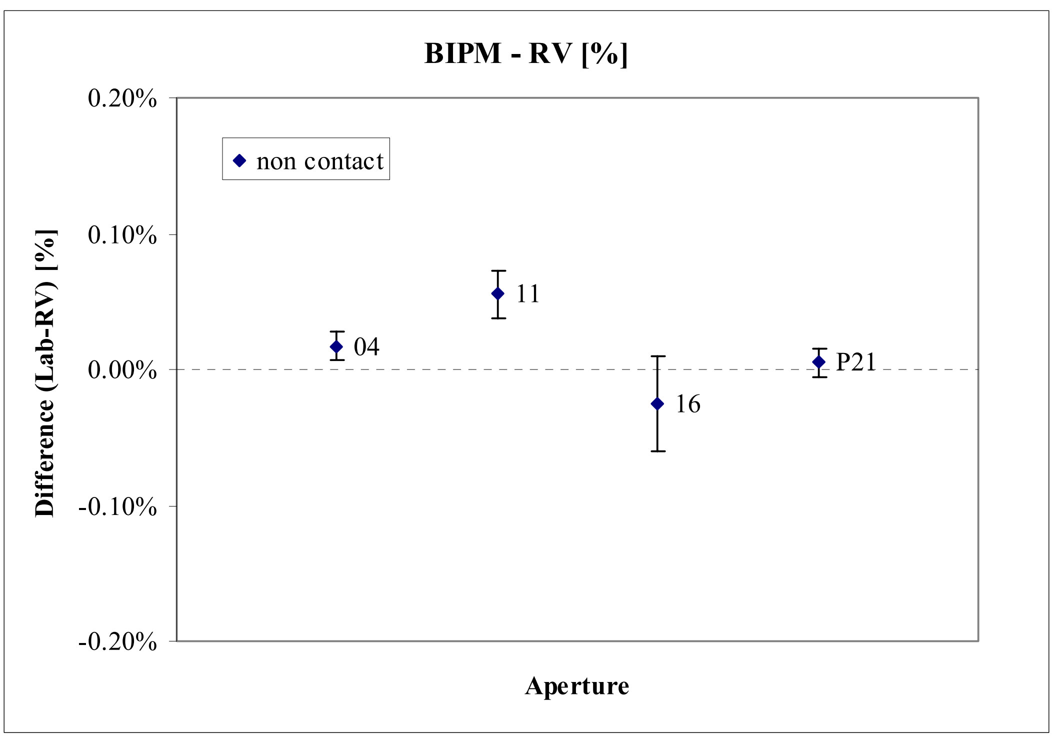

Figure D.9 OMH Lab differences from RV of apertures measured using revised values

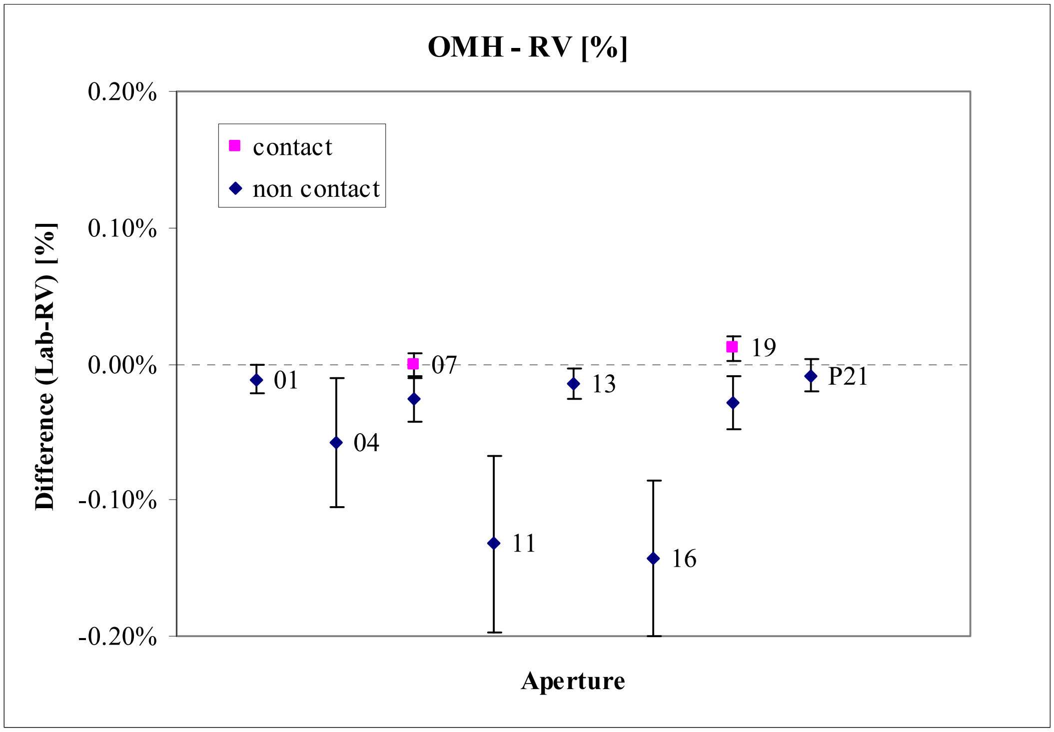

Figure D.10 NIST Lab differences from RV of apertures measured using revised values